4-25-2016

Phenological Responses of Deciduous Woody Plants to Climate Variability and Change from Individuals to Communities

Yingying Xie
yingying.xie1@gmail.com

Phenological Responses of Deciduous Woody Plants to Climate Variability and Change from Individuals to Communities

Yingying Xie, PhD

University of Connecticut, 2016

Shifts in plant phenology can have direct impacts on community and ecosystem-level processes as well as substantial economic impacts including declines in maple syrup production and changes in the timing and vividness in fall foliage as this affects ecotourism. Understanding how plant phenology mechanistically responds to environmental variation is vital to assessing the effects of climate change on ecological processes and to making predictions about the future. This dissertation focuses on understanding the mechanisms of phenological responses of Northeastern North American deciduous forests to climate change from ground-based individual level to the community at landscape scales. Mechanism-based plant phenological models were developed that incorporate spatio-temporal responses from local to regional scales. These models incorporated ground-based, visual phenological observations on individual trees, time-lapse digital photography, and remotely-sensed land surface phenology. A novel, mechanistic modeling framework that utilizes Bayesian survival analysis is developed in Chapter one. This model using remotely-sensed satellite data identified significant effects from chill and heat units on deciduous forest green-up and predicted the future change across the landscapes of the Northeast. In the second chapter, significant environmental factors affecting the timing of fall dormancy of deciduous forests in New England, based on remotely sensed data, were identified and quantified using multiple statistical variable selection methods. Future predictions of fall dormancy timing suggested complex effects from temperature, precipitation, drought-, heat-stress and floods on forests autumn phenology across the landscape. Chapter three focuses on the phenological responses of individual trees to climate/weather variables based on ground-based, visual observations. Linear mixed effects models revealed species-

specific phenological responses of leaf coloration and leaf drop to precipitation, drought and floods. In fourth chapter, color indices derived from time-lapse camera imagery of tree canopies were analyzed to determine how fall foliage coloration responds to variation in climate/weather variables. The red color index matched better with visual defined autumn phenology across the dominant species than did the green color index. Linear mixed effects model results suggested that chill in autumn, drought stress in summer and autumn, and heat-stress in summer are all important factors of the timing of peak color in fall foliage.

Phenological Responses of Deciduous Woody Plants to Climate Variability and Change from Individuals to Communities

Yingying Xie

B.A., Beijing Forestry University, 2007

M.S., Beijing Forestry University, 2010

A Dissertation

Submitted in Partial Fulfillment of the

Requirements for the Degree of

Doctor of Philosophy

at the

University of Connecticut

2016

APPROVAL PAGE

Doctor of Philosophy Dissertation

Phenological Responses of Deciduous Woody Plants to Climate Variability and Change from Individuals to Communities

Presented by

Yingying Xie, B.A., M.S.

Major Advisor _____
John A. Silander, Jr.

Associate Advisor _____
Robin L. Chazdon

Associate Advisor _____
Eldridge S. Adams

Associate Advisor _____
Daniel L. Civco

Associate Advisor _____
Richard B. Primack

University of Connecticut
2016

ACKNOWLEDGEMENTS

I have many thanks to my adviser, John Silander, who guides me in scientific research and provides critical suggestions and feedback on my research projects. I am grateful to have a great adviser committee. Robin Chazdon and her lab members gave me great suggestions and invaluable encouragement especially at the beginning of my Ph.D research period. I learnt population ecology and linear mixed effects models from Eldridge Adams, who inspired me in my research leading me to a new statistical tool. Daniel Civco provided guidance on the remote sensing component of my projects, who brought me the powerful tools in satellite data analysis, spatial analysis and imaging processing. The discussions on plant phenology with Richard Primack were inspiring to my future direction of research.

My research was supported by NSF grants DEB 0842465 to John A. Silander and EEB Bamford fund. I was fortunate to have great lab mates in Silander's lab, wonderful research environment in EEB department in UCONN and very helpful staff in the department. My former lab mates, Jenica Allen, Adam Wilson, Sarah Bois, Cory Merow, and Mattew Aiello-Lammens gave me a lot of help in discussion ideas, brainstorms, solving problems, and research improvements. Special thanks to my collaborator, Xiaojing Wang, from Department of Statistics, UCONN.

I could not finish my Ph.D research in the USA without the strong support from my family. My parents, Weimin Shentu and Qin Xie, gave great encouragement and support far from China. My friends (Wen Chen, Xin Xie, Ju Zhang, Shuai Yang, etc.) in the USA always provide kind helps and positive energy to my academic and non-academic life. Finally, I thank my dear husband, Chengjie Tian, who quits his job in China and comes to the USA to take good care of me and make his best efforts for our own family.

TABLE OF CONTENTS

LIST OF FIGURES

LIST OF TABLES

Introduction

Climate change has brought substantial temporal changes in plant phenology (Walther et al. 2002; Ibanez et al. 2010) including advanced spring phenology and delayed fall phenology in temperate regions around the world, resulting in longer growing seasons (Linderholm 2006). Plant phenological shifts can have a direct impact on community and ecosystem level processes, such as mismatched food web interactions, faster carbon cycling in spring, and changes in community composition and biodiversity patterns (Cleland et al. 2007; Berg et al. 2010; Vittoz et al. 2013). In addition to ecological effects, phenological changes may also have substantial economic impacts on the fall foliage ecotourism in northeastern North America (Rustad et al. 2011), and elsewhere. Given these impacts, mechanistically understanding how plant phenology responds to spatial and temporal environmental variation now and in the future is vital to assessing the effect of climate changes on ecological processes and to making predictions about the future.

Currently our understanding of the mechanisms controlling plant phenology is surprisingly poor. Regional mechanistic plant phenology models are needed for predictions of both temporal and spatial responses at large scales. Although different species are known to show different phenological responses spatially and temporally (Ibanez et al. 2010, Diez et al. 2012), no study has examined community or landscape level phenological responses to environmental variation. General mechanisms of spring plant phenology involving gene regulatory and hormonal responses to chilling and heating temperatures have been studied in some temperate woody plant species (Li et al. 2009; Jiménez et al. 2010). However, the mechanisms of fall phenology (senescence and dormancy) remain poorly understood and little studied (Lim et al. 2007, Gallinat et al. 2015). Most published work has focused only on the role of day-length and chilling or frost (Archetti et al. 2013, Jeong and Medvigy 2014). Although ground-based phenology observation and Land Surface Phenology (LSP, i.e. seasonal pattern of vegetation dynamics on land

surface observed by satellites), have been conducted for decades, a major challenge is integrating information from these two data sources and to link their ecological signals to yield an integrated understanding of phenology as a predictive science across spatial and temporal scales.

This dissertation contains four chapters that focus on understanding how phenology of temperate deciduous forests responds mechanistically to environmental variation from ground-based individual level to communities at the landscape scales.

In Chapter One, I investigated how variation in weather and climate relate to the known physiological chilling and heating requirements of deciduous forest tree species that result in spring green-up in New England, USA over nine years (2001-2009). I used remotely sensed phenology data from MODIS satellite images. Both warming and chilling temperatures had large influences on the timing of green-up in New England deciduous forests. The effects of community composition across the landscape were also significant. Greater oak dominance had later green-up, while sites with more birch tended to have earlier green-up dates. Future predictions (2046-2065) based on climate change scenarios suggested that higher heating and chilling accumulations will lead to earlier green-up (8-48 days). However, in coastal areas green-up may be delayed due to reduced chilling accumulation. This chapter provides an innovative statistical modeling method combining plant physiological mechanisms, topographic spatial heterogeneity, and species composition to predict how land surface phenology responds to climate and weather variation and in turn allows future projections.

In Chapter Two, I used remotely sensed MODIS satellite phenology data from 2001 to 2012, and identified and quantified significant effects of a suite of environmental factors on the timing of fall dormancy of deciduous forest communities in New England, USA. While earlier dormancy of deciduous forests was induced by cold, frost, wet conditions, high heat-stress, moderate heat- and drought-stress delayed dormancy, which was also affected by species composition in forest communities. I made future predictions of fall dormancy in two eco-regions for two periods (2041-2050 and 2090-2099) based on climate change scenario projections. Later dormancy dates were predicted in northern areas, whereas in

coastal areas earlier dormancy dates were predicted. The findings suggested that changes in frost and moisture conditions as well as extreme weather events (e.g. drought- and heat-stress, and flooding) should be considered in future predictions of autumn phenology for temperate deciduous forests. While climate change brings more frequent and intensity of extreme weather events, the phenological responses of deciduous forests to these events will be complicated.

Chapter Three focused on the analysis of ground-based, visually-scored, phenology observations in New England USA. I identified a suite of weather/climatic factors that significantly affect the autumn phenology (leaf coloration and leaf drop) of 12 dominant deciduous tree species. These factors included autumn chill, frost, heat- and, drought-stress, and precipitation across the growing season. Linear mixed effects models are applied to phenology responses for the first time. Due to different physiological requirements among species, species-specific sensitivities to those factors were also quantified in the models. I also found a positive relationship between spring and autumn phenology. Based on future climate projections along with projected spring phenological changes, I predicted future changes in autumn phenology for all individual tree species from 2015 to 2099. Autumn phenology in general will be later in the future by 1 to more than 20 days, and the length of coloration process will be shorter for most species. Climatic stresses play a critical role in affecting autumn phenology, and divergent phenological responses are found in different tree species. This will have a profound effect in predicting future impacts from climate change on forest community and ecosystem patterns and processes.

In Chapter Four I focused on the analysis of digital cameras images that capture color variation in canopy foliage aver the growing season. These digital images captured multiple deciduous tree species canopies with continuous observations, and with enough spatial resolution to identify temporal changes in individual over the growing season. These provided a bridge linking ground-based visual observation to remotely sensed changes in phenology. Color indices and phenological transition dates were derived from three color channels from the images for each tree canopy at each of several sites. Start of season (SOS) dates from green color indices matched the period between onset and peak of leaf unfolding dates, based

on visual observations. In contrast, red color index had better performance in matching with visually observed autumn phenology across the dominant species. I also investigated how the timing of peak red color of fall foliage and the increased redness during the growing season of each species responded to a suite of climatic/weather factors. Temperature and precipitation in autumn, drought-stress in the summer and autumn, and heat-stress in the summer were all important factors affecting the timing of peak color in fall foliage. The findings help in understanding phenological timing in deciduous trees as captured by digital cameras. As well this provides insights in scaling phenology of individuals observed in the field to the remote sensed forest stands.

References

Archetti M, Richardson AD, O'Keefe J, Delpierre N (2013) Predicting Climate Change Impacts on the Amount and Duration of Autumn Colors in a New England Forest. PLoS ONE 8(3): e57373. doi:10.1371/journal.pone.0057373.

Berg MP, Kiers ET, Driessen G, Heijden MVD, Kool BW, Kuenen F, Liefting M, Verhoef HA, Ellers J (2010) Adapt or disperse: understanding species persistence in a changing world. Glob Change Biol 16:587–598.

Cleland EE, Chuine I, Menzel A, Mooney HA, Schwartz MD (2007) Shifting plant phenology in response to global change. Trends Ecol Evol 22:358–365.

Diez MJ, Ibanes I, Miller-Rushing AJ, Mazer SJ, Crimmins MA, Bertelsen CD, Inouye DW (2012) Forecasting phenology: from species variability to community patterns. Ecol Lett 15:545–553.

Gallinat AS, Primack RB, Wagner DL (2015) Autumn, the neglected season in climate change research. Trends in Ecology and Evolution 30: 169-176.

Ibanez I, Primack RB, Miller-Rushing AJ, Ellwood E, Higuchi H, Lee SD, Kobori H, Silander JA (2010) Forecasting phenology under global warming. Philos T Roy Soc B 365:3247–3260.

Jeong S, Medvigy D (2014) Macroscale prediction of autumn leaf coloration throughout the continental United States. Global Ecology and Biogeography 23: 1245-1254.

Jiménez S, Reighard GL, Bielenberg DG (2010) Gene expression of DAM5 and DAM6 is suppressed by chilling temperatures and inversely correlated with bud break rate. Plant Mol Biol 73:157–167.

Li Z, Reighard GL, Abbott AG, Bielenberg DG (2009) Dormancy associated MADS genes from the EVG locus of peach [Prunus persica (L.) Batsch] have distinct seasonal and photoperiodic expression patterns. J Exp Bot 60:3521–3530.

Lim PO, Kim HJ, Nam HG (2007) Leaf Senescence. Annual Review of Plant Biology 58:115–136

Linderholm HW (2006) Growing season changes in the last century. Agricultural and Forest Meteorology 137:1–14.

Rustad, L, Campbell J, Dukes JS, Huntington T, Lambert KF, Mohan J, and Rodenhouse N. (2011) Changing Climate, Changing Forests: The Impacts of Climate Change on Forests of the Northeastern United States and Eastern Canada. USDA Forest Service Northern Research Station General Technical Report NRS-99. 48 p.

Vittoz P, Cherix D, Gonseth Y, Lubini V, Maggini R, Zbinden N, Zumbach S (2013) Climate change impacts on biodiversity in Switzerland: A review. J Nat Conserv 21:154–162.

Chapter 1

Green-up of deciduous forest communities of northeastern North America in response to climate variation and climate change

The following paper was published in *Landscape Ecology* in January 2015. Kazi F. Ahmed calculated climatic variables using downscaled future climate projection data. Jenica M. Allen offered ideas using Bayesian survival models and improve the models and comments on the manuscript. Adam M. Wilson provided suggestions on modeling and data analysis. John A. Silander Jr. provided suggestions on data analysis and comments on the manuscript.

Landscape Ecol
DOI 10.1007/s10980-014-0099-7

RESEARCH ARTICLE

Green-up of deciduous forest communities of northeastern North America in response to climate variation and climate change

Yingying Xie · Kazi F. Ahmed · Jenica M. Allen · Adam M. Wilson · John A. Silander Jr.

Received: 11 December 2013 / Accepted: 6 October 2014

Abstract Temporal shifts in phenology are important biotic indicators of climate change. Satellite-derived Land Surface Phenology (LSP) offers data for the study of vegetation phenology at landscape to global spatial scales. However, the mechanisms of plant phenological responses to temperature are rarely considered at broad spatial scales, despite the potential improvements to spatiotemporal predictions. Geographical gradients in community species composition may also affect LSP spatially and temporally. Using a modified survival analysis, we reveal how weather and climate relate to physiological chilling and heating requirements and affect deciduous forest green-up in New England, USA over 9 years (2001–2009). While warm daily temperatures lead to earlier green-up of deciduous forests, chilling temperatures had a larger influence on green-up. We also found that the effects of community composition across the landscape were as important as the effects of weather. Greater oak dominance led to later green-up, while sites with more birch tended to have earlier green-up dates. Projection into the future (2046–2065) with statistically downscaled, bias corrected climate model output suggested advanced green-up (8–48 days) driven by higher heating and chilling accumulations, but green-up in coastal areas may be delayed due to reduced chilling accumulation. This study provides an innovative statistical method combining plant physiological mechanisms, topographic spatial heterogeneity, and species composition to predict how LSP responds to climate and weather variation and makes future projections.

Keywords Land surface phenology · Bayesian survival model · Chilling · Spatial heterogeneity · Species composition · Vernalization · New England

Electronic supplementary material The online version of this article (doi:10.1007/s10980-014-0099-7) contains supplementary material, which is available to authorized users.

Y. Xie (✉) · J. M. Allen · J. A. Silander Jr.
Department of Ecology and Evolutionary Biology, University of Connecticut, 75 North Eagleville Road, Unit 3043, Storrs, CT 06269-3043, USA
e-mail: yingying.xie1@gmail.com

K. F. Ahmed
Department of Civil and Environmental Engineering, University of Connecticut, 261 Glenbrook Road, Unit 2037, Storrs, CT 06269-2037, USA

A. M. Wilson
Department of Ecology and Evolutionary Biology, Yale University, 165 Prospect St, New Haven, CT 06520, USA

Introduction

Plant phenology is an indicator of climate change, with earlier phenological events for many species in response to rising winter and spring temperatures (Walther et al. 2002; Ibanez et al. 2010). Plant phenological shifts can have a direct impact on

Published online: 06 November 2014

community and ecosystem level processes, such as mismatched food web interactions, faster carbon cycling in spring, and change in community composition and biodiversity patterns (Cleland et al. 2007; Berg et al. 2010; Vittoz et al. 2013). Other than ecological effects, phenological changes may also bring substantial economic impacts. In 2012, a warm spring led to early bud burst and flowering of sugar maples, resulting in a significant drop (32–42 %) in maple syrup production and reduced product quality across New England, USA (Keough 2012). Given these impacts, mechanistically understanding how plant phenology responds to environmental change is vital to assessing the effects of associated changes on ecological processes and to making predictions about the future projected changes.

Experiments on forest trees from different genera (*Alnus, Betula, Fagus, Larix, Picea,* and *Populus*) in Europe (Sarvas 1974; Cannell and Smith 1983; Heide 1993; Rinne et al. 2011) and 50 woody plant species in northeastern USA (Polgar et al. 2013) have provided insight into the general mechanisms controlling spring phenology in woody plants. Specifically a set amount of chilling is required to break the dormancy and heating temperatures then induce budburst and leafing-out of temperate woody plants. Chilling and heating requirements vary among species, as well as genetically within species (Li et al. 2009; Rinne et al. 2011). The general molecular and physiological control of the onset and breaking of bud dormancy in temperate woody plants has been identified and studied in detail in *Prunus* cultivars and *Populus* genotypes. This involves the expression of a cluster of several "Dormancy Associated MADS-box transcription factors" (DAM genes) (Li et al. 2009; Jiménez et al. 2010; Paul et al. 2014). DAM genes are up-regulated by decreasing day length, which results in the onset of plant dormancy in the fall until peak expression around the winter solstice. DAM genes are antagonistically down-regulated by exposure to chilling temperatures after the winter solstice. Thus, the chilling requirement for breaking dormancy is a function of the level of expression of DAM genes, and genetic variation in chilling requirements among species can be related to variation in gene expression. A recent review of the mechanisms involved in breaking bud dormancy in woody plants by Paul et al. (2014), shows a complex interaction among DAM and other genes, their gene products, and hormone levels as these in turn alter structural and physiological changes in plant meristems that then lead to bud break. Nevertheless, these processes are all modulated environmentally by chilling and heating requirements (Paul et al. 2014). In at least some temperate woody species, if chilling requirements are not met spring bud break is delayed or may even fail to occur (Rinne et al. 2011).

Mechanistic models at the species level have been built to detect plant phenological responses and predict projected changes under climate change (Chuine 2000; Vitasse et al. 2011; Clark et al. 2013; Allen et al. 2014), however, little is known about the responses at the community or landscape level to environmental variation (Pau et al. 2011; Elmore et al. 2012). What are the dominant regional drivers of community phenology? How do differences in species phenology affect community responses spatially and temporally? To answer these questions, long-term phenological observations over large spatial domains are informative. Relating Land Surface Phenology (LSP) derived from remotely sensed imagery over space and time to a suite of environmental factors permits the development of explanatory phenological models (White et al. 1997; Zhou et al. 2003; Kim and Wang 2005; Dunn and de Beurs 2011; Yang et al. 2012). Unlike species-level, ground-based studies, plant phenological responses to chilling and heating requirements are not often considered at the broad spatial scales inherent in LSP that can be used to make broad scale spatio-temporal predictions.

Regional scale variation in community composition, regional climate, soils, and land management result in complex spatiotemporal variation in plant phenology that are difficult to quantify and interpret (Zhang et al. 2003). Moreover, inter-annual phenological variation observed from satellite data may not be easily interpreted using weather data alone (Fisher et al. 2007). Phenological models need to include factors other than simply weather, such as elevation, slope, aspect, and soil moisture, to capture such spatiotemporal variability (Hwang et al. 2011; Dunn and de Beurs 2011). Additionally, since species differ in physiological chilling and heating requirements for breaking dormancy, different species within the same community or landscape may show divergent phenological responses to the same weather conditions (Diez et al. 2012). A study of European leaf phenology of deciduous forests showed earlier bud burst onset

(2 days on median) and leaf spread (2 days on median) of *Acer platanoides* than *Quecus robur* during 1997 and 2005 (Wesolowski and Rowinski 2006). In New Hampshire, USA, sugar maple (*Acer saccharum*) reached each spring development stage 3 days earlier than yellow birch (*Betula alleghaniensis*) and 2 days earlier than American beech (*Fagus grandifolia*) during 1989 and 2002 (Richardson et al. 2006). Therefore, we would expect different phenological responses from communities and landscapes with different species compositions. Combining physiological mechanisms and topographical heterogeneity with community composition may provide a more effective, precise, mechanistic way to explain and predict plant phenological responses across large spatial domains.

Survival analysis is often used in time-to-event statistical models in biological and mechanical systems (Cox and Oakes 1984; Wilson et al. 2010), but is only infrequently used in phenological models (Gienapp et al. 2005; van de Pol and Cockburn 2011; Terres et al. 2013; Allen et al. 2014; Diez et al. 2014). Here we have adapted a Bayesian survival model to explain green-up of deciduous forest landscapes using the MODIS phenology product during 2001–2009 in New England, USA. The objectives of this study are: (1) determine the dominant environmental drivers of green-up date of deciduous forests across a region; (2) assess the spatial and temporal influences of those drivers on phenological change; and (3) forecast future changes in phenology given projected climate change scenarios.

Methods

Study area

A rectangular area (72.6°W–71.8°W, 41.3°N–45°N) in New England, USA, was selected as the study area (Fig. 1). Topographically, this region varies from sea level along the south coast to approximately 1,500 m in the White Mountains of New Hampshire. The natural vegetation is broadleaf deciduous, needle-leaf evergreen, and mixed forests, dominated by oak communities in the south and northern-hardwoods with pockets of spruce-fir communities in the north (Foster and Aber 2004). Overlaying the natural forest is a mosaic of human altered, urban to suburban and agricultural landscapes. Annual mean temperature varies north to south from about 4 to 10 °C; annual precipitation varies across the region from about 1,000 to 1,250 mm (Hijmans et al. 2005).

Data and processing

Estimates of the timing of vegetation phenology at global scale were provided by MODIS Land Cover Dynamics (MCD12Q2) product downloaded from U.S. Geological Survey, Land Processes Distributed Active Archive Center (LP DAAC) (https://lpdaac.usgs.gov). This is the only remote-sensing product that best optimizes temporal and spatial resolution that can be used in modeling landscape-scale phenology (Zhang et al. 2009), although there are some rarely discussed challenges in using and interpreting these data (e.g. estimate errors and spatio-temporal resolutions). We discuss these issues below in more detail and in supplementary materials (Supplementary Materials 3). Version 005 products include four key phenological transition dates (green-up, maturity, senescence, and dormancy) from 2001 to 2010 with a spatial resolution of 500 m (Zhang et al. 2003). We focused on the green-up date of deciduous forests in New England, a metric of beginning of spring.

We extracted MODIS pixels corresponding to deciduous forest from the all of the pixels in the MODIS dataset. To accomplish this, we used 30 m resolution land cover data from the 2001 Coastal Change Analysis Program (C-CAP) dataset at the NOAA Coastal Services Center (http://www.csc.noaa.gov/) because the MODIS land-cover product is too coarse to assess sub-pixel land cover composition. We overlaid the 500 m MODIS grid on the 30 m LULC data and calculated the percentage of deciduous forest cover in each MODIS cell. We retained all MODIS pixels with at least 75 % deciduous forests for the phenological analysis. We removed pixels with estimated green-up dates that occurred before Julian day 60 (March 1st or February 29th) or after Julian day 150 (May 30th or 31th) because these green-up dates are unrealistic for our study biome in the current climate. The outliers accounted for less than 1 % of the selected deciduous forest MODIS data, and are likely due to green-up of sub-pixel patches of agricultural fields in the winter, summer or fall, or the appearance of green grassy areas with snow melt in the winter.

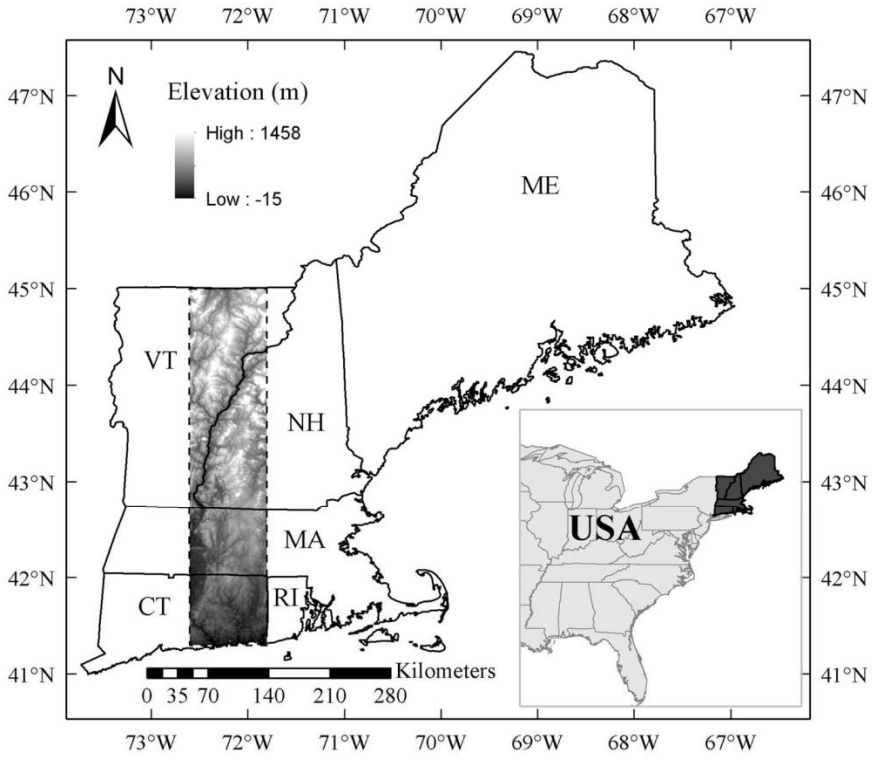

Fig. 1 Study area in northeastern USA covering the Connecticut River Valley from 41.3 to 45°N, 71.8 to 72.6°W and parts of the states of Connecticut (CT), Rhode Island (RI), Massachusetts (MA), New Hampshire (NH) and Vermont (VT). The southern area has lower elevations (*dark*) close to the coast, and the northern area has higher elevations (*light*) with mountains. (Color figure online)

The final phenology data set included about 9,500 500 m grid cells for each year across the study region.

Temperature is typically the most important factor for plant phenology in temperate regions (Walther et al. 2002; Cleland et al. 2007; Bertin 2008). Growing Degree Day (GDD) and Chilling Unit (CU) metrics have been used to quantify plant responses in phenology models (Chuine 2000; Kim and Wang 2005; Kaduk and Los 2011; Yang et al. 2012). GDD is a measure of heat accumulation to predict plant development rate and is calculated as $\mathrm{GDD} = \sum(\mathrm{T}_i - \mathrm{T}_\mathrm{b})$, in which T_i is daily mean temperature and T_b is base temperature. CU is a measure of chilling temperatures and can be used to determine if chilling requirements of buds are fulfilled. Methods of calculating CU have been studied experimentally in fruit and nut trees, using several different CU models (Bennett 1949; Richardson et al. 1974; Shaltout and Unrath 1983).

We used gridded daily average temperature with a spatial resolution of 0.125° (~12 km) from Maurer et al. (2002) covering the period from 2001 to 2009 to calculate daily GDD and CU as explanatory weather factors in our model. In the absence of known GDD or CU base temperatures for the species in our system, we explored the likely range of temperatures using four base temperatures: 4, 5, 6 and 7 °C (Richardson et al. 2006; Fisher et al. 2007). Three standard chilling unit models (Table S1) were used: the Chilling Hours Model (CH) (Luedeling et al. 2009), the Utah Model (UT) (Richardson et al. 1974), and the North Carolina Model (NC) (Shaltout and Unrath 1983). We set the start date for GDD and CU accumulation, assuming simultaneous accumulation of chill and heat, to 1 January each year, a reasonable proxy date for the effective start date of CU accumulation following known gene regulation mechanisms (Jiménez et al. 2010).

We used statistically downscaled and bias corrected daily weather projection data for 2046–2065 for New England from multiple General Circulation Models (GCMs) and Regional Climate Models (RCMs) (Ahmed et al. 2013) to predict future green-up dates. The spatial resolution of data, which follow emission scenario SRES A2, is 0.125°, the same as the weather data used for model fitting. We used an 8-model, 20 year average of daily mean temperature, to create an ensemble prediction dataset with one mean value

for each day across a year. To illustrate the potential range of future values (in addition to the multi-model and multi-year mean), we also explored extreme predictions by selecting the warmest (2057, MIROC model) and coolest (2047, GFDL model) model-years (based on January to May mean temperatures) from the 20-year ensemble projection dataset. Cumulative GDD and CU were calculated from future projection data in the same way as the historical data.

Digital elevation model (DEM) data with a spatial resolution of 90 m from NASA Shuttle Radar Topographic Mission (SRTM) (http://srtm.csi.cgiar.org/) were used to generate our topographic variables. Aspect and slope were calculated through ArcGIS Spatial Analyst Toolset (ESRI ArcMap 9.3, Redlands, California, 2009). The spatial resolution of the outputs was aggregated to 500 m using zonal mean values of DEM data, corresponding to the resolution of the MODIS grid cells. Aspect and slope were transformed into a north-southness index (−1: South with 90° slope, 1: North with 90° slope) and an east-westness index (−1: West with 90° slope, 1: East with 90° slope), following Sherman et al. (2008).

We estimated species composition using inventory data from 1,211 plots surveyed across our region between 2003 and 2010 by the Forest Inventory and Analysis (FIA) Program (http://fia.fs.fed.us/). Specifically, we aggregated 1,211 extant FIA plots into the 206 climate grid cells used in this study yielding 6 plots on average in each grid cell. We quantified the relative biomass of each genus in each plot and then averaged the mean relative biomass for all plots in each climate data grid cell (0.125°). Three dominant (data not shown) genera (*Quercus*, *Acer*, *Betula*) were chosen to represent most of the spatial variation in deciduous forest species biomass composition across our study region (Fig. S3-4).

Statistical modeling

Survival analysis involves modeling time-to-an-event, based on a sequence of observations as to whether or not the event has occurred. It attempts to attribute the probability of an event to one or more explanatory variables. These variables provide insight into the particular circumstances that may increase or decrease the probability of the event. The timing of a phenological event can be analyzed in a survival modeling framework, with observed environmental factors used as explanatory variables (Terres et al. 2013; Allen et al. 2014).

Here we adopt survival model analysis, with "events" defined as green-up dates of forest pixels. The survival function is $S(t) = P(T > t)$, which gives the probability that green-up has not occurred by the end of time step t. T represents the waiting time until the occurrence of the event of interest (i.e., green-up). Although MODIS green-up dates determined from 8 day vegetation index data are continuous, the uncertainty is approximately 8 days (Fig. S3-1). Thus, time steps of green-up are modeled as 8 day intervals when fitting the survival model to incorporate the uncertainty of MODIS green-up dates (Fig. S3-1).

For each 8 day time step, beginning January 1, we model the probability of green-up not occurring by the end of the time step given that green-up has not yet occurred, which is $p_{iyt} = P(T_{iy} > t | T_{iy} > t-1)$, where i indicates grid cell, y indicates year, and t indicates time step. To assess the relationship between environmental factors and green-up probability, a probit link function, probit $(p_{iyt}) = X_{iyt}^{T}\beta$, was used, where X_{iyt}^{T} is a matrix of time varying (GDD and CU) and time invariant (EW, NS, species composition) covariates, and β is a vector of regression coefficients. Standardized coefficients of covariates were estimated using a Bayesian framework (Wilson et al. 2010; Terres et al. 2013; Allen et al. 2014). We used a random sample from normal, uninformative prior distributions for all parameters. The posterior distribution of each coefficient was obtained using a custom mcmc sampler written in R version 2.13 (R Development Core Team 2011). Models were run for three chains and approximately 20,000 iterations for each chain. After a burn in of 2,000 iterations, we thinned the 18,000 samples from the posterior probability distribution by 100 to reduce auto-correlation, resulting in a posterior sample size of 540. The autocorrelation function for each chain was plotted to check autocorrelation, and convergence were assessed visually by plots from three independent chains using functions in the R package "coda" (Plummer et al. 2006). See Supplementary Material File 1 for modeling R code. We used Deviance Information Criterion (DIC), a model comparison metric that indicates how well the model fits the data penalizing for model complexity (Spiegelhalter et al. 2002), to compare

alternative models. DIC can be calculated more readily using MCMC in Bayesian framework, which is analogous to AIC and BIC for model selection using frequentist approaches. By convention, models with smaller DIC are preferred to models with larger DIC and reductions of DIC value by more than 10 units are considered significant and reductions of less than 5 units are considered non-significant.

Three components, weather (GDD and CU), landscape (NS and EW), and species composition (oak, maple and birch), are considered as important factors explaining the date of green-up of deciduous forest in New England. Five combinations of the three components were used in a set of models, the best of which was selected using DIC values (cf. Table 1). After selecting the covariates, 12 candidate models, based on four base temperatures of GDD and three chill unit models, were assessed to select among the most appropriate base temperature and chill unit model for our system (cf. Table 2).

Probability of green-up not occurring in each grid cell at each time step in every year is based on the explanatory variables in the model and the estimated coefficients. The probability of green-up at each time step is calculated as $p(t-1 < T_{iy} \leq t) = [1-S(t)]-[1-S(t-1)] = S(t-1)-S(t)$, resulting in posterior probability distributions over all 8 day time steps in each year for each grid cell. From the mean and 95 %

Table 1 DIC values of five candidate models

No.	Model	DIC	ΔDIC
A	$GDD_5 + CU_{UT}$	387924	19134
B	$GDD_5 + CU_{UT}$ + NS + EW	386107	17317
C	$GDD_5 + CU_{UT}$ + oak + maple + birch	370972	2182
D	NS + EW + oak + maple + birch	618059	249269
E	$GDD_5 + CU_{UT}$ + NS + EW + oak + maple + birch	**368790**	**0**

Best fit model indicated in bold and ΔDIC calculated as the difference from the smallest DIC value. Candidate covariates include growing degree days with base temperature 5 °C (GDD_5), chilling units calculated by Utah model (CU_{UT}), topographic indices north-southness (NS) and east-westness (EW), and the relative biomass of the three genera of deciduous trees (oak, maple, and birch)

Table 2 Model comparison based on DIC values of twelve models with different base temperatures and chilling models

No.	Model			DIC	ΔDIC
	GDD	CU	Other covariates		
1	GDD_4	CU_{CH}	NS + EW + oak + maple + birch	366751	1998
2	GDD_5			365308	555
3	GDD_6			**364753**	**0**
4	GDD_7			364819	66
5	GDD_4	CU_{UT}		370326	5573
6	GDD_5			368790	4037
7	GDD_6			367563	2810
8	GDD_7			367138	2385
9	GDD_4	CU_{NC}		374065	9312
10	GDD_5			373173	8420
11	GDD_6			372275	7522
12	GDD_7			370970	6217

The best fit model is indicated in bold and ΔDIC calculated as the difference from the smallest DIC value. GDD represents growing degree days and the number indicates the base temperature (4, 5, 6, or 7 °C). CU represents chilling units, where CH, UT, and NC indicate three chilling unit models (Chilling Hour model, Utah model, and North Carolina model, respectively). NS and EW indicate two topographic indices, north-southness and east-westness. Three variables, oak, maple, and birch, represent relative biomass of the group of deciduous species

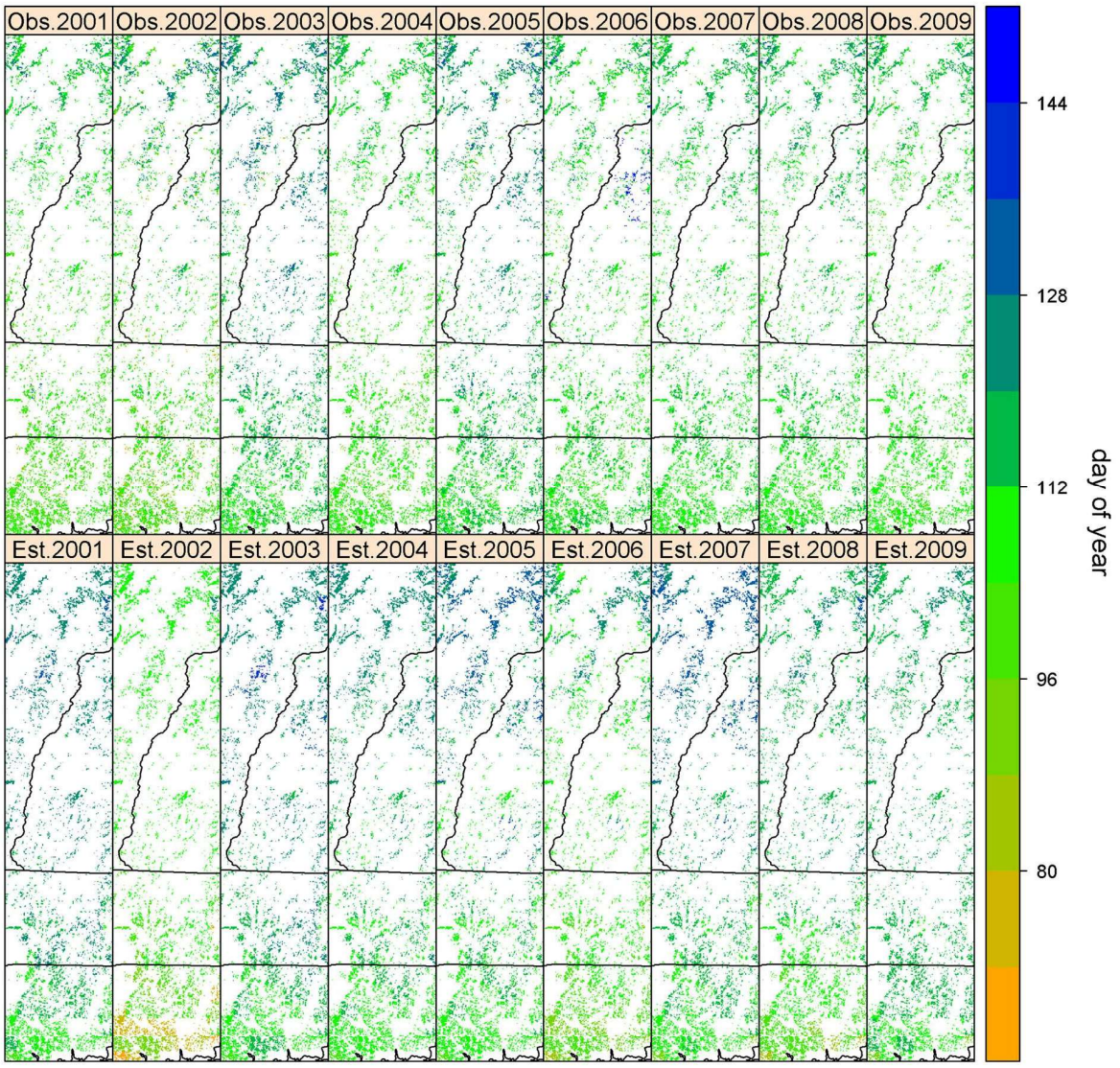

Fig. 2 Green-up dates (as day of year) from MODIS product (*top panels*) and green-up time steps from model estimations (*bottom panels*) for the deciduous forest in study area from 2001 to 2009. For comparisons, green-up dates and time steps are both shown in 8-day intervals by colors. Each color in the color ramp represents one 8 day interval and is labelled as the day of year corresponding to successive time intervals. Small values (*orange pixels*) indicate early green-up dates and large values (*blue pixels*) indicate late green-up dates. *Black lines* are state boundaries (CT at the bottom, MA next, then VT upper left and NH upper right). *White areas* indicate non-deciduous forest area. (Color figure online)

credible interval probability distributions, we computed the 8 day step green-up probability [S(t−1)–S(t)] curve for the mean estimate and its associated uncertainty. We report the time step with the highest probability as the expected time step of green-up (Fig. S2-1). MODIS green-up dates from 2001 to 2009 were used as training data for the model, and green-up dates in 2010 were used for model validation. We calculated residuals between MODIS green-up time steps and model estimation, and root mean square error (RMSE) to assess model predictive performance.

We predicted the future green-up based on projected weather data for the period (2046–2065) including the 20 year model ensemble average and

two extreme projected model years (2057 MIROC and 2047 GFDL). The dynamics of species composition and landscape change over time in New England over the next 30 to 50 years are likely to be relatively modest (see Supplementary Materials 3). Thus no change of species composition of forest and landscape was applied to predictions, and the change of green-up dates is only driven by change of GDD and CU. Mean green-up time steps during 2001 and 2009 were estimated using the best model, as green-up time steps in current weather conditions to compare to predicted future green-up time steps. The differences between prediction in the future period and estimation of current period were calculated to assess how many time steps green-up will change in the future across the study area.

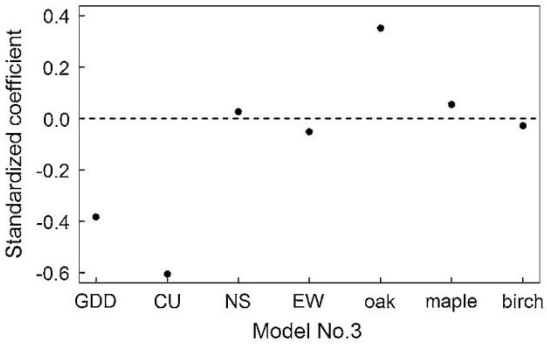

Fig. 3 Standardized coefficients of explanatory variables in our best fit model (model No. 3). GDD represents cumulative Growing Degree Day with base temperature 6 °C, CU represents cumulative Chilling Unit calculated by Chilling Hour model, NS means North-Southness, and EW means East-Westness. Oak, maple and birch represent relative biomass of oaks, maples and birches. The credible interval of each variable is too narrow to show due to large sample size. All coefficients are significant. The *dashed line* shows zero. (Color figure online)

Results

From 2001 to 2009, observed MODIS green-up dates of the deciduous forest region showed obvious landscape-level spatial and temporal variation (Fig. 2 top panels). The forests in southern areas usually became green earlier than the forests in northern areas. In 2003 and 2005, the green-up dates were generally later than other years, and in 2001 and 2002, the dates were earlier than other years (Fig. 2 top panels).

Among five candidate models, the one containing weather, landscape characteristics and species composition had the smallest DIC value (model E, Table 1). To determine the most appropriate GDD base temperature and CU formulation, we used models that included weather, landscape topography, and species composition in 12 candidate models (Table 2). The best of the 12 candidate models had GDD with 6 °C as the base temperature and CU calculated from the Chilling Hours model (model No. 3, Table 2).

The standardized coefficients of all variables in the best model (model No. 3, Table 2) were significantly different from zero (Fig. 3). Positive coefficients mean green-up date will be earlier, while negative coefficients mean a delayed green-up date, with increased variable values. Overall, CU had the greatest effect on green-up, and the standardized coefficient (with 95 % credible interval) was −0.604 (−0.607, −0.599). GDD, −0.382 (−0.387, −0.380) had the second greatest effect on green-up, and the third most influential covariate was relative biomass of oaks, 0.353 (0.347, 0.359). The best fit model indicated that higher GDD and CU lead to earlier green-up date. Based on standardized coefficients for topographic variables (NS: 0.027 (0.020, 0.031), EW: −0.051 (−0.054, −0.048)), green-up dates of deciduous forest for southern and eastern aspects would be earlier than the forests at northern or western aspect; higher slope amplifies this pattern (Fig. 3). In terms of species composition, the coefficients (with 95 % credible interval) of maple, and birch, were 0.056 (0.051, 0.060), and −0.028 (−0.035, −0.024) respectively (Fig. 3). We therefore expect forests with more oaks will have later green-up dates, and that greater birch dominance will lead to earlier green-up dates. The positive effect of maple dominance is similar to oaks but the magnitude of the effect was much smaller.

We used the best fit model, model No. 3, to estimate green-up time steps of all grid cells from 2001 to 2009. As expected, the northern region had later green-up dates and southern region had early green-up across years (Fig. 2 bottom panels). We observed considerable year to year variation in the predicted green-up time steps as well as spatial variation (Fig. 2 bottom panels). Most points in the predicted versus observed green-up plot correspond to a 1:1 line, indicating a good fit of the model, given the minimum 8 day temporal resolution of the MODIS product data (Fig. S3-2). The Pearson correlation coefficient between MODIS green-up dates from 2001 to 2009 and model

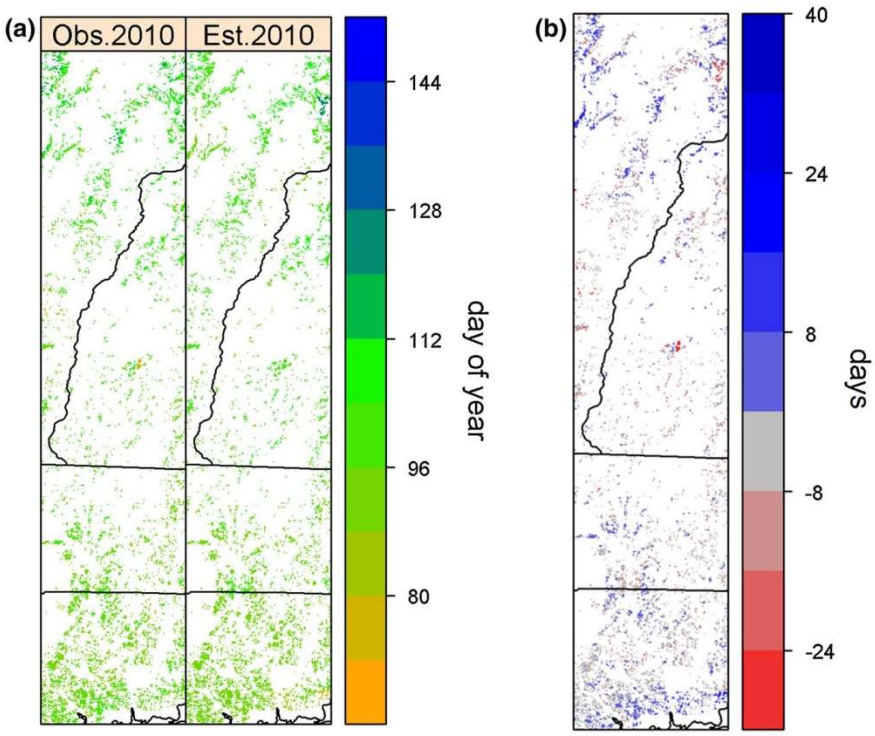

Fig. 4 **a** Observed MODIS and model estimated green-up dates in 2010. The unit is converted from 8 day time steps to day of year. **b** Residual between MODIS green-up time steps and estimated green-up time steps in 2010. The unit is converted from 8 day time steps to days. *Positive values* indicate early estimation and *negative values* indicate late estimation. In both plots, *black lines* are state boundaries and *white areas* indicate non-deciduous forest areas. (Color figure online)

estimation was 0.361, $p < 0.001$ (Fig. S3-2). Residuals between observed green-up time steps (MODIS) and estimated time steps vary among years. Generally, 50 % residuals fall in the range of -2 and $+1$ time step (-16 to $+8$ days). The RMSE of residuals is 1.5 time steps (12 days) indicating how close the observed green-up dates are to the model's predicted values, given the temporal resolution of the data; recall that our minimum temporal resolution for the MODIS phenology product is 8 days. The map of time step residuals shows more earlier estimations in 2002 and 2006, and in southern area in 2008, and more later estimations in 2001, 2004 and 2007 (Fig. S2-2).

We also used the best fit model to validate green-up dates of deciduous forest in 2010. Comparison between MODIS green-up time steps and estimated time steps shows similar pattern of green-up across the area (Fig. 4a), and 91 % of residuals are in the range of -1 to $+1$ time step (-8 to $+8$ days) (Fig. 4b). The predicted versus observed plot shows that most points fall near the 1:1 line (Fig. S3-3). The Pearson correlation coefficient between MODIS green-up dates in 2010 and model estimation is 0.419, $p < 0.001$ (Fig. S3-3). The RMSE of residuals for the validation, as a measure of model fit, is 1.0 time step (8 days). All metrics suggest that the predictive accuracy of the model is near the temporal resolution of the data (8 days). As the uncertainty of MODIS green-up dates is about 8 days (Fig S3-1), this predictive accuracy suggests a good fit for model predictions.

Compared to model estimated mean green-up dates under current weather conditions (2001–2009), earlier green-up dates are predicted by mid-21st century (2046–2065) including two extreme model years (Fig. 5). Overall, 96 % of grid cells in the study area are projected to have earlier green-up dates for the future period (2046–2065). How many days earlier green-up occurs in the future will depend on the specific weather condition in each year. For example, green-up dates were shifted 45 days earlier on average across grid cells in the warmest model year (model year 2057), compared to 2001–2009, and in the coolest model year (model year 2047) green-up dates shifted 12 days earlier on average (Fig. 5). The green-up dates and the change in the future showed considerable spatial variation (Fig. 6). Given the projected climate ensemble average for the 2046–2065 period, the northern and central area are predicted to have a small advancement (about 1 time step earlier, i.e. 8 days) in

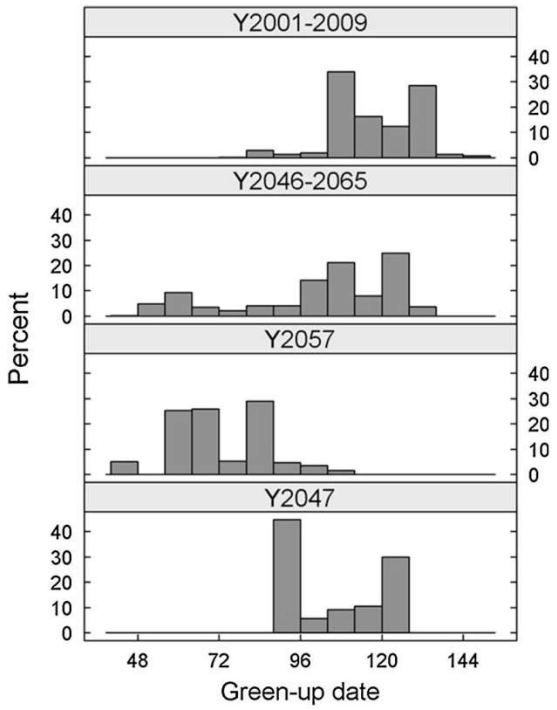

Fig. 5 Histograms of model estimated green-up dates for two periods, current (2001–2009) and future (2046–2065), and for two extreme years, the warmest model year 2057 (MIROC) and the coolest model year 2047 (GFDL). The unit is converted from 8 day time steps to day of year

green-up, while the most southern coastal areas predicted to have a much greater shift of up to 6 time steps (i.e. 48 days) earlier in the spring (Fig. 6b). In the coolest model year (2047), the southern coastal areas actually show a significantly delayed green-up date (8–16 days), while inland areas indicate advanced green-up of (0–24 days) (Fig. 6b). We assessed the effect of parameter uncertainty on our green-up predictions by creating predictions using the upper and lower 95 % credible interval bounds. Under future ensemble climate, we found ± 8 days of uncertainty due to parameter uncertainty (Fig. S3-5). These uncertainties are small relative to the temporal scale of the data and we therefore use the mean predicted green-up dates for most comparisons. We also did predictions using upper and lower bonds of 95 % quartile variation of GDD and CU from 20 year and 8-climate-model data. Results suggested spatial variation of uncertainty from GDD and CU caused spatial variation of green-up dates predictions. The uncertainty of 95 % of predicted green-up dates from climate projection is no more than ± 8 days in central and northern areas, but the uncertainty in the coastal areas ± 24 days.

Discussion

Our study shows that weather variables of chilling and heating, along with topographic heterogeneity, and species composition all contribute to explaining the spatial and temporal variation in LSP. We found warmer spring temperatures contributed significantly to advanced forest green-up, similar to other studies (Cleland et al. 2007; Ibanez et al. 2010; Kaduk and Los 2011; Yang et al. 2012; Clark et al. 2013). However, the contribution of chilling temperatures may be more important, as indicated by the larger effect of CU relative to GDD on green-up in our model. This reflects what others have shown for woody plants, delving experimentally into environmental and gene regulation control of breaking bud dormancy in *Populus* (Rinne et al. 2011). While topographic conditions, such as elevation, slope and aspect have been the most commonly used non-climate variables for characterizing broad spatial variation in phenology (Dunn and de Beurs 2011; Hwang et al. 2011), our study shows that community composition had a greater influence on observed phenology. In fact, the effect of species composition was as great as that of GDD. Despite our findings, the effect of variation in species composition as it influences broad spatial patterns in landscape phenology remains little explored (Isaacson et al. 2012).

The contribution of species composition to LSP responses reflects variation in the physiological requirements of species in response to climate and weather (e.g., Jeong et al. 2013; Clark et al. 2013; Allen et al. 2014). Differences in vessel construction may explain physiologically why oaks (ring porous species) typically leaf out later than maples and birches (diffuse porous species) (Polgar and Primack 2011). The positive coefficients for maples may reflect differences in the phenology of understory species or co-occurring canopy species in maple dominated stands. Understory composition does in fact vary among areas with different dominant canopy tree species (Metzler and Barrett 2006) and mixed species reflectance signals in the MODIS data may yield a different estimated green-up date than dominant

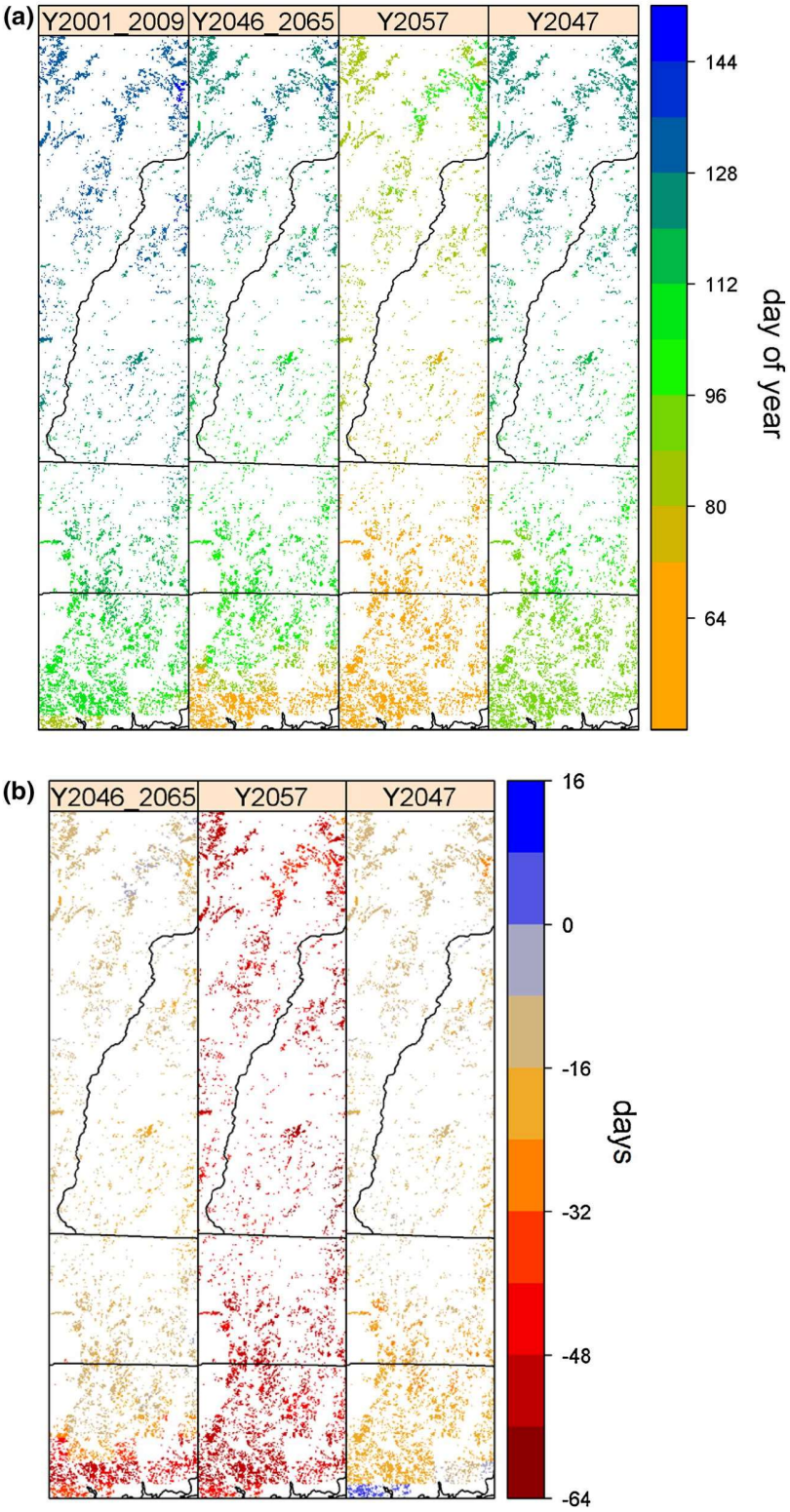

Fig. 6 Estimation of mean green-up dates for the current period (2001–2009), prediction of mean green-up dates for the future period (2046–2065), and prediction in 2057 (MIROC) and 2047 (GFDL), and the change between current and future periods. **a** shows model predications of green-up dates for two periods and two extreme years. Each color in the color ramp represents one 8 day interval and is labelled as the day of year corresponding to successive time intervals. **b** shows change between two periods (2001–2009 – 2046–2065), and between current and future extreme years. The unit is day indicating the difference of green-up dates between two periods. Each color in the color ramp represents one 8 day difference. Negative values (*warm color*) indicate earlier green-up in the future relative to the current period, and positive values (*cold color*) indicate delayed green-up in the future. In both plots, black lines are state boundaries and white areas indicate non-deciduous forest areas. (Color figure online)

canopy species alone. Unmeasured site conditions associated with the prevalence of maples may have similar effects. For example, delayed leaf out is known to occur in red maple swamps relative to upland red maple stands (Mathews and Dwyer 1990). These other site-level effects merit further investigation as they likely contribute to unexplained spatial variation in phenology.

Given the future projected climate data, we predicted that green-up dates of deciduous forests in northern and central areas will be considerably advanced on average by mid-21st century given higher GDD and CU. In northern and central areas higher winter and spring temperatures cause greater accumulations of not only GDD but also CU (Fig. S2-3). This is because most positive accumulation of CU occurs between 1 and 7 °C (Table S1) (Guy 2014) and climate warming is projected to induce more days with mild temperatures (i.e., between 1 and 7 °C) in late winter and early spring relative to historical conditions. Therefore, based on the mechanism of woody plants dormancy, we expect that greater CU accumulation will lead to earlier dormancy release of deciduous forests, and greater GDD accumulation will lead to earlier bud break and leaf development, and hence earlier green-up of our deciduous forests.

However, the situation is a bit different in the southern-most areas of our region (<41.5°N). The extreme cold and warm years from the ensemble of climate projections for this region both show CU accumulation in the winter and spring to be lower than current years (Fig. S2-3); there are simply fewer days projected with temperatures between 1 and 7 °C for optimal CU accumulation. Although both years are projected to have higher GDD accumulation (Fig. S2-3), the effect of GDD is not adequate to compensate for unfulfilled chilling requirement, especially in the coldest model year 2047 (GFDL), but there is also more uncertainty in the predictions for this region. More heating would be required to overcome lack of chilling (Kaduk and Los 2011; Rinne et al. 2011), thus the predicted green-up of deciduous forest is delayed in 2047 (GFDL). Of course, these years only represent possible scenario years in the future rather than what might actually occur in specific years, but it is noteworthy that delayed green-up has been reported in some warm temperate to subtropical regions, and on the Tibetan Plateau (Sunley et al. 2006; Baldocchi and Wong 2008; Yu et al. 2010; Pope et al. 2013). Our study suggests how green-up date changes in the future may depend not only on projected average changes in CUs and GDDs in the future, but how these may vary temporally and spatially across the region with differential effects on landscape phenology.

Model predictions on green-up dates include several sources of uncertainties, such as data uncertainty, model uncertainty and climate projection uncertainty: (1) The temporal resolution of the 8 day, of MODIS phenology product results in added temporal uncertainty for event timing (cf. Fig. S3-1), which yields added temporal error for the model predictions (Zhang et al. 2009). (2) Setting thresholds (75 %) for deciduous forest cover may have introduced additional noise in our data. The remaining 25 % land cover (e.g., grassy areas, agricultural fields, etc.) may affect landscape phenology as detected by MODIS. (3) Model uncertainty of predictions is ± 8 days (Fig. S3-5). (4) There is a spatial variation of uncertainty from climate projection for green-up date predictions, which is no more than ± 8 days in central and northern areas, while the uncertainty in the coastal areas is ± 24 days. Additionally, long term changes in species composition (e.g. species demographic changes, species migration and landscape change) will also contribute to uncertainty in landscape phenology over longer time scales (i.e. century time scales) (see further detail in Supplementary Materials 3). Finally we acknowledge that the time interval of this study (10 years) is relatively short to fully evaluate the MODIS phenology product and the model predictions, despite the large sample size for the data (95,000 pixels) and the fact that spatially and temporally the data span a broad range of weather and climate conditions. The models and predictions developed here merit further testing and evaluation as additional data become available.

Our results suggest that the Chilling Hour model provides a much better fit to the data than the North Carolina or Utah models, but we have no explicit mechanistic bases to explain the difference. Our results also suggest that the optimal GDD base temperature is 6 °C. This is higher than the base temperature (5 °C) suggested for some mechanistic models (e.g., Chuine 2000), but is close to the base temperature of Heating Degree Days used by Fisher et al. (2007), (i.e., 5.8 °C for forests in New England). In our study, we used parallel CU-GDD models, which means forcing temperatures were accumulated simultaneously with

chilling temperatures. The sequential model and alternating (partial parallel) models were not used, because we had no information as to when chilling requirements are fulfilled or when GDD forcing temperatures start to be effective for our system. Empirical evidence as to when chilling requirements are met for specific species could be used for calibrating and evaluating the sequential model (e.g., Alburquerque et al. 2008; Allen et al. 2014, Clark et al. 2013), but we lack species-specific phenological response information of all dominant tree species for the deciduous forest communities in this study. Experimental studies (e.g. Caffarra et al. 2011; Caffarra and Donnelly 2011; Fu et al. 2012; Polgar et al. 2013) are now providing some insight into the phenology mechanisms that ultimately will allow for species-specific phenological modeling at the landscape level (see more detail in Supplementary Material 3). We suggest that physiological experiments are needed on a larger range of species and sites to provide for greater understanding of chilling and heating requirements that lead to the breaking of winter dormancy and thus improved phenological models.

Earlier forest green-up across the New England landscape was predicted as a consequence of climate warming, which may lead to substantial economic and ecological impacts. The advancement up to 48 days may induce much more serious damage on maple syrup industry than what happened in New England in 2012 (Keough 2012). Although fewer frost days are predicted in spring during the future period (2046–2065) than the current years (2001–2009) in study area, the risk of frost damage to trees will still exist since frost days are predicted to occur well after projected bud-burst and leaf-out (1–10 frost days after green-up in 2057 and 2047 model years in this study), which may lead to the deleterious consequence of killing new leaf tissue if the weather follows current patterns of frost damage (Augspurger 2013). Developing better phenology models and predicting future phenological responses are necessary to help assess potentially deleterious impacts of climate change.

Survival analysis provides a mechanistic, physiologically-based statistical model that incorporates more of the underlying mechanisms (cf. Paul et al. 2014) of spatiotemporal responses of LSP to environmental change. Our approach can be applied to a variety of different ecological systems using analogous explanatory covariates, or to different temporal and spatial scales. For example, survival models have been used in some recent studies on cherry flowering phenology (Terres et al. 2013; Allen et al. 2014), modeling wildfire probabilities (Wilson et al. 2010), and bird phenology (Gienapp et al. 2005; van de Pol and Cockburn 2011). However, the application of a survival modeling framework is novel in LSP and may provide future opportunities for scaling up ground observations to the landscape scale. Relating observational datasets at multiple spatial scales using hierarchical models (Wilson et al. 2011) and building bridges between ground observations and satellite images using digital cameras (Richardson et al. 2009; Bater et al. 2011; Ide and Oguma 2013) are possible extensions of our approach. Methods to integrate across spatial and temporal scales facilitate our understanding of phenological responses to climate change and will aid economic and ecological impact assessments of future change.

Acknowledgments This study was supported in part by an US National Science Foundation grant (DEB 0842465) to J.A.S. and by NASA headquarters under the NASA Earth and Space Science Fellowship Program Grant NNX09AN82H to AMW. We thank R. B. Primack for helpful comments and X. Wang and A. E. Gelfand for statistical advice.

References

Ahmed KF, Wang G, Silander JA, Wilson AM, Allen JM, Horton R, Anyah R (2013) Statistical downscaling and bias correction of climate model outputs for climate change impact assessment in the US Northeast. Glob Planet Change 100:320–332

Alburquerque N, García-Montiel F, Carrillo A, Burgos L (2008) Chilling and heat requirements of sweet cherry cultivars and the relationship between altitude and the probability of satisfying the chill requirements. Environ Exp Bot 64:162–170

Allen JM, Terres MA, Katsuki T, Iwamoto K, Kobori H, Higuchi H, Primack RB, Wilson AM, Gelfand A, Silander JA (2014) Modeling daily flowering probabilities: expected impact of climate change on Japanese cherry phenology. Glob Change Biol 20:1251–2063

Augspurger CK (2013) Reconstructing patterns of temperature, phenology, and frost damage over 124 years. Ecology 94:41–50

Baldocchi D, Wong S (2008) Accumulated winter chill is decreasing in the fruit growing regions of California. Clim Change 87:153–166

Bater CW, Coops NC, Wulder MA, Hilker T, Nielsen SE, McDermid G, Stenhouse GB (2011) Using digital time-lapse cameras to monitor species-specific understory and

overstory phenology in support of wildlife habitat assessment. Environ Monit Assess 180:1–13
Bennett JP (1949) Temperature and bud rest period. Calif Agric 3:9–12
Berg MP, Kiers ET, Driessen G, Heijden MVD, Kool BW, Kuenen F, Liefting M, Verhoef HA, Ellers J (2010) Adapt or disperse: understanding species persistence in a changing world. Glob Change Biol 16:587–598
Bertin R (2008) Plant phenology and distribution in relation to recent climate change. J Torrey Bot Soc 135:126–146
Caffarra A, Donnelly A (2011) The ecological significance of phenology in four different tree species: effects of light and temperature on bud burst. Int J Biometeorol 55:711–721
Caffarra A, Donnelly A, Chuine I, Jones MB (2011) Modeling the timing of Betula pubescens bud burst. I. Temperature and photoperiod: a conceptual model. Clim Res 46:147–157
Cannell MGR, Smith RI (1983) Thermal time, chill days and prediction of budburst in Picea Sitchensis. J Appl Ecol 20:951–963
Chuine I (2000) A unified model for budburst of trees. J Theor Biol 207:337–347
Clark JS, Melillo J, Mohan J, Salk C (2013) The seasonal timing of warming that controls onset of growing season. Glob Change Biol (in press). doi: 10.1111/gcb.12420
Cleland EE, Chuine I, Menzel A, Mooney HA, Schwartz MD (2007) Shifting plant phenology in response to global change. Trends Ecol Evol 22:358–365
Cox DR, Oakes D (1984) Analysis of survival data. CRC Press, New York
Diez MJ, Ibanes I, Miller-Rushing AJ, Mazer SJ, Crimmins MA, Bertelsen CD, Inouye DW (2012) Forecasting phenology: from species variability to community patterns. Ecol Lett 15:545–553
Diez JM, Ibáñez I, Silander J, Primack RB, Higuchi H, Kobori H, Sen A, James TY (2014) Beyond seasonal climate: statistical estimation of phenological responses to weather. Ecol Appl (In press)
Dunn AH, de Beurs KM (2011) Land surface phenology of North American mountain environments using moderate resolution imaging spectroradiometer data. Remote Sens Environ 115:1220–1233
Elmore AJ, Guinn SM, Minsley BJ, Richardson AD (2012) Landscape controls on the timing of spring, autumn, and growing season length in mid-Atlantic forests. Glob Change Biol 18:656–674
Fisher J, Richardson A, Mustard JF (2007) Phenology model from surface meteorology does not capture satellite-based greenup estimations. Glob Change Biol 13:707–721
Foster DR, Aber JD (2004) Forests in time: the environmental consequences of 1,000 years of change in New England. Yale University Press, New Heaven and London
Fu YH, Campioli M, Deckmyn G, Janssens JA (2012) The impact of winter and spring temperatures on temperate tree budburst dates: results from an experimental climate manipulation. PLoS ONE 7(10):e47324. doi:10.1371/journal.pone.0047324
Gienapp P, Hemerik L, Visser ME (2005) A new statistical tool to predict phenology under climate change scenarios. Glob Change Biol 11:600–606
Guy R (2014) The early bud gets to warm. New Phytol 202:7–9
Heide OM (1993) Dormancy release in beech Buds (Fagus sylvatica) requires both chilling and long days. Physiol Plant 89:187–191
Hijmans RJ, Cameron SE, Parra JL, Jones PG, Jarvis A (2005) Very high resolution interpolated climate surfaces for global land areas. Int J Climatol 25:1965–1978
Hwang T, Song C, Vose JM, Band LE (2011) Topography-mediated controls on local vegetation phenology estimated from MODIS vegetation index. Landscape Ecol 26:541–556
Ibanez I, Primack RB, Miller-Rushing AJ, Ellwood E, Higuchi H, Lee SD, Kobori H, Silander JA (2010) Forecasting phenology under global warming. Philos T Roy Soc B 365:3247–3260
Ide R, Oguma H (2013) A cost-effective monitoring method using digital time-lapse cameras for detecting temporal and spatial variations of snowmelt and vegetation phenology in alpine ecosystems. Ecol Inform 16:25–34
Isaacson BN, Serbin SP, Townsend PA (2012) Detection of relative differences in phenology of forest species using Landsat and MODIS. Landscape Ecol 27:529–543
Jeong S-J, Medvigy D, Shevliakova E, Brown ME (2013) Predicting changes in temperate forest budburst using continental-scale observations and models. Geophys Res Lett 40:1–6
Jiménez S, Reighard GL, Bielenberg DG (2010) Gene expression of DAM5 and DAM6 is suppressed by chilling temperatures and inversely correlated with bud break rate. Plant Mol Biol 73:157–167
Kaduk JD, Los SO (2011) Predicting the time of greenup in temperate and boreal biomes. Clim Change 107:277–304
Keough GR (2012) Maple Syrup 2012. USDA, National Agricultural Statistics Service, New England Field Office, Concord, pp 1–8
Kim Y, Wang G (2005) Modeling seasonal vegetation variation and its validation against moderate resolution imaging spectroradiometer (MODIS) observations over North America. J Geophys Res 110:D04106. doi:10.1029/2004JD005436
Li Z, Reighard GL, Abbott AG, Bielenberg DG (2009) Dormancy associated MADS genes from the EVG locus of peach [*Prunus persica* (*L.*) *Batsch*] have distinct seasonal and photoperiodic expression patterns. J Exp Bot 60:3521–3530
Luedeling E, Zhang M, Luedeling V, Girveta EH (2009) Sensitivity of winter chill models for fruit and nut trees to climatic changes expected in California's Central Valley. Agr Ecosyst Environ 133:23–31
Mathews NS, Dwyer KW (1990) Floodplain vegetation phenology in southeastern USA: optimizing the timing of aerial imagery acquisition. Wetl Ecol Manag 1:65–72
Maurer EP, Wood AW, Adam JC, Lettenmaier DP, Nijssen B (2002) A long-term hydrologically-based data set of land surface fluxes and states for the conterminous United States. J Climate 15:3237–3251
Metzler KJ, Barrett JP (2006) The vegetation of Connecticut: a preliminary classification. State geological and natural history survey of Connecticut. Hartford, CT, pp 29–30
Pau S, Wolkovich EM, Cook BI, Davies TJ, Kraft NJB, Blomgren K, Betancourt JL, Cleland EE (2011) Predicting phenology by integrating ecology, evolution and climate science. Glob Change Biol 17:3633–3643

Paul LK, Rinne PLH, van der Schoot C (2014) Shoot meristems of deciduous woody perennials: self-organization and morphogenetic transitions. Curr Opin Plant Biol 17:86–95

Plummer M, Best N, Cowles K, Vines K (2006) CODA: convergence diagnosis and output analysis for MCMC. R News 6:7–11

Polgar AC, Primack BR (2011) Leaf-out phenology of temperate woody plants: from trees to ecosystems. New Phytol 191:926–941

Polgar AC, Gallinat A, Primack BR (2013) Drivers of leaf-out phenology and their implications for species invasions: insights from Thoreau's Concord. New Phytol 202:106–115

Pope KS, Dose V, Da Silva D, Brown PH, Leslie CA, Dejong TM (2013) Detecting nonlinear response of spring phenology to climate change by Bayesian analysis. Glob Change Biol 19:1518–1525

R Core Team (2011) R: a language and environment for statistical computing. R Foundation for Statistical Computing, Vienna, Austria. http://www.R-project.org/

Richardson EA, Seeley SD, Walker DR (1974) A model for estimating completion of rest for 'Redhaven' and 'Elberta' peach trees. HortScience 9:331–332

Richardson AD, Bailey AS, Denny EG, Martin CW, O'Keefe J (2006) Phenology of a northern hardwood forest canopy. Glob Change Biol 12:1174–1188

Richardson AD, Braswell BH, Hollinger DY, Jenkins JP, Ollinger SV (2009) Near-surface remote sensing of spatial and temporal variation in canopy phenology. Ecol Appl 19:1417–1428

Rinne PLH, Welling A, Vahala J, Ripel L, Ruonala R, Kangasjarvi J, van der Schoot C (2011) Chilling of dormant buds hyperinduces Flowering Locus T and recruits GA-inducible 1,3-b-Glucanases to reopen signal conduits and release dormancy in *Populus*. Plant Cell 23:130–146

Sarvas R (1974) Investigation on the annul cycle of development of forest trees. II. Autumn dormancy and winter dormancy. Commun Inst For Fenn 76:1–110

Shaltout AD, Unrath CR (1983) Rest completion prediction model for 'Starkrimson Delicious' apples. J Am Soc Hortic Sci 108:957–961

Sherman R, Mullen R, Haomin L, Zhendong F, Yi W (2008) Spatial patterns of plant diversity and communities in alpine ecosystems of the Hengduan Mountains, northwest Yunnan, China. J Plant Ecol 1:117–136

Spiegelhalter DJ, Best NG, Carlin BP, van der Linde A (2002) Bayesian measures of model complexity and fit (with discussion). J R Stat Soc B 64:583–640

Sunley RJ, Atkinson CJ, Jones HG (2006) Chill unit models and recent changes in the occurrence of winter chill and Spring frost in the United Kingdom. J Hortic Sci Biotech 81:949–958

Terres MA, Gelfand AE, Allen JM, Silander JA (2013) Analyzing first flowering event data using survival models with space and time-varying covariates. Environmetrics 24:317–331

Van de Pol M, Cockburn A (2011) Identifying the critical climatic time window that affects trait expression. Am Nat 177:698–707

Vitasse Y, Francios C, Delpierre N, Dufrene E, Kremer A, Chuine I, Delzon S (2011) Assessing the effects of climate change on the phenology of European temperate trees. Agr Forest Meteorol 151:969–980

Vittoz P, Cherix D, Gonseth Y, Lubini V, Maggini R, Zbinden N, Zumbach S (2013) Climate change impacts on biodiversity in Switzerland: a review. J Nat Conserv 21:154–162

Walther G, Post E, Convey P, Menzel A, Parmesan C, Beebee TJC, Fromentin J, Hoegh-Guldberg O, Bairlein F (2002) Ecological responses to recent climate change. Nature 416:389–395

Wesolowski T, Rowinski P (2006) Timing of budburst and tree-leaf development in a multispecies temperate forest. For Ecol Manag 237:387–393

White MA, Thornton PE, Running SW (1997) A continental phenology model for monitoring vegetation responses to interannual climatic variability. Glob Biogeochem Cycles 11:217–234

Wilson AM, Latimer AM, Silander JA, Gelfand AE, de Klerk H (2010) A hierarchical bayesian model of wildfire in a mediterranean biodiversity hotspot: implications of weather variability and global circulation. Ecol Model 221:106–112

Wilson AM, Silander JA, Gelfand AE, Glenn JH (2011) Scaling up: linking field data and remote sensing with a hierarchical model. Int J Geogr Inf Sci 25:509–521

Yang X, Mustard JF, Tang J, Xu H (2012) Regional-scale phenology modeling based on meteorological records and remote sensing observations. J Geophys Res 117:G03029. doi:10.1029/2012JG001977

Yu H, Luedeling E, Xu J (2010) Winter and spring warming result in delayed spring phenology on the Tibetan Plateau. Proc Natl Acad Sci 107:22151–22156

Zhang X, Friedl MA, Schaaf CB, Strahler AH, Hodges JCF, Gao F, Reed BC, Huete A (2003) Monitoring vegetation phenology using MODIS. Remote Sens Environ 84:471–475

Zhang X, Friedl MA, Schaaf CB (2009) Sensitivity of vegetation phenology detection to the temporal resolution of satellite data. Int J Remote Sens 30:2061–2074

Zhou L, Kaufmann RK, Tian Y, Myneni RB, Tucker CJ (2003) Relation between interannual variations in satellite measures of northern forest greenness and climate between 1982 and 1999. J Geophys Res 108(D1):4004. doi:10.1029/2002JD002510

Appendix 1.1

```
##############################################################################

## Time-to-event model R code for green-up phenology of deciduous forest in the paper:

## Title: Green-up of deciduous forest communities of northeastern North America in response to climate variation and climate change.

## Authors: Yingying Xie, Kazi F. Ahmed, Jenica M. Allen, Adam M. Wilson, John A. Silander. Jr.

## These codes are running in R version 2.13


##############################################################################

#######                  Model Functions                  ########

##############################################################################


#### Functions to calculate likelihood and posterior probability values

CalcLogLik <- function(Y, X,Beta,GUrows) {

   logp = pnorm(ifelse(Y == 1, -1, 1) * ((X%*%Beta) ), log.p = TRUE)

   logp[GUrows+1] = 0  # set likelihood contribution to 0 (i.e p=1) for the seasons immediately following fires

   loglik = sum(logp)

   return(loglik)

}


CalcPostNonspatial <- function(Y, X, Beta,GUrows){

   loglik = CalcLogLik(Y, X, Beta,GUrows)

   logpost = loglik + sum(

      ##Priors

      sum(dnorm(Beta, 0, 1000,log=T))

   )

   return(logpost)

}
```

```
#### Generic MCMC functions

metrop.norm <- function(x0, propsd, f, params, this.par) {
   # x0 = current value of parameter to be sampled
   # propsd = proposal standard deviation
   # f = function with value proportional to posterior probability function
   # params = list of current values of all parameters supplied to f()
   # this.par = name tag for parameter to be sampled among names(params)
   this.par = match.arg(this.par, names(params))
   pos = match(this.par, names(params)) # get position of current parameter in argument list
   K = length(x0)
   postcurrent = do.call(f, params)
   paramsnew = params
   #print(K)
   #print(x0)
   #print(propsd)
   propx = rnorm(K, x0, propsd)
   paramsnew[[pos]] = propx
   postnew = do.call(f, paramsnew)
   a = min(1, exp(postnew-postcurrent))
   #print(a)
   if (runif(1) < a) { # test for acceptance
      return(propx)
   }
   return(x0)
}

################################################################################
###############  New England Green-up Phenology Survivial Model  ################
```

```
library(MCMCpack)
library(coda)
library(MASS)
library(Hmisc)

#############################################################################################
########                    read data                    ######
#############################################################################################
## load full dataset, truncated to observed phenology dates for each individual for each year, standardized covariates
load("Data.Rdata") ##load your dataset
ls()
head(data_std)    #look at it
summary(data_std)  #check it-- make sure there are no NAs in covariate or response data
data=data_std
head(data)
dim(data)

## data set up
summary(data)
head(data)
dim(data)

N = length(data$greenup) ##total number of time steps for dataset
greenup = data$greenup   ## creates vector of 0/1 events for dataset
select=c("cumuGDD6_std","cumuCH_std","ns_std","ew_std","oak_std","maple_std","birch_std") ##specify names of covariates from dataset that will go into model
datamatrix = as.matrix(cbind(intercept=1,subset(data,select=select)))  # create design matrix for current model from dataset
nBeta=ncol(datamatrix)   # number of regression parameters to be estimated (same as number of columns in design matrix)
```

```
GUrows = grep(1, data$greenup) ## create index for pheno events-- returns a list of row numbers with greenup==1


###############################################################################
######                    MCMC runs                    #######
###############################################################################
iterations=20000    ##set total number of iterations per chain.
# Initial Values
 beta={}
 log={}


##### CHAIN 1
setup <- function(iterations){
   ## Data Structures (editing not needed)
   nBeta <<- ncol(datamatrix)
   ## Intital values
   beta.init=function() rnorm(nBeta,0,0.5) #initial values for beta, probably don't need to edit unless you have informative priors
      propsd_Beta <<- c(0.05,0.005,0.005,0.005,0.005,0.005,0.005,0.005)    ##must be same number as betas; these are step sizes, so may need to tune these


# Data Structure (editing not needed)
   beta <<- matrix(ncol=nBeta,nrow=iterations[length(iterations)]+1) ; beta[1,] <<- beta.init()
      PLF <<- matrix(ncol=2,nrow=iterations[length(iterations)]+1);colnames(PLF)=c("Gm","Pm");PLF[1,]=c(0,0)
   Dbar <<- vector(length=iterations[length(iterations)]+1); Dbar[1]=0
   sigma.beta <<- vector(length=iterations[length(iterations)]+1); sigma.beta[1]=0.1
}


setup(iterations)
```

```
## MCMC Loop-- this runs the model

## note: if error is generated during first run (usually related to runif line in metrop.norm): check that the number of proposed betas matches the number of covariates + intercept

system.time(  for(i in 1:iterations) {

  params.nonspatial = list(Y=greenup,X=datamatrix,Beta=beta[i,], GUrows=GUrows) #For CalcPostNonspatial

  beta[i+1,] <- metrop.norm(beta[i,], propsd_Beta, CalcPostNonspatial, params.nonspatial, "Beta")

          Dbar[i] <- -2*CalcLogLik(Y=greenup, X=datamatrix, Beta=beta[i,], GUrows=GUrows)

        print(i)   ## will print the iteration number, so you can see how far the model has progressed

   }  )  ##this will report out total processing time, so you can run some tests on a small number of iterations to estimate per iteration computation time


### CHAIN 2  (same as CHAIN 1, so anything you edited there should be edited here)

setup <- function(iterations){

   ## Data Structures

   nBeta <<- ncol(datamatrix)

   ## Intital values

   beta.init=function() rnorm(nBeta,0,0.5)

      propsd_Beta <<- c(0.05,0.005,0.005,0.005,0.005,0.005,0.005,0.005)


### Data Structure

   beta1 <<- matrix(ncol=nBeta,nrow=iterations[length(iterations)]+1) ; beta1[1,] <<- beta.init()

      PLF1 <<- matrix(ncol=2,nrow=iterations[length(iterations)]+1);colnames(PLF1)=c("Gm","Pm");PLF1[1,]=c(0,0)

   Dbar1 <<- vector(length=iterations[length(iterations)]+1); Dbar1[1]=0

   sigma.beta1 <<- vector(length=iterations[length(iterations)]+1); sigma.beta1[1]=0.1

}

setup(iterations)

### MCMC Loop-- this runs the model

for(i in 1:iterations) {

  params.nonspatial = list(Y=greenup,X=datamatrix,Beta=beta1[i,], GUrows=GUrows)     #For CalcPostNonspatial
```

```
  beta1[i+1,] <- metrop.norm(beta1[i,], propsd_Beta, CalcPostNonspatial, params.nonspatial, "Beta")
          Dbar1[i] <- -2*CalcLogLik(Y=greenup, X=datamatrix, Beta=beta[i,], GUrows=GUrows)
      print(i)
   }

### CHAIN 3 (same as CHAIN 1, so anything you edited there should be edited here)
setup <- function(iterations){
   ## Data Structures
   nBeta <<- ncol(datamatrix)
   ## Intital values
   beta.init=function() rnorm(nBeta,0,0.5)
      propsd_Beta <<- c(0.05,0.005,0.005,0.005,0.005,0.005,0.005,0.005)

### Data Structure
   beta2 <<- matrix(ncol=nBeta,nrow=iterations[length(iterations)]+1) ; beta2[1,] <<- beta.init()
      PLF2 <<-
matrix(ncol=2,nrow=iterations[length(iterations)]+1);colnames(PLF2)=c("Gm","Pm");PLF2[1,]=c(0,0)
   Dbar2 <<- vector(length=iterations[length(iterations)]+1); Dbar2[1]=0
   sigma.beta2 <<- vector(length=iterations[length(iterations)]+1); sigma.beta2[1]=0.1
}
setup(iterations)

### MCMC Loop-- runs the model
   for(i in 1:iterations) {
  params.nonspatial = list(Y=greenup,X=datamatrix,Beta=beta2[i,], GUrows=GUrows)     #For
CalcPostNonspatial
  beta2[i+1,] <- metrop.norm(beta2[i,], propsd_Beta, CalcPostNonspatial, params.nonspatial, "Beta")
          Dbar2[i] <- -2*CalcLogLik(Y=greenup, X=datamatrix, Beta=beta[i,], GUrows=GUrows)
      print(i)
   }
```

```
savedate = "data_model" # label for saved files, prefix will be added to this for all save commands below
outputdir <- function(x) paste("C:/",x,sep="") ##set the directory where output should be written

### save betas
beta=as.mcmc(beta)   #convert chain 1 output to MCMC object
beta1=as.mcmc(beta1) #convert chain 2 output to MCMC object
beta2=as.mcmc(beta2) #convert chain 3 output to MCMC object
beta_all=mcmc.list(beta,beta1,beta2)   #make MCMC list from 3 chains (for Coda analysis)
varnames(beta_all)=c(colnames(datamatrix))   #gives names to parameters in MCMC list
save(beta_all,file=outputdir(paste("beta",savedate, ".Rdata", sep="")))  #saves beta MCMC list as Rdata

### can do identical for Dbar (for calculating DIC-- model comparison)
Dbar=as.mcmc(Dbar)   #convert chain 1 output to MCMC object
Dbar1=as.mcmc(Dbar1) #convert chain 2 output to MCMC object
Dbar2=as.mcmc(Dbar2) #convert chain 3 output to MCMC object
Dbar_all=mcmc.list(Dbar,Dbar1,Dbar2)   #make MCMC list from 3 chains (for Coda analysis)
save(Dbar_all,file=outputdir(paste("Dbar",savedate, ".Rdata", sep="")))  #saves Dbar MCMC list as
Rdata

#########################################################################
####  load beta posteriors for model of interest, explore, subset, and plot   ######
#########################################################################
beta=beta_all

## explore mcmc chains
plot(beta, auto.layout = TRUE, smooth=TRUE)  ##plot chains and density plots to check convergence
autocorr.plot(beta, lag.max=50)   ## autocorrelation plots for each chain and covariate
gelman.plot(beta,ylim=c(0,3))     ## BGR plots to check convergence

## subset posterior as needed
```

```
s=2000  #start iteration (eliminate burn-in) -- explore for your data

t=100  #thinning (to reduce autocorrelation) -- explore for your data

beta=window(beta_all, start=s,thin=t)  #subset posterior (be sure to replot the above 3 plots to check convergence & autocorrelation)

str(beta)   #structure of posterior sample


## Parameter estimates

betastats=as.data.frame(summary(beta,quantiles=c(0.025,.5,0.975))[2]) #betas for post-burn-in and thinned posterior

betastats$names=c("intercept",select)    #puts names on fitted coefficients

betastats       #print the coefficient estimates

save(betastats,file=outputdir(paste("betastats",savedate, ".Rdata", sep=""))) #save the coefficient estimates


#########################################################################

#####              Model Comparison: DIC                #####

#########################################################################

Dbar_mean=summary(window(Dbar_all,start=s,thin=t))$statistics["Mean"] #mean Dbar of post-burn-in and thinned posterior

DThetabar= -2*CalcLogLik(Y=greenup, X=datamatrix, Beta=betastats[,"quantiles.50."], GUrows=GUrows)

pD=Dbar_mean-DThetabar

DIC=pD+Dbar_mean    #prints the DIC summary

DICsummary=rbind("Dbar_mean = "=Dbar_mean,"D(Thetabar) = "=DThetabar,"pD = "=pD,"DIC = "=DIC);DICsummary  #create dataframe for DIC summary

write.csv(DICsummary,outputdir(paste("DICsummary", savedate, ".csv", sep="")))   #save DIC summary


#############################################################################################

######                    unstandardize coefficients                    #######

#############################################################################################

beta=as.matrix(beta)
```

```
beta=as.data.frame(beta)  #convert for ease of handling in unstandardization process


## intercept adjustment: numerator are means used to standardize each covariate, denominator is standard deviation used to standardize each covariate

beta$inter_us = beta$intercept - ((beta$cumuGDD6_std*(9.049559/18.5106)) +
(beta$cumuCH_std*(14.36484/13.9272))            + (beta$ns_std*(-0.04902559/0.06465616)) +
(beta$ew_std*(0.02009537/0.08097351))              + (beta$oak_std*(0.2188244/0.2105303)) +
(beta$maple_std*(0.3213264/0.1660717)) + (beta$birch_std*(0.1266706/0.1051982)))  #adjust intercept


## beta unstandardization: denominator is standard deviation used to standardize each covariate

beta$cumuGDD6_us = beta$cumuGDD6_std/18.5106    #unstandardize beta1

beta$cumuCH_us = beta$cumuCH_std/13.9272   #unstandardize beta2

beta$ns_us= beta$ns_std/0.06465616  #unstandardize beta3

beta$ew_us= beta$ew_std/0.08097351  #unstandardize beta4

beta$oak_us= beta$oak_std/0.2105303  #unstandardize beta5

beta$maple_us= beta$maple_std/0.1660717

beta$birch_us= beta$birch_std/0.1051982


beta1=subset(beta,select=c("inter_us","cumuGDD6_us","cumuCH_us","ns_us","ew_us","oak_us","maple
_us","birch_us"))

head(beta1)

dim(beta1)


## convert beta1 to matrix for multiplication in prediction

beta1=as.matrix(beta1)

head(beta1)

dim(beta1)


#############################################################################

######                    prediction data                    #######

#############################################################################

load(file='NEMODIS_greenup_modeling_full_xdata.Rdata')
```

```
#a dataset setup like the fitting dataset, but including non-standardized variables and 47 8-day time steps per year (not truncated to event dates)

# when load dataset of all nine years (2001-2009), the model is making estimations of all nine years

# when load dataset of 2010, it is doing model validation

# when load dataset of mean values of current period (2001-2009) and future period (2046-2065) and two model years (2047 and 2057), it is doing model prediction for two periods and two model years

# so this part of code actually run for multiple times depending on the needs


head(xdata)

dim(xdata)

str(xdata)

data=xdata ## rename your dataset to data


data=data[order(data$celln, data$doy),]    #order the data by individual and date, here each individual is each grid cell, celln is cell number as id number

data$IDyr=paste(data$celln,data$year,sep="_")      #add unique identifier for each individual


head(data)

summary(data)


##############################################################################

#########                 generate predictions                 ########

##############################################################################

select=c("cumuGDD6","cumuCH","ns","ew","oak","maple","birch")  #covariates used in the model (non-standardized)

datamatrix = as.matrix(cbind(intercept=1,subset(data,select=select)))    #create the design matrix for the model in question

head(datamatrix)

dim(datamatrix)


ls()

rm(beta,beta_all,data)  #remove unneeded data to maximize available memory
```

```
gc()


##

p=apply(beta1,1,function(x) pnorm(datamatrix%*%x))  #calculate the p's for each individual at each time for each iteration (slow with large datasets)

dim(p)  #length = datamatrix, columns = iterations

pmean=apply(p,1,mean)  #mean across iterations-- same length as p

plower=apply(p,1,quantile,prob=0.025)

pupper=apply(p,1,quantile, prob=0.975)


# generate cumulative probabilities of green-up

cumid=as.matrix(data$IDyr)

cumid_order=cbind(data$celln,data$year, data$doy,data$IDyr)

colnames(cumid_order)=c("celln","year","doy","IDyr")

head(cumid_order)

cumid_order=cumid_order[order(cumid_order[,4]),]


q=tapply(pmean,cumid,function(x2) 1-cumprod(x2))   ##mean prediction cumulative probability

q1=do.call(c,q)

qb=tapply(plower,cumid,function(x2) 1-cumprod(x2))  ##lower CL prediction cumulative probablility

q2=do.call(c,qb)

qc=tapply(pupper,cumid,function(x2) 1-cumprod(x2))  ##upper CL prediction cumulative probablility

q3=do.call(c,qc)

qfinal=rbind(q1,q2,q3)    ##one observation for each individual for each day in the dataset (length qfinal = length datamatrix)

qfinalA=t(qfinal)

head(qfinalA)

qfinal1=as.data.frame(cbind(qfinalA,cumid_order))      #append the unique identifiers with cell number, year and doy


qfinal1$q1=as.numeric(as.character(qfinal1$q1))
```

```
qfinal1$q2=as.numeric(as.character(qfinal1$q2))
qfinal1$q3=as.numeric(as.character(qfinal1$q3))
qfinal1$celln=as.numeric(as.character(qfinal1$celln))
qfinal1$doy=as.numeric(as.character(qfinal1$doy))
qfinal1$year=as.numeric(as.character(qfinal1$year))
head(qfinal1)
library(gdata)
qfinal1=rename.vars(qfinal1, from="q1", to="mean")
qfinal1=rename.vars(qfinal1, from="q2", to="lower")
qfinal1=rename.vars(qfinal1, from="q3", to="upper")
head(qfinal1)

#############################################################################
#######              create p(t) and p(t-1) vectors                ######
#############################################################################
qfinal2=qfinal1
qfinal2$st1=rep(0)

n=length(qfinal2$celln)/47          # number of individuals
a={}
b={}
for (j in 1:n)
{for (i in 2:47)
{ a=c(a,i+47*(j-1))
  b=c(b,i-1+47*(j-1))
}
}        # this loop generates row number of s(t-1) from s(t)

qfinal2$st1[a]=qfinal2$mean[b]    # generate a column of s(t-1)
qfinal2$sdiff=qfinal2$mean-qfinal2$st1  #calculate probability of green-up in each time interval
```

```
# get probability of green-up in each time interval for lower and upper bound of credible interval
qfinal2$st1_l=rep(0)
qfinal2$st1_u=rep(0)
qfinal2$st1_l[a]=qfinal2$lower[b]
qfinal2$sdiff_l=qfinal2$lower-qfinal2$st1_l
qfinal2$st1_u[a]=qfinal2$upper[b]
qfinal2$sdiff_u=qfinal2$upper-qfinal2$st1_u
head(qfinal2)

#############################################################################################
#######                    HPD credible interval                    #######
#############################################################################################
## get metrics of highest green-up probability
sq=as.data.frame(tapply(qfinal2$sdiff,qfinal2$IDyr,max))
sq=rename.vars(sq,from="tapply(qfinal2$sdiff, qfinal2$IDyr, max)",to="max_sdiff")
sq$IDyr=row.names(sq)
head(qfinal2)
dim(qfinal2)
head(sq)
dim(sq)

# get the row number of highest green-up probability and determine estimated green-up date
max_nrow={}
for (i in 1:n)
{max_nrow=c(max_nrow,which((qfinal2$IDyr==sq$IDyr[i])&(qfinal2$sdiff==sq$max_sdiff[i])))}
head(max_nrow)
est_date=qfinal2$doy[max_nrow]      ## this date is actually the end day of the time step
sq$est_date=as.integer(est_date)
sq$celln=qfinal2$celln[max_nrow]
```

```
sq$year=qfinal2$year[max_nrow]
head(sq)

# get lower and upper bounds of HPD credible interval
sq_l=as.data.frame(tapply(qfinal2$sdiff_l,qfinal2$IDyr,max))
sq_l=rename.vars(sq_l,from="tapply(qfinal2$sdiff_l, qfinal2$IDyr, max)",to="max_sdiff")
sq_l$IDyr=row.names(sq_l)
max_nrow={}
for (i in 1:n)
{max_nrow=c(max_nrow,which((qfinal2$IDyr==sq_l$IDyr[i])&(qfinal2$sdiff_l==sq_l$max_sdiff[i])))}
sq_l$est_date_l=qfinal2$doy[max_nrow]
sq_l$celln=qfinal2$celln[max_nrow]
sq_l$year=qfinal2$year[max_nrow]

sq_u=as.data.frame(tapply(qfinal2$sdiff_u,qfinal2$IDyr,max))
sq_u=rename.vars(sq_u,from="tapply(qfinal2$sdiff_u, qfinal2$IDyr, max)",to="max_sdiff")
sq_u$IDyr=row.names(sq_u)
max_nrow={}
for (i in 1:n))
{max_nrow=c(max_nrow,which((qfinal2$IDyr==sq_u$IDyr[i])&(qfinal2$sdiff_u==sq_u$max_sdiff[i])))
}
sq_u$est_date_u=qfinal2$doy[max_nrow]
sq_u$celln=qfinal2$celln[max_nrow]
sq_u$year=qfinal2$year[max_nrow]
head(sq)
```

Appendix 1.2

Table 1.2-1 Conversion of temperatures to chill units using Chill Hour (CH), Utah (UT) and North Carolina (NC) Model.

Chill Hour model		Utah model		North Carolina model	
Temperature(°C)	Chill units	Temperature(°C)	Chill units	Temperature(°C)	Chill units
T≤0	0	T≤ 1.4	0	T≤ 1.6	0
0 < T < 7.2	1	1.4< T≤ 2.4	0.5	1.6< T≤ 7.2	0.5
T≥ 7.2	0	2.4< T≤ 9.1	1	7.2< T≤ 13	1
		9.1< T≤ 12.4	0.5	13< T≤ 16.5	0.5
		12.4< T≤ 15.9	0	16.5< T≤ 19	0
		15.9< T≤ 18	-0.5	19< T≤ 20.7	-0.5
		T> 18	-1	20.7< T≤ 22.1	-1
				22.1< T≤ 23.3	-1.5
				T> 23.3	-2

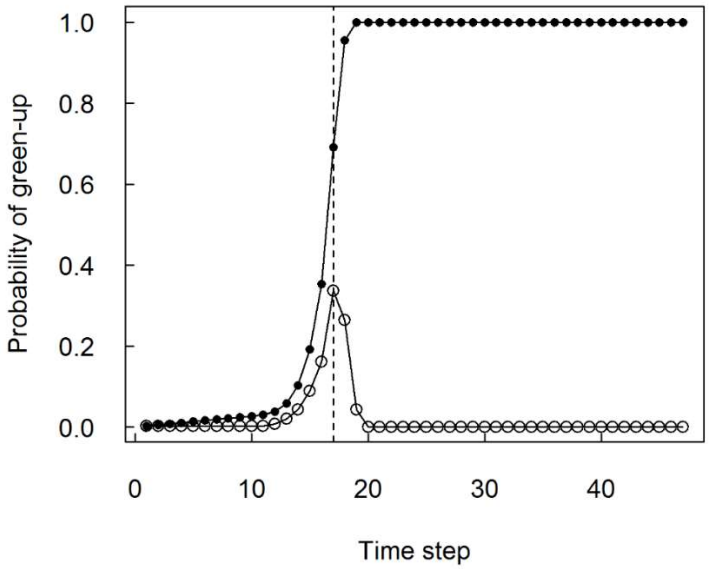

Figure 1.2-1 Plot of estimated probability of green-up from model output. The 8-day time steps are on the horizontal axis. Open circles indicate the estimated probability of green-up of each 8-day time step ((S(t-1)-S(t)) curve), and closed circles indicate the estimated cumulative probability of green-up. The vertical dashed line indicates the time step with highest predicted probability of green-up, which we used as the estimated time step of green-up. The 95% HPD interval for the estimated probability of green-up at each time step is too narrow (about ±0.001) to show in the figure.

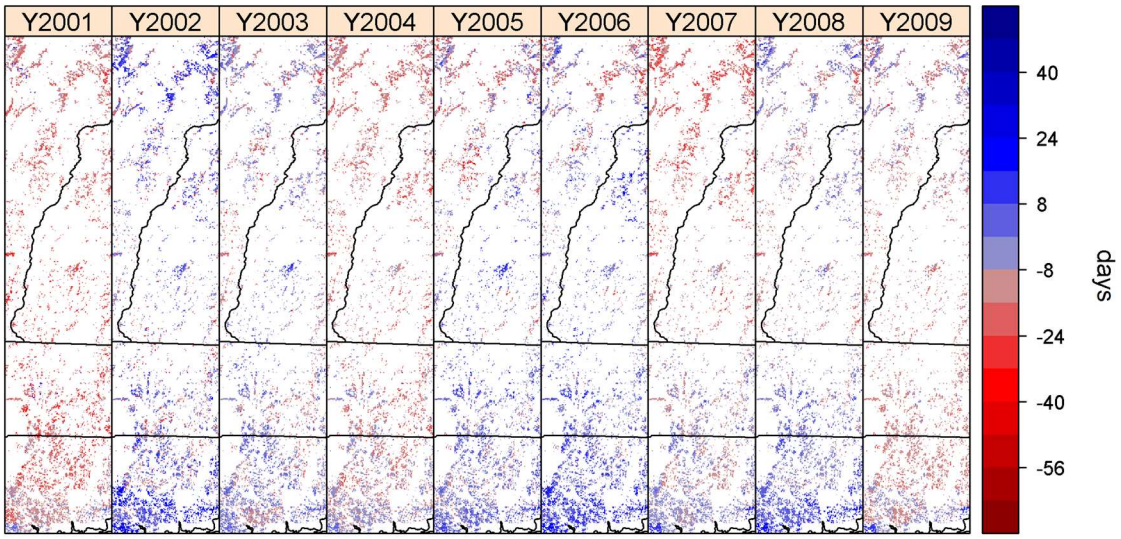

Figure 1.2-2 Maps of residuals of green-up dates for nine years. The unit is converted from 8-day time step to days. Black lines are state boundaries. White areas indicate non-deciduous forest area.

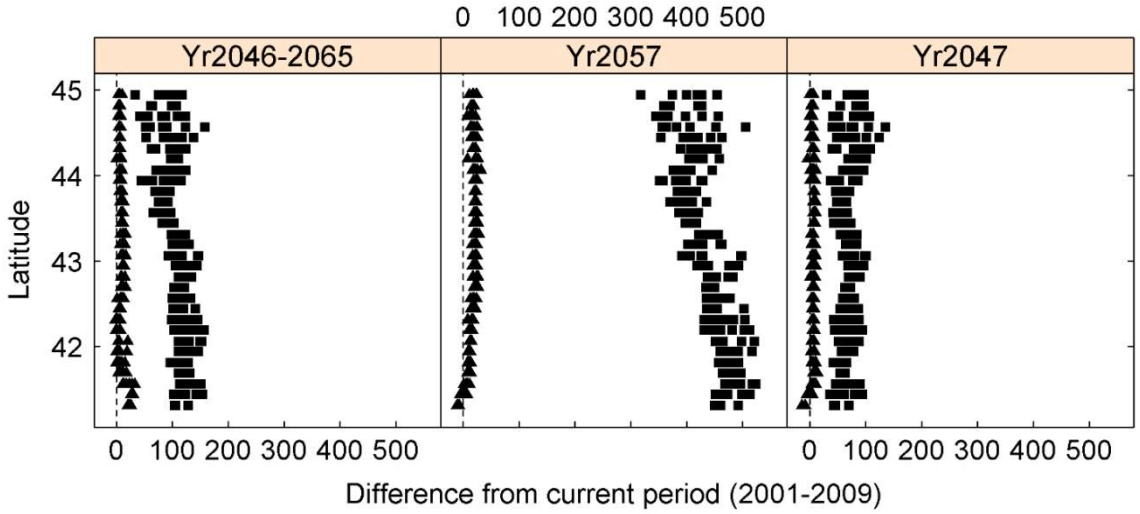

Figure 1.2-3 Difference of cumulative GDD and CU on 150th day of year between the current period (2001-2009) and the ensemble future period (2046-1065), 2057 (MIROC) and 2047 (GFDL) across the latitudinal gradient. Cumulative CU is represented by triangles and cumulative GDD is represented by squares. The dashed line indicates zero difference. A positive difference indicates higher values in the future period or year.

Appendix 1.3: Spatio-temporal uncertainty in the MODIS phenology product and implications for the analyses and modeling thereof.

1. Known issues with the MODIS Land Cover Dynamics (MCD12Q2) product.

This product uses EVI calculated from composited 8-day Normalized BRDF Adjusted Reflectance data, MCD43A4 (User Guide of MODIS Land Cover Dynamics product). MCD43A4 data are produced every 8-days using overlapping 16-day compositing windows. Thus, there are a maximum of 46 possible EVI values for any year at any given 500m pixel location. According to Zhang et al. (2003), the phenophase transition dates were estimated from the rate of change of curvature of logistic curves made by 8-day EVI values. So the dates are estimated with daily precision by fitting a continuous function through data with 8-day resolution. In consequence there can be significant uncertainties in the date of green-up estimated using noisy EVI time series. Ideally, the temporal uncertainty would be accounted for within the model (with a measurement error component), but developing this is well beyond the scope of this initial (and innovative) effort to use a survival model framework to model remotely sensed data. Indeed incorporating uncertainty in the analysis of remotely sensed images constitutes an important future objective in ecological studies such as ours (cf. our figure S3A below). But rarely, if ever, has this been done. In addition, we could have relied on the QC data provided with the product, but the product group has reported that the QC layer was not performing as intended and they plan to solve the issue for the next version of the product. This information about the QC issue can be found in a document updated in 2012 to show the known issues about this MODIS product (see link below).

Our objective in working with 8-day intervals is to acknowledge the uncertainty in the estimated dates by coarsening the temporal resolution of the analysis and predictions to that of the underlying EVI data. At the same time, we did our best to use high spatial resolution land cover data to identify the MODIS pixels with deciduous forest cover higher than 75% in order to get more reliable locations (typically the seasonal cycle of EVI in deciduous forest is regular and well defined). In future analysis, we would like to revisit this important issue and perhaps add a measurement error component that incorporates the QC information that should be available in the next version of the land cover dynamics product.

User Guide: http://www.bu.edu/lcsc/files/2012/08/MCD12Q2_UserGuide.pdf

Known issues: http://www.bu.edu/lcsc/files/2012/08/MCD12Q2_Known_Issues.pdf

2. Preliminary assessment of temporal uncertainty in the MODIS phenology product.

Using the logistic regression method from Zhang et al. (2003), we fit two logistic curves for NDVI in one year (2001) of one MODIS 500m pixel with 100% deciduous forest (Fig. S3-1). Circles are 8-day NDVI. The solid line combines two logistic regression curves including spring and fall periods. Dashed curves are 95% confidence intervals of NDVI curves. Based on the method from Zhang et al. (2003), we calculated the change of curvature to determine green-up dates for this deciduous forest pixel. Vertical dashed lines represent the 95% confidence interval of green-up date for this pixel based on the change of curvature, which spans about an 8-day interval. Analyses such as these for each pixel in the landscape in each year could provide the basis for characterizing and summarizing the temporal uncertainty in the MODIS phenology product. This figure also illustrates added sources of error in the NDVI reflectance over the time course of a year for this one pixel: notice the outliers in reflectance around days 10, 180 and 220.

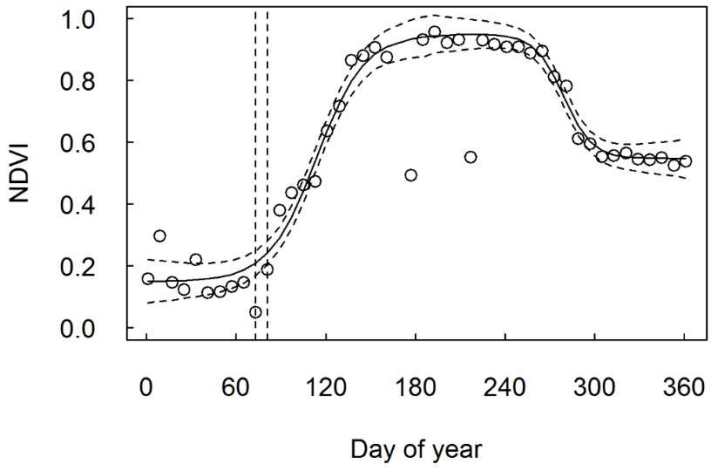

Figure 1.3-1Eight-day NDVI (open circles), fitted logistic curves (solid line), 95% confidence intervals for fitted curve (dashed curves), and 95% confidence interval of the estimated green-up date (vertical dashed lines) for one MODIS pixel with 100% deciduous forest cover in 2001.

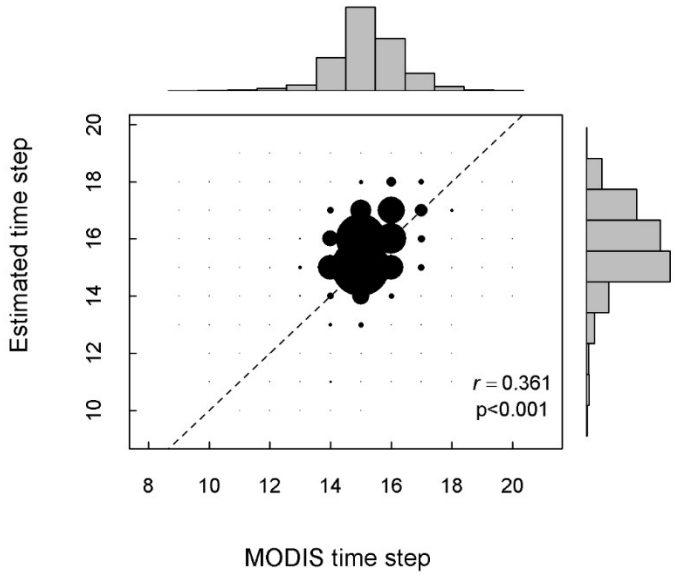

Figure 1.3-2 MODIS green-up time steps and estimated time steps by model No.3 for nine years (2001-2009). The horizontal histogram is for MODIS time steps, and the vertical histogram is for model estimated time steps. Every time step represent 8-day interval (e.g. time step 10 represents 73-80 day of year). Size of points in the plot represents frequency matching to the histograms. The largest point represents frequency of 12920/85358 and the smallest point represents frequency of 1/85358. The dashed line is the 1:1 line. Black points on the dashed line suggest that estimation is equal to observation. Points under the dash line indicate early estimation, and points above the dash line indicate late estimation. The Pearson's correlation coefficients is 0.361, $p<0.001$.

3. How temporal uncertainty and temporal resolution translate into model and prediction uncertainty.

Given the 8-day temporal resolution of green-up time steps from the MODIS product, comparison between MODIS green-up dates and model estimated 8-day time steps had relatively small r values (correlation coefficients). This can be attributed to several factors, including the coarse temporal resolution, uncertainty in the curve and associated inflection point for bud burst and outliers (cf. fig. S3-1), unknown quality issues with the MODIS data (cf. point 1 above), etc. Nevertheless, from figure S3-2 and S3-3, we can see the majority of data fall on the 1:1 line or with only 1 time step residual (73% of points are within 1 time step for 2001-2009, 91% for 2010). Moreover, the reported RMSE (12 days for 2001 to 2009, and 8 days for 2010) does indicate a reasonably good fit given the temporal 8-day resolution of the data.

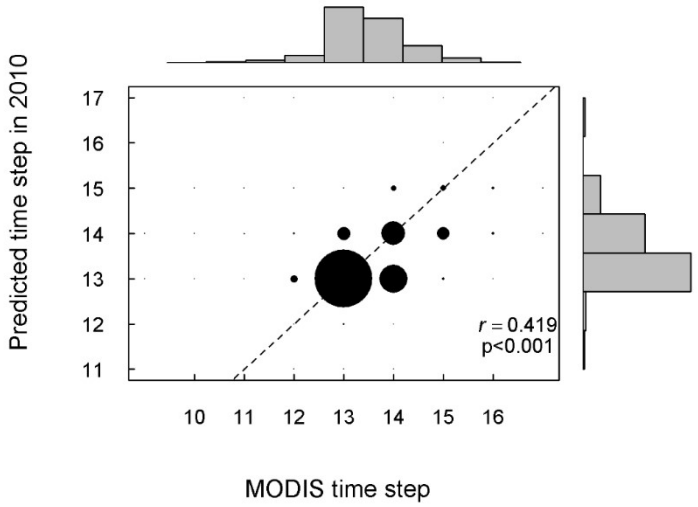

Figure 1.3-3 MODIS green-up time steps and estimated time steps for the year 2010. The horizontal histogram is for MODIS time steps, and the vertical histogram is for estimated time steps. Every time step represent 8-day interval (e.g. time step 10 represents 73-80 day of year). Size of points in the plot represents frequency matching to the histograms. The dashed line is the 1:1 line. Black points on the dash line suggest that estimation is equal to observation. The largest point represents frequency of 2653/8050 and the smallest point represents frequency of 1/8050. Points under the dashed line indicate early estimation, and points above the dashed line indicate late estimation. Pearson's correlation coefficient is 0.419, $p<0.001$.

4. Contribution of uncertainty in species composition and landscape coverage.

Variation of species composition may contribute to variation of landscape phenology in a large region. In our study area, data of three genera (Acer, Betula, Quercus) of dominant deciduous trees from 1211 FIA plots were aggregated into 206 climate grid cells to represent variation of species composition (Fig. S3-4). There are about 6 plots on average in each cell. 2 grid cells have no plot and areshown as white pixels in Figure S3-4. Given the spatial resolution of climate grid cell, 1/8 degree (12 km), and uncertainty (fuzziness) of FIA plot coordinates, 0.5 mile (0.8 km) or 1 mile (1.6 km) (http://fia.fs.fed.us/), the aggregation on FIA data onto our climate grid may bring a very small level of inaccuracy at a local scale,

but still provide sufficient information to specify the spatial variation of species composition at the landscape-level across the broad community types of our study area.

Setting thresholds for deciduous forest cover may have introduced additional noise in our data. Since the land cover and land-use data we used has finer resolution (30 m) than MODIS data (500 m), we used 75% as the threshold for including deciduous forest pixels, but we do not know the extent to which the remaining 25% cover (e.g., grassy areas, agricultural fields, etc.) may affect phenology as detected by MODIS. This sub-pixel effect may bring an added extent of uncertainty of the data into the modeling.

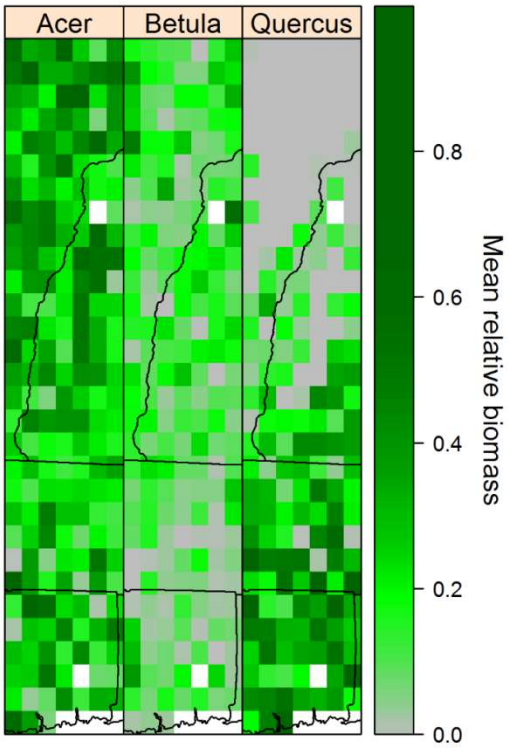

Figure 1.3-4 Mean relative biomass of three genera of deciduous species (Acer, Betula, and Quercus) for each climate grid cell in the study area. Each grid cell is 1/8*1/8 degree. Dark grid indicates high relative biomass, and light grid indicates low relative biomass. White areas mean no data.

5. Uncertainty in species-specific phenological responses to climate and weather variation.

The general physiological mechanism by which plants respond phenologically to variation in weather and climate has shown to hold experimentally in a number of different woody plant species across different genera (Acer, Alnus, Betula, Carya, Fagus, Fraxinus, Larix, Picea, Populus, Prunus, Quecus, Ulmus) of forest woody plant species. In order to incorporate species-specific effects in our model, it would be necessary to obtain specific mechanistic response for every dominant species in the forest community across the region and then to incorporate the phenological performances of each species in the model at the community level. The different species-specific responses would include specifying the parameters associated with growing degree days, chilling unit models, as well as specifying model structures (i.e. parallel or sequential models). The extant published studies simply do not provide the necessary or

sufficient parameterization information on the species we find in our landscape to accomplish that goal. It is also unclear whether weighted species specific models would translate to the observed community level phenology. Given both of these substantial challenges, we use community composition proxies rather than weighted species level models to address our research questions. This undoubtedly adds noise and uncertainty to the models and their predictions. It also points to the need for appropriate physiological experiments and development of statistical methods to parameterize species-specific models of phenological change that translate to the community and landscape scale.

6. Unmeasured climate and weather variables as a potential source of model and prediction uncertainty.

Of course we have incorporated only a few of the many possible climate and weather variables that may affect variation in phenological responses. The mechanism of breaking dormancy and development of leaves is triggered by temperatures linking the regulation of dormancy associated genes (cf. Paul et al. 2014 for the most recent review). Although moisture is necessary for plant development, precipitation was not considered in the model, because water is not typically a limiting factor for temperate forests in New England. Winters and springs in New England provide enough precipitation for plant leaf out in spring. In our early model exploration, precipitation was not identified as a significant explanatory variable. In another phenology study of bud break, Doi & Katano (2008) found no significant relationship between spring phenology and monthly precipitation, even for the monsoonal (winter drought) climates in their study area. We also did not find any other mechanistic models of temperate plant phenology involving precipitation. We checked monthly precipitation from January to May for each model year from 2046 to 2065 and compared it to monthly precipitation from 2001 to 2009. The comparisons suggested similar mean values and standard deviation of monthly precipitation during 9-year period and 20-year period. Since the two periods are quite similar, we do not expect precipitation to become a limiting factor in this system by 2065.

7. Model uncertainty, parameter uncertainty and prediction uncertainty.

The Bayesian framework in our model generated posterior distributions of every parameter, which is one source of model uncertainty (parameter uncertainty). The model prediction used posterior mean values of parameters as the coefficients in the model. Additionally, we also did predictions using the lower and upper bounds of 95% credible intervals for every parameter in the model. The difference among these predictions indicated the uncertainty from the model, which is ±8 days across the study region (Fig. S3-5).

For model prediction of the future period, we used averaged weather data from ensemble of 8 climate models for 20 years period (2046-2065). Four models are from General Circulation Models (GCMs) and the other four are from Regional Climate Models (RCMs) (see: Ahmed et al. 2013). Our predictions on green-up dates generally represented the averaged condition from the 8 model projections for future period. However, due to different model structures on processes and parameterizations, projection of future weather conditions generated by those models have variations and uncertainties. So we calculated 95% quartile of variation of GDD (growing degree day) and CU (chilling units) for future 20 years using projection data provided by 8 climate models. Then we did model predictions using upper and lower bounds of 95% quartile variation of GDD and CU for future period. The difference among predictions indicate an extent of uncertainty. The results indicated spatial variation of predictions, which is caused by

spatial variation of climate model projections. In northern and central area the uncertainty is ±8 days, but the uncertainty is larger in coastal area, which is ±24 days.

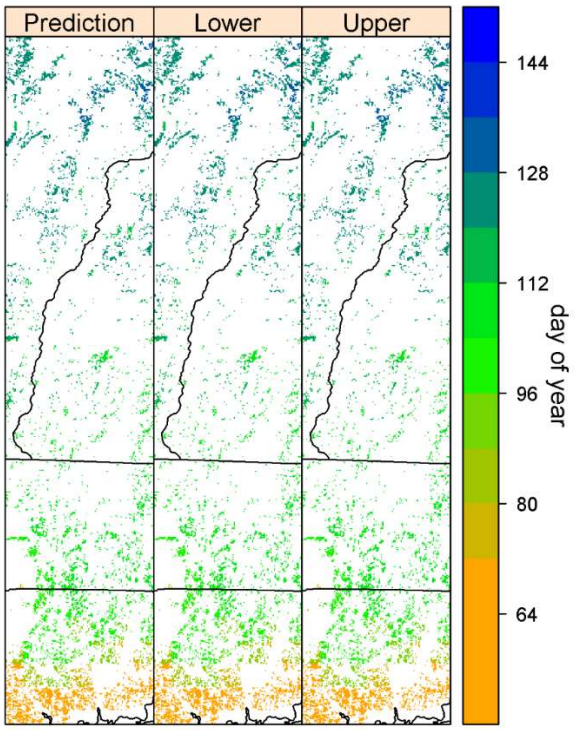

Figure 1.3-5 Prediction of mean green-up dates in 2046-2065 with lower and upper bounds of 95% credible intervals of model parameters. "Prediction" panel shows prediction of green-up dates by ensemble average weather projection data. "Lower" and "Upper" panels show prediction by 95% credible intervals lower and upper bounds of model parameters. The unit is converted from 8-day time step to day of year. Black lines are state boundaries. White areas indicate non-deciduous forest area. The variations among three panels of predictions indicate model uncertainty.

8. Issues related to projecting changes in forest communities over time.

Species compositional change over time may cause spatial phenological variation, but the dynamics of projected forest change in New England over the next 30 to 50 years are likely to be relatively small, given the generation time of trees and gap-phase dynamics for our system. For example Pacala et al. (1996) showed that dynamical changes in these forests are on the order of centuries not decades. Also, changes in species geographical distributions are likely to occur on a similar long temporal scale in the absence of human assistance (i.e. migration of <100m/yr: McLachlan et al 2005). Past land use changes, on the scale of centuries, have had the greatest impact on species distributions across the region (e.g. Foster & Aber. 2004). But projections of future changes over the next 50-100 years are more about changes in forest cover and geographic patterns thereof, than species compositional changes (cf. Foster et al. 2010). In the absence of human assisted species migration, we are unlikely to see new species augmenting local species pools or having much of an effect on forest canopy composition over the next 30-50 years. In comparison, climate change effects on species distributions will likely be considerably less over this time frame, given little change projected in rainfall, limited migration potential and long

generation times for trees. Thus no change of species composition of forest and landscape was applied to our predictions; the change of green-up dates is driven by change of GDD and CU.

9. Issue with length of data for modeling and model predictions.

There are 10 years data (2001-2010) for our modeling, so 9 years (2001-2009) for model estimation and 1 year (2010) for model validation. If a factor affecting green-up (like chilling or GDD) had a small variation over 9 years (2001-2009) but larger variation in projected 20 year period (2046-2065), then our 9 years of data could be too short to detect the association between the environmental factors and green-up dates. Since our projection is only based on change of cumulative GDD and CU, we checked the variation of cumulative GDD and CU for two time periods (2001-2009 and 2046-2065). We compared the mean value and standard deviation of cumulative GDD and CU on the 100th, 120th and 140th day of year for two periods. From the comparison we found the change of mean values between two periods, but the standard deviations are similar across the study area. It suggested that similar variations of explanatory variables during two time periods (2001-2009 and 2046-2065) allow the model predictions for the future period. Thus, we believe prediction of 20 years green-up dates based on 9 years data is practical.

References:

Allen JM, Terres MA, Katsuki T, Iwamoto K, Kobori H, Higuchi H, Primack RB, Wilson AM, Gelfand A, Silander JA (2014) Modeling daily flowering probabilities: expected impact of climate change on Japanese cherry phenology. Glob Change Biol 20:1251–2063

Doi H, Katano I (2008) Phenological timings of leaf budburst with climate change in Japan. Agricultural and Forest Meteorology 148: 512–516

Foster DR, Aber JD (2004) Forests in Time: the environmental consequences of 1,000 years of change in New England. Yale University Press, New Heaven and London.

Foster DR, Donahue BM, Kittredge DB, Lambert KF, HunterML, Hall BR, Irland LC, Lilieholm RJ, Orwig DA, D'Amato AW, Colburn EA, Thompson JR, Levitt JN, Ellison AM, Keeton WS, Aber JD, Cogbill CV, Driscoll CT, Fahey TJ, Hart CM (2010) Wildlands and woodlands: A vision for the New England landscape. Harvard Forest, Petersham

McLachlan JS, Clark JS and Manos PS (2005) Molecular indicators of tree migration capacity under rapid climate change. Ecology, 86:2088–2098

Pacala SW, Canham CD, Saponara J, Silander JA Jr., Kobe RK, Ribbens E (1996) Forest models defined by field measurements: esimtation, error analysis and dynamics. Ecological Monographs, 66:1–43

Paul L.K., Rinne P.L.H., van der Schoot C. (2014) Shoot meristems of deciduous woody perennials: self-organization and morphogenetic transitions. Current Opinion in Plant Biology 17:86–95

Terres MA, Gelfand AE, Allen JM, Silander JA (2013) Analyzing first flowering event data using survival models with space and time-varying covariates. Environmetrics 24:317–331

Zhang X, Friedl MA, Schaaf CB, Strahler AH, Hodges JCF, Gao F, Reed BC, Huete A (2003) Monitoring vegetation phenology using MODIS. Remote Sens Environ 84:471–475

Chapter 2

Deciduous forest responses to temperature, precipitation, and drought imply complex climate change impacts

The following paper was published in *Proceedings of the National Academy of Sciences of the United States of America* in November 2015. Xiaojing Wang offered ideas to improve the models and the text of modeling in the Methods. John A. Silander, Jr. provided suggestions on the data analysis and comments on the manuscript.

Deciduous forest responses to temperature, precipitation, and drought imply complex climate change impacts

Yingying Xie[a,1], Xiaojing Wang[b], and John A. Silander Jr.[a]

[a]Department of Ecology and Evolutionary Biology, University of Connecticut, Storrs, CT 06269-3043; and [b]Department of Statistics, University of Connecticut, Storrs, CT 06269-4120

Edited by William H. Schlesinger, Cary Institute of Ecosystem Studies, Millbrook, NY, and approved September 23, 2015 (received for review May 21, 2015)

Changes in spring and autumn phenology of temperate plants in recent decades have become iconic bio-indicators of rapid climate change. These changes have substantial ecological and economic impacts. However, autumn phenology remains surprisingly little studied. Although the effects of unfavorable environmental conditions (e.g., frost, heat, wetness, and drought) on autumn phenology have been observed for over 60 y, how these factors interact to influence autumn phenological events remain poorly understood. Using remotely sensed phenology data from 2001 to 2012, this study identified and quantified significant effects of a suite of environmental factors on the timing of fall dormancy of deciduous forest communities in New England, United States. Cold, frost, and wet conditions, and high heat-stress tended to induce earlier dormancy of deciduous forests, whereas moderate heat- and drought-stress delayed dormancy. Deciduous forests in two eco-regions showed contrasting, nonlinear responses to variation in these explanatory factors. Based on future climate projection over two periods (2041–2050 and 2090–2099), later dormancy dates were predicted in northern areas. However, in coastal areas earlier dormancy dates were predicted. Our models suggest that besides warming in climate change, changes in frost and moisture conditions as well as extreme weather events (e.g., drought- and heat-stress, and flooding), should also be considered in future predictions of autumn phenology in temperate deciduous forests. This study improves our understanding of how multiple environmental variables interact to affect autumn phenology in temperate deciduous forest ecosystems, and points the way to building more mechanistic and predictive models.

Land-surface phenology | dormancy date | frost | New England

Plant phenological shifts in recent decades are iconic bio-indicators of climate change (1–4). These phenological changes in turn have cascading ecological effects on species demography, biotic interactions, and ecosystem functions (5–8). Whereas mechanisms of spring phenology (i.e., bud burst, leafing out, and flowering) are well studied (9–13), fall phenology (i.e., leaf senescence and dormancy, indicated by visual signals from leaf coloration and leaf drop) remains little studied (14–16). Changes in timing of autumn phenology play a significant role in growing season length prediction, C and N cycling, and biotic interactions (8, 17–19). Furthermore, delayed leaf coloration and more muted autumn foliage in response to climate change will likely significantly affect the multibillion dollar fall foliage ecotourism industry (20–22). Although delayed leaf coloration and leaf drop in deciduous forests have been observed across the northern hemisphere in recent decades (14, 23, 24), the full range of environmental triggers and how they influence fall phenological changes now or in the future remain poorly understood.

Autumn phenology of deciduous woody plant species in temperate regions is the timing of the developmental stages of leaf senescence and dormancy. Plant physiologists demark leaf senescence beginning with onset of leaf coloration, and dormancy with leaf drop and the development of dormant apical meristems (25, 26). As detected by remotely sensed satellite images, autumn phenology dates describe the timing of loss of leaf greenness. Leaf senescence dates correspond to when greenness starts to decrease (i.e., onset of leaf coloration) and dormancy dates occur when greenness reaches a minimum value (brown leaves with leaf drop) (27) (*SI Appendix*, Figs. S1 and S2). Currently, most studies consider short day length and low temperature as the primary or only external triggers of autumn phenology (28, 29). However, over the past 60 y (25, 30, 31), researchers studying the physiology of leaf senescence and dormancy have enumerated a range of other environmental conditions that may influence autumn phenology, including frost, moisture conditions, and extreme weather events (e.g., drought- and heat-stress, and flooding). Although the effects of a subset of these factors on plant leaf coloration and leaf drop were reported by a handful of physiological experiments (32, 33), few studies have quantified the response of fall phenology to a full suite of potential explanatory factors. Ongoing climate changes are likely to introduce higher frequency and intensity of climatic stress factors (34), so it is important to include these in developing more predictive, mechanistic models of fall phenology.

To study landscape-scale forest phenology, we used satellite remotely sensed autumn dormancy dates of deciduous forests in New England, United States, from the Moderate Resolution Imaging Spectroradiometer (MODIS) data product (27) (*SI Appendix*, Fig. S1). Greenness of forest canopy reaches the minimum values at the dormancy date (27), a proxy for plant fall dormancy (*SI Appendix*, Figs. S1 and S2). We examined dormancy dates of deciduous forest communities in two eco-regions (NH, Northeastern Highlands; NCZ, Northeastern Coastal Zone) from 2001 to 2012 (Figs. 1 and 2). Multiple environmental factors affecting fall forest dormancy were identified representing spatially and temporally varying chill and frost-stress, heat-stress, drought-stress, precipitation,

Significance

Autumnal phenological shifts (leaf senescence and dormancy) because of climate change bring substantial impacts on community and ecosystem processes (e.g. altered C and N cyding and phenological mismatches) and the fall foliage ecotourism industry. However, the understanding of the environmental control of autumn phenology has changed little over the past 60 y. We found that cold, frost, wet, and high heat-stress lead to earlier dormancy dates across temperate deciduous forest communities, whereas moderate heat- and drought-stress delayed dormancy. Divergent future responses of fall dormancy timing were predicted: later for northern regions and earlier for southern areas. Our findings improve understanding of autumn phenology mechanisms and suggests complex interactions among environmental conditions affecting autumn phenology now and in the future.

Author contributions: Y.X. and J.A.S. designed research; Y.X. and J.A.S. performed research; X.W. contributed new reagents/analytic tools; Y.X. and X.W. analyzed data; Y.X., X.W., and J.A.S. wrote the paper.

The authors declare no conflict of interest.

This article is a PNAS Direct Submission.

[1]To whom correspondence should be addressed. Email: yingying.xie1@gmail.com.

This article contains supporting information online at www.pnas.org/lookup/suppl/doi:10.1073/pnas.1509991112/-/DCSupplemental.

and flooding events (Table 1), as well as latitude (a proxy for photoperiod) and elevation. We built models independently using eight different statistical regression methods [including multiple linear regression, penalized regression methods, Bayesian model averaging (BMA) (35), and Bayesian spike and slab regression (36)] to select significant environmental drivers of dormancy dates of deciduous forest communities, and to assess spatiotemporal responses of dormancy dates to those drivers. By model selection criteria and root mean square error (RMSE), the best models were selected to predict future dormancy dates of deciduous forest communities in two 10-y periods (2040–2050 and 2090–2099) with two greenhouse gas concentration scenarios [representative concentration pathway (RCP) 4.5 and RCP 8.5] under future climate change projections (37).

Results

Statistical regressions between fall dormancy dates and the suite of predictor variables showed that a number of environmental/weather conditions significantly affect dormancy dates. The different variable selection methods converged on very similar, best-fit models with only slightly different values for predictor coefficients (*SI Appendix*, Tables S1 and S2). The posterior median model (38) from the BMA procedure was selected as the best model explaining deciduous forest dormancy dates in the NH eco-region, and the multiple linear regression model as the best model in the NCZ eco-region. Predictors included in the two best models (Table 2) show that dormancy dates of deciduous forests in New England were significantly affected by latitude (a proxy for photoperiod), elevation, plus temperature conditions [cold degree days (CCD), frosts, and heat-stress], and precipitation [rain days (RD), drought-stress, and extreme flooding events] summarized from daily data over the course of the growing season. Deciduous forests at higher latitude and elevation showed earlier fall dormancy dates. Generally, cold, wet, or extremely hot conditions tended to induce earlier dormancy, whereas moderately hot and dry conditions delayed fall dormancy. Quadratic terms in the models indicated significant nonlinear relationships between dormancy dates and frost, drought, and rainfall conditions.

Coefficients in the best models indicate sensitivities of fall dormancy dates to changes of environmental conditions. Dormancy dates for the deciduous forest communities in the two eco-regions showed different sensitivities to environmental variation (Table 2). We found that deciduous forests in the NH were more sensitive to changes of latitude (i.e., photoperiod), drought, and summer rainfall than the NCZ forests, whereas deciduous forests in the NCZ were more sensitive to change of elevation, chill-stress, autumn rainfall, and heavy rain events (Table 2 and *SI Appendix*, Fig. S3). The interaction between summer rain and heat in two models suggested that to some extent summer rain reduced the effect of heat-stress on forest dormancy dates, especially for NCZ forests.

The variables that were unique to each of the two models indicate that dormancy dates for deciduous forests in two eco-regions had different responses to frost, seasonal drought-stress, and seasonal rainfall conditions (Table 2). Dormancy dates of NH deciduous forests were influenced by frost in both spring (earlier) and autumn (nonlinear), whereas dormancy dates in the NCZ were affected significantly only by autumn frost (earlier). Moreover, the response of dormancy dates in NCZ forests to frost was also related to elevation; the significant interaction between frost days (FD) and elevation in the model indicated that the sensitivity of deciduous forests at higher elevation to FD was smaller than the forests at lower elevation. In terms of drought effects, dormancy dates in NCZ forests were affected by spring, summer, and autumn drought-stress (respectively earlier, later, and later dormancy dates), but dormancy dates in the NH were more sensitive to summer and autumn drought (later dormancy dates and nonlinear effects). Although droughts in autumn lead to later dormancy dates in the two eco-regions, the quadratic term (growing season drought, GDR) $GDR_{(Sep.1–Nov.15)}^2$ indicates a delaying effect on dormancy dates in NH forests, but that as drought continues to increase, dormancy comes earlier.

Precipitation affected fall dormancy dates of deciduous forests in the NH across the growing season from spring to autumn. For NCZ forests, dormancy dates were affected by rainfall in summer (earlier) and autumn (later and with a nonlinear response). More summer rainfall lead to later dormancy dates in the NH but earlier dormancy dates in the NCZ; but the quadratic effect of summer rainfall $[RD_{(Jul.1–Aug.31)}^2]$ in the NH indicates that initially as rainfall increases, fall dormancy is later but as the rainfall further increases, dormancy progressively comes earlier. More autumn rainfall lead to earlier dormancy dates in the NH but later dormancy dates in the NCZ, but given the quadratic coefficient associated with autumn rainfall in the NCZ $[RD_{(Sep.1–Nov.15)}^2]$, initially as rainfall increases, dormancy is later, and as this continues to increase, dormancy comes earlier. Because there are more heavy rainfall days in autumn in the NCZ, dormancy is earlier, but with a significant positive quadratic term (heavy rainy days, ECA) $[ECA_{(Sep.1–Nov.15)}^2]$ there is nonlinearity to this trend.

Predicted fall dormancy dates in the two eco-regions showed different responses to projected future climate change. Although later dormancy dates were predicted in the NH, earlier dormancy dates were predicted for the NCZ (Fig. 3). Dormancy dates in the NH were predicted to be 0.5 ± 3 d (RCP 4.5) and 1.1 ± 3 d (RCP 8.5) later on average (±SD) for 2041–2050 compared with recent dates (2001–2010). In contrast, dormancy dates for NCZ forests were predicted to be 2.6 ± 3 d (RCP 4.5) and 1.3 ± 3 d (RCP 8.5) earlier on average across the region compared with current (2001–2010) conditions (first to third rows in Fig. 3). For the two scenarios in 2090–2099, dormancy dates in the NH were projected to be further delayed: 1.4 ± 3 d (RCP 4.5) and 3.8 ± 3 d (RCP 8.5). However, dormancy dates in the NCZ in 2090–2099 were 1.0 ± 3 d earlier (RCP 4.5) and were strongly advanced (12.2 ± 5 d earlier) under the RCP 8.5 scenario (fourth and fifth rows in Fig. 3). Across the landscape, dormancy dates of deciduous forest in northern region occurred earlier than in southern region over 2001–2012. Similar spatial variation of dormancy dates was predicted under the RCP 4.5 scenario for the two 10-y periods and under the RCP 8.5 scenario for the 2041–2050 period (Fig. 4*A*). However, the spatial pattern in the late century RCP 8.5 scenario is projected to be quite different (Fig. 4*A*, fifth column): the latest dormancy dates are projected for midlatitude forests and earlier dormancy is projected for southern latitudes, mirroring northern

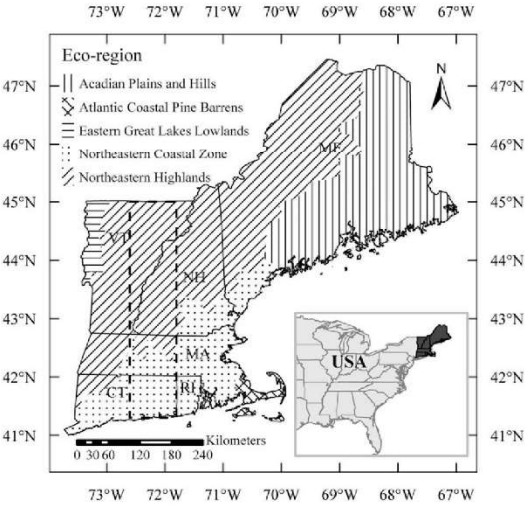

Fig. 1. Study area (dashed rectangular box) in New England, United States, covering the Connecticut River Valley from 41.3 to 45°N, 71.8 to 72.6°W, and parts of the states of Connecticut (CT), Rhode Island (RI), Massachusetts (MA), New Hampshire (NH), and Vermont (VT). Study area covers two eco-regions, NH and NCZ.

Table 1. Candidates of explanatory variables for dormancy dates

Name	Description
Cold degree day (CDD)	$\sum(T_b - T_i)$
Hot days (HD)	No. of days with $T_{max} \geq 32$ or 35 °C
Frost days (FD)	No. of days with $T_{min} \leq 0$ °C
Growing season drought (GDR)	No. of events when ≥ 7 consecutive days without precipitation
Rainy days (RD)	No. of days with precipitation ≥ 2 mm
Heavy rainy days (ECA)	No. of days with precipitation ≥ 20 mm

T_b: base temperature; T_i: daily mean temperature; T_{max}: daily maximum temperature; T_{min}: daily minimum temperature.

latitudes. Note that for the NCZ, dormancy dates are projected to be as much as 20+ days earlier than at present, whereas for the NH eco-region dormancy dates are projected to be as much as 10+ days later (Fig. 4*B*).

Discussion

Autumn phenology determining timing of the end of the growing season (i.e., dormancy), reflects plant strategic responses to all environmental stressors during the entire growing season in maximizing survival (39). Leaf senescence and dormancy result from the integration of developmental and environmental signals (40). Developmental signals including hormones and molecular regulations of growth cessation, bud set, and leaf senescence leading to dormancy have been identified in studies (30, 40, 41). However, the controlling environmental factors and how they interact to affect timing of these events is still unclear. We found that timing of fall dormancy of deciduous forest communities was affected not only by temperature, but also by a number of other environmental conditions over the growing season, including frost events, heat-stress, rainfall patterns, and drought-stress. Moreover, our models suggest nonlinear responses of dormancy to these factors, implying a complex environmental regulation of plant growth and development. Our findings support the results from previous studies: regression models with monthly precipitation had smaller RMSE than CDD-photoperiod models for autumn phenology of selected tree species (28), and summer severe drought followed by rains in autumn caused delayed leaf senescence of selected deciduous tree species in Europe in 2013 (42).

At least two possible interpretations relating plant phenological responses in the autumn to environmental stresses may be relevant in interpreting our results. One is viewed as the traditional explanation for autumnal dormancy in plants, that arresting growth and entering dormancy early avoids unfavorable, or damaging growing season conditions and facilitates the diversion of more resources for use in subsequent years, thus maximizing longer-term fitness (25, 30, 43). This finding explains negative correlations between dormancy dates and autumnal CDD, frost, and high heat-stress days (Table 2). An alternative possibility is that some environmental stressors may actually delay leaf senescence; a very limited number of studies that have examined the effects of a range of environmental stressors on fall phenology support this interpretation. We found that moderate summer heat-stress, summer and fall drought-stress, and summer heavy rain events, all lead to later autumn dormancy, counter to the traditional expectations. Studies on economically important plants (e.g., apples, soybeans, birch) have shown that under moderate heat- or water-stress in summer and fall, associated changes occur in gene-regulated levels of plant hormones and stress-shock proteins (44–46). The regulatory and physiological changes not only induce greater drought tolerance in plant leaves (47), but also prevent drought-induced cell death in leaves (that would otherwise lead to leaf senescence), and alter photosynthate source-sink relationships among plant organs (roots, stems, and leaves). The net result is delayed autumn senescence and dormancy. This finding suggests a long-term advantage in resource storage and reallocation for plant growth in the spring. However, this phenomenon has been little studied (45). Few studies have mentioned either the effects of heat- and drought-stress on fall phenology (45, 48) or the potential role of the underlying molecular and physiological mechanisms (44, 46). We have an ongoing project of ground-based phenological observations (*SI Appendix*, Fig. S2*A*) suggesting delayed effects from autumn drought on leaf coloration and leaf drop based on preliminary results. Clearly there is much to be done to fully elucidate the role that environmental factors, other than simply cold and frost, have on determining autumnal phenological events, as well as their underlying gene-regulatory and physiological bases.

We found higher sensitivities to CDD and heat stress for the southern region (NCZ) than the northern region (NH) of the study area. These results are similar to previous studies (23, 24) reporting higher phenological sensitivities of deciduous trees to temperature change at lower latitudes. However, we also found the sensitivity of fall dormancy dates to drought was higher in northern areas than in southern areas. These differences are likely a result of differences in forest tree species compositions in two eco-regions. Maples and birches dominate (45% biomass on average) the north (NH), whereas oaks dominate (35% biomass on average) the south (NCZ) (*SI Appendix*, Table S3). With higher drought tolerance, oaks may show lower sensitivity to drought stress than maples or birches (49, 50).

The studies that typically only considered projected warming effects (28, 29) all showed a consistent, progressive delay in the onset of fall leaf senescence and dormancy under projected climate change, but our study projected a slightly later dormancy in northern areas and earlier dormancy in coastal areas, especially under the RCP 8.5 scenario. Comparing climatic variables between the current and future periods, we found that lower values for CDD, fewer frosts, and more moderate heat-stress days in summer, were the main drivers for delaying dormancy dates in two eco-regions (*SI*

Table 2. Coefficients of variables in the best models of two eco-regions (mean value and SD)

Variables	Northeastern Highlands	Northeastern Coastal Zone
Latitude	−4.255 (0.097)	−3.955 (0.151)
Elevation	−0.007 (0.0004)	−0.017 (0.001)
$CDD_{20(Aug.1–Nov.15)}$	−0.022 (0.001)	−0.029 (0.001)
$FD_{(Sep.1–Nov.15)}$	—	−0.269 (0.018)
$FD_{(Sep.1–Nov.15)}^2$	0.004 (0.0003)	—
$FD_{(Apr.1–un.30)}$	−0.059 (0.009)	—
$HD_{32(Jul.1–Aug.31)}$	1.111 (0.076)	1.611 (0.033)
$HD_{35(Jul.1–Aug.31)}$	−0.821 (0.161)	−1.706 (0.051)
$GDR_{(May.1–Jun.30)}$	—	−0.079 (0.012)
$GDR_{(Jul.1–Aug.31)}$	0.088 (0.022)	0.050 (0.013)
$GDR_{(Sep.1–Nov.15)}$	0.755 (0.028)	0.111 (0.009)
$GDR_{(Sep.1–Nov.15)}^2$	−0.029 (0.002)	—
$RD_{(May.1–Jun.30)}$	−0.192 (0.012)	—
$RD_{(Jul.1–Aug.31)}$	0.578 (0.068)	−0.099 (0.012)
$RD_{(Jul.1–Aug.31)}^2$	−0.012 (0.002)	—
$RD_{(Sep.1–Nov.15)}$	−0.067 (0.012)	0.743 (0.085)
$RD_{(Sep.1–Nov.15)}^2$	—	−0.019 (0.002)
$ECA_{(May.1–Jun.30)}$	−0.206 (0.025)	−0.243 (0.022)
$ECA_{(Jul.1–Aug.31)}$	0.124 (0.022)	0.372 (0.023)
$ECA_{(Sep.1–Nov.15)}$	0.286 (0.021)	−0.795 (0.064)
$ECA_{(Sep.1–Nov.15)}^2$	—	0.083 (0.006)
$FD_{(Sep.1–Nov.15)}$ × Elevation	—	0.002 (0.0008)
$HD_{32(Jul.1–Aug.31)}$ × $RD_{(Jul.1–Aug.31)}$	−0.058 (0.006)	−0.093 (0.002)

All coefficients are significantly different from zero. T_b of CDD is 20 °C, and HD has two thresholds, 32 °C and 35 °C. The time period calculated for the variables are shown in subscript in brackets for different seasons (spring: May–June; summer: July–August; fall: September1–November 15). Positive coefficients promote later fall dormancy; negative coefficients promote earlier fall dormancy. Dash indicates variables not included in the best models.

ECOLOGY

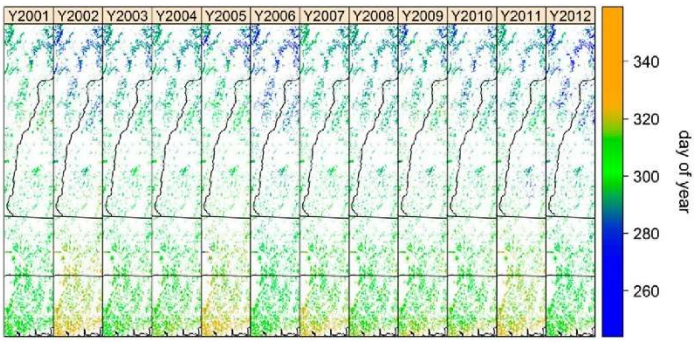

Fig. 2. Dormancy dates (day of year) for deciduous forests across study area from 2001 to 2012. Small values (blue pixels) indicate early dormancy dates and large values (orange pixels) indicate late dormancy dates. Black lines are state boundaries (Connecticut at the bottom, Massachusetts next, then Vermont upper left, and New Hampshire upper right). White areas indicate nondeciduous forest area; see also study area shown in Fig. 1.

Appendix, Figs. S4 and S5). However, there are also antagonistic factors operating at the same time that lead to earlier fall dormancy: that is, in the future higher heat-stress, slightly less drought, and significant interaction effects between moderate heat-stress and summer rainfall. The heat-stress effects were stronger than the lower chill effects in NCZ eco-region, leading to earlier dormancy dates (*SI Appendix*, Fig. S5). Although warmer autumn may extend forest growing season, earlier leaf dormancy can be forced under higher heat-stress during the summer from climate change. This finding suggests that multiple impacts from projected climate with more identified stresses, in addition to warming, will in concert affect autumn phenology of deciduous forest trees in the future. Recent studies pointing out the positive correlation between spring and fall phenology (51, 52), further support our finding that autumn phenology responds to weather spanning the full growing season.

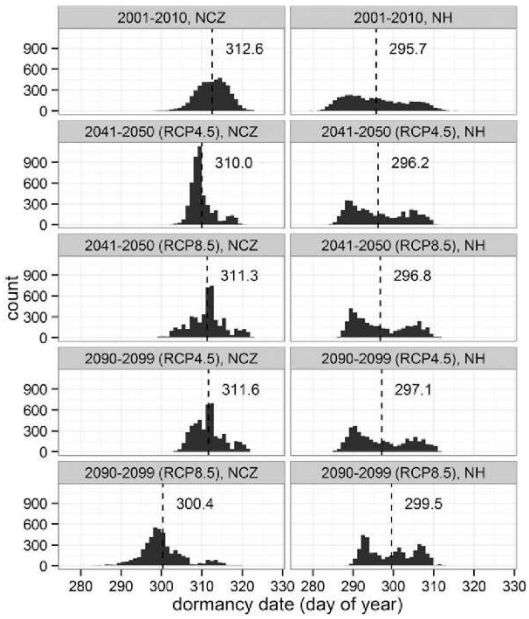

Fig. 3. Histogram of 10-y averaged dormancy dates in three 10-y periods (current: 2001–2010, and projected future: 2041–2050, 2090–2099) with two climate change projection scenarios (RCP 4.5 and RCP 8.5) across the two eco-regions (NCZ and NH). Dashed lines and numbers indicate mean values of predicted dormancy dates.

Moreover, these responses will be spatially and temporally complex: different phenological responses will likely occur in different regions, given the spatial variation in climate variables across the landscape.

From the variable selection methods, the very slight difference in predictor coefficients, model selection criteria, and RMSE (*SI Appendix*, Tables S1 and S2) suggested that multicollinearity does not significantly affect model fitting or predictions. RMSE in model validation (2011–2012) suggested predictive uncertainties were about 14.2 (NH) and 6.7 (NCZ) days (*SI Appendix*, Tables S1 and S2), which include data uncertainty in the MODIS and climate data because of data quality and model uncertainties; this is within the limits of the temporal resolution of MODIS phenology data summarized at 8-d intervals.

We encourage further investigations on physiological responses of autumn phenology to multiple environmental stresses, including interactions among stresses and nonlinear effects, and collecting long-term datasets across more species, communities, and ecosystems, including field observations and physiological experiments, to better inform future predictions and narrow model uncertainties. Species-specific phenological responses also need to be integrated into forest community phenology models in the future to better predict individual species- and community- or landscape-level responses (53). Indeed the bimodality in dormancy responses for the NH (Fig. 3) may reflect this issue.

Materials and Methods

Study Area. A rectangular area (72.6°W to 71.8°W, 41.3°N to 45°N) was selected in New England, United States as the study area (Fig. 1). This area covers two ecological regions: the Northeastern Highlands (NH) and Northeastern Coastal Zone (NCZ) (archive.epa.gov/wed/ecoregions/web/html/na_eco.html). These two eco-regions are geographically and ecologically different representing a large variation of landscape, species composition, and environmental conditions in deciduous forest communities in New England (*SI Appendix*, Fig. S6). The NH is a mountainous area with elevations up to 1,000 m higher than the NCZ, which comprises coastal plains with hills rising to about 400 m, and overall the NH has a cooler and wetter climate than the NCZ. For forest tree species composition, deciduous forests in the NH are dominated by maples and birches, whereas the NCZ deciduous forest is dominated by oaks (*SI Appendix*, Table S3).

Data and Processing. The MODIS Land Cover Dynamics (MCD12Q2) product (the NASA Land Processes Distributed Active Archive Center, US Geological Survey/Earth Resources Observation and Science Center) provides estimates of the timing of vegetation phenology at regional to global scale based on the remotely sensed vegetation index summarized at 8-d temporal resolution. The MODIS data product derives four phenological transition dates (green-up, maturity, senescence, and dormancy) from 2001 to 2012 with a spatial resolution of 500 m (28) (*SI Appendix*, Fig. S1). This study focuses on dormancy dates in fall. By using 30-m resolution land cover data from National Oceanic and Atmospheric Association's Coastal Services Center C-CAP 2001 dataset (coast.noaa.gov/dataregistry/search/collection/info/ccapregional), we extracted MODIS pixels corresponding to deciduous forest in the study area. The percentage of deciduous forest cover in each MODIS grid cell was calculated by combining land cover and phenology data. MODIS pixels with at least 75% deciduous forests were retained for analysis. We

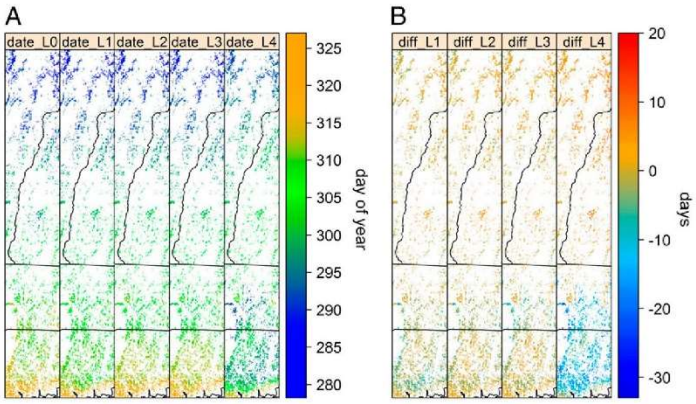

Fig. 4. (*A*) Maps of 10-y averaged dormancy dates for deciduous forests across the region over different 10-y periods with two climate change projection scenarios. L0: 2001–2010; L1: 2041–2050, RCP 4.5; L2: 2090–2099, RCP 4.5; L3: 2041–2050, RCP 8.5; L4: 2090–2099, RCP 8.5. (*B*) Difference of dormancy dates between current period and predicted periods in study area. Positive values (warm color) indicate delayed dormancy dates in the future compared with the current period, and negative values (cold color) indicate earlier dormancy dates in the future. In both plots, black lines are state boundaries and white areas indicate nondeciduous forest areas; see also study area shown in Fig. 1.

removed outliers from the analyses that showed dormancy occurring before Julian day 244 (September 1 or August 31) or after Julian day 360 (December 26 or 25). These outliers are less than 1% of the MODIS phenology data in the deciduous forest region, and are likely because of subpixel patches of agricultural fields being plowed, forest patches being defoliated or harvested, or the occurrence of grassy areas that remain green well into the winter. The final phenology data set included about 9,500 grid cells for each year for two eco-regions. Digital elevation data (srtm.csi.cgiar.org/) with a spatial resolution of 90 m were aggregated to generate elevation data for the 500-m MODIS grid cells.

We used gridded daily weather data from 2001 to 2012 obtained from PRISM climate group to develop the explanatory weather variables. The data included daily mean, maximum, and minimum temperature and daily precipitation with a spatial resolution of 4 km (54), which can be used to summarize a broad range of different weather indices (55). Statistically downscaled climate projection data for one global climate model (GCM, GFDL-ESM2G) with two future scenarios (RCP 4.5 and RCP 8.5) were obtained from Multivariate Adaptive Constructed Analogs group for model predictions (37). We used daily maximum and minimum temperature and daily precipitation over two 10-y periods (2041–2050 and 2090–2099) with a spatial resolution of 4 km, which is comparable to the PRISM data.

To find the relationships between environmental factors and dormancy of deciduous forests, we first built a list of weather variables of potential environmental conditions that may affect fall phenology including cold, frost, heat, rainfall, drought, and flood events (Table 1 and *SI Appendix*, Fig. S6). Accumulating CDDs (28, 56) and decreasing day length that occur in fall have long been considered as the primary triggers of leaf senescence and dormancy. Because day length does not have year-to-year variation, we did not investigate the effect of day length effect; rather this effect is taken into account in the latitudinal variation (57). The other variables in Table 1 represent environmental/weather stressors potentially affecting tree performance (55, 58, 59). Plant responses to stresses may differ depending on when stresses occur in different seasons, and the specific species involved (56, 60–62). The physiological requirements of trees may also differ in different phenophases (62, 63). We calculated three sets of weather variables, growing season drought, rainy days, and heavy rainy days, for three periods (May 1 to June 30, July 1 to August 31, and September 1 to November 15). For CDD, we examined the effects of three different base temperatures (10°, 15°, and 20 °C) and starting dates (July 1, August 1, and September 1) to determine which period of CDD with what base temperature may best explain dormancy timing variation across the deciduous forest landscape. The end date of CDD was set as November 15, the 90th percentile of dormancy dates in the whole study region. We also used different threshold temperatures (32° and 35 °C) for hot days and we found hot days only occurred in July and August in the study area. There was no frost between June 30 and September 1 in study area, so we only calculated FD for two periods (April 1 to May 31 and September 1 to November 15), representing spring and fall growing season frosts.

Statistical Modeling. Datasets from two eco-regions were analyzed separately because dormancy dates in two eco-regions fall in two different normal distributions. Data from 2001 to 2010 were used as model training data, and data from 2011 to 2012 were used in model validation. From initial exploratory data analyses, we selected one CDD variable with the highest correlation coefficient with dormancy dates plus other variables with a limited number of quadratic and interaction terms between predictors for each eco-region in subsequent analyses. Large number of explanatory variables from a large-scale dataset with multicollinearity among variables (e.g., correlations between temperature and latitude, latitude, and elevation) make variable selection and interpretation quite challenging (64). Thus, in addition to multiple linear regression, we used several complementary statistical methods to select important predictors explaining variation in dormancy dates. Variable selection methods include penalized regression methods, BMA (35), and Bayesian spike and slab regression (36). The penalized regression methods used were: ridge regression (65), Bayesian Least Absolute Shrinkage and Selection Operator (Bayesian LASSO) (66), the Elastic Net (67), and Pairwise Absolute Clustering and Sparsity method (PACS) (68). Penalized regression methods apply penalties to estimate coefficients with shrinkage effects of driving coefficients to be zero, which can simultaneously select important variables and estimate coefficients in the model. PACS and Elastic Net can especially select groups of correlated variables to deal with multicollinearity (67, 68). BMA provides a coherent mechanism to take account of model uncertainty by determining the coefficient of each variable using the weighted average of the parameter's posterior estimate in each model on the entire model space (35). To choose a model for future prediction, the model consisting of those variables that have overall posterior inclusion probability equal to or greater than 0.5 was considered as the optimal predictive model (38); this is termed the "posterior median model" and is easily found in BMA procedures. Bayesian spike and slab regression used a mixture of "slab distribution" (e.g., normal distribution) and "spike distribution" (e.g., a probability mass at zero) as a prior distribution to segregate the variable coefficients to be exactly zero in the induced posterior (36). Data were analyzed using software R (69) (see *SI Appendix* for R codes).

The Akaike Information Criterion (AIC) (70), Bayesian Information Criterion (BIC) (71), and RMSE were used for model selection. Models from all eight methods were used to predict dormancy dates for 2011–2012 as model validation. AIC, BIC, and RMSE were calculated for model estimation (2001–2010) and validation (2011–2012) (*SI Appendix*, Tables S1 and S2). Best models were selected by smallest AIC, BIC, and RMSE indicating best model fitting and prediction. Based on future climate projection data, dormancy dates of deciduous forests in two eco-regions were predicted by the best models for two 10-y periods, 2041–2050 and 2090–2099, with two scenarios (RCP 4.5 and RCP 8.5). We calculated 10-y average dormancy dates of period, 2001–2010, as a base line, and then compared these to 10-y averaged dormancy dates in future periods.

ACKNOWLEDGMENTS. We thank R. Primack, J. Allen, M. Aiello-Lammens, C. Merow, E. Adams, and two anonymous reviewers for helpful comments. This study was supported in part by National Science Foundation Grant DEB 0842465 (to J.A.S.).

1. Peñuelas J, Filella I (2001) Phenology. Responses to a warming world. *Science* 294(5543):793–795.
2. Parmesan C, Yohe G (2003) A globally coherent fingerprint of climate change impacts across natural systems. *Nature* 421(6918):37–42.
3. Miller-Rushing AJ, Primack RB (2008) Global warming and flowering times in Thoreau's Concord: A community perspective. *Ecology* 89(2):332–341.
4. Ibáñez I, et al. (2010) Forecasting phenology under global warming. *Philos Trans R Soc Lond B Biol Sci* 365(1555):3247–3260.

5. Cleland EE, Chuine I, Menzel A, Mooney HA, Schwartz MD (2007) Shifting plant phenology in response to global change. *Trends Ecol Evol* 22(7):357–365.
6. Cook BI, Wolkovich EM, Parmesan C (2012) Divergent responses to spring and winter warming drive community level flowering trends. *Proc Natl Acad Sci USA* 109(23):9000–9005.
7. Ovaskainen O, et al. (2013) Community-level phenological response to climate change. *Proc Natl Acad Sci USA* 110(33):13434–13439.
8. Estiarte M, Peñuelas J (2014) Alteration of the phenology of leaf senescence and fall in winter deciduous species by climate change: Effects on nutrient proficiency. *Glob Change Biol* 21(3):1005–1017.
9. Chuine I (2000) A unified model for budburst of trees. *J Theor Biol* 207(3):337–347.
10. Körner C, Basler D (2010) Plant science. Phenology under global warming. *Science* 327(5972):1461–1462.
11. Polgar CA, Primack RB (2011) Leaf-out phenology of temperate woody plants: From trees to ecosystems. *New Phytol* 191(4):926–941.
12. Clark JS, Melillo J, Mohan J, Salk C (2014) The seasonal timing of warming that controls onset of the growing season. *Glob Change Biol* 20(4):1136–1145.
13. Allen JM, et al. (2014) Modeling daily flowering probabilities: Expected impact of climate change on Japanese cherry phenology. *Glob Change Biol* 20(4):1251–1263.
14. Estrella N, Menzel A (2006) Responses of leaf colouring in four deciduous tree species to climate and weather in Germany. *Clim Res* 32(3):253–267.
15. Vitasse Y, Porté AJ, Kremer A, Michalet R, Delzon S (2009) Responses of canopy duration to temperature changes in four temperate tree species: Relative contributions of spring and autumn leaf phenology. *Oecologia* 161(1):187–198.
16. Gallinat AS, Primack RB, Wagner DL (2015) Autumn, the neglected season in climate change research. *Trends Ecol Evol* 30(3):169–176.
17. Weih M (2009) Genetic and environmental variation in spring and autumn phenology of biomass willows (*Salix* spp.): Effects on shoot growth and nitrogen economy. *Tree Physiol* 29(12):1479–1490.
18. Fridley JD (2012) Extended leaf phenology and the autumn niche in deciduous forest invasions. *Nature* 485(7398):359–362.
19. Pépino M, Proulx R, Magnan P (2013) Fall synchrony between leaf color change and brook trout spawning in the Laurentides Wildlife Reserve (Québec, Canada) as potential environmental integrators. *Ecol Indic* 30:16–20.
20. Spencer DM, Holecek DF (2007) A profile of the fall foliage tourism market. *J Vacation Marketing* 13(4):339–358.
21. Rustad L, et al. (2011) *Changing Climate, Changing Forests: The Impacts of Climate Change on Forests of the Northeastern United States and Easter Canada*. USDA Forest Service Northern Research Station General Technical Report NRS-99. (US Department of Agriculture, Forest Service, Newtown Square, PA) 48 pp.
22. Ge Q, Dai J, Liu J, Zhong S, Liu H (2013) The effect of climate change on the fall foliage vacation in China. *Tour Manage* 38:80–84.
23. Doi H, Takahashi M (2008) Latitudinal patterns in the phenological responses of leaf colouring and leaf fall to climate change in Japan. *Glob Ecol Biogeogr* 17(4):556–561.
24. Dragoni D, Rahman AF (2012) Trends in fall phenology across the deciduous forests of the Eastern USA. *Agric For Meteorol* 157:96–105.
25. Paul LK, Rinne PL, van der Schoot C (2014) Shoot meristems of deciduous woody perennials: Self-organization and morphogenetic transitions. *Curr Opin Plant Biol* 17:86–95.
26. Hänninen H, Tanino K (2011) Tree seasonality in a warming climate. *Trends Plant Sci* 16(8):412–416.
27. Zhang X, et al. (2003) Monitoring vegetation phenology using MODIS. *Remote Sens Environ* 84(3):471–475.
28. Archetti M, Richardson AD, O'Keefe J, Delpierre N (2013) Predicting climate change impacts on the amount and duration of autumn colors in a New England forest. *PLoS One* 8(3):e57373.
29. Jeong S-J, Medvigy D (2014) Macroscale prediction of autumn leaf coloration throughout the continental United States. *Glob Ecol Biogeogr* 23(11):1245–1254.
30. Lim PO, Kim HJ, Nam HG (2007) Leaf senescence. *Annu Rev Plant Biol* 58:115–136.
31. Samish RM (1954) Dormancy in woody plants. *Annu Rev Plant Physiol* 5(1):183–204.
32. Rosenthal SI, Camm EL (1997) Photosynthetic decline and pigment loss during autumn foliar senescence in western larch (*Larix occidentalis*). *Tree Physiol* 17(12):767–775.
33. Frachebourd Y, et al. (2009) The control of autumn senescence in European aspen. *Plant Physiol* 149(4):1982–1991.
34. Garcia RA, Cabeza M, Rahbek C, Araújo MB (2014) Multiple dimensions of climate change and their implications for biodiversity. *Science* 344(6183):1247579.
35. Hoeting JA, Madigan D, Raftery AE, Volinsky CT (1999) Bayesian Model Averaging: A tutorial. *Stat Sci* 14(4):382–417.
36. Ishwaran H, Rao JS (2005) Spike and slab variable selection: Frequentist and Bayesian strategies. *Ann Stat* 33(2):730–773.
37. Abatzoglou JT, Brown TJ (2012) A comparison of statistical downscaling methods suited for wildfire applications. *Int J Climatol* 32(5):772–780.
38. Barbieri MM, Berger JO (2004) Optimal predictive model selection. *Ann Stat* 32(3):870–897.
39. Günthardt-Goerg MS, Vollenweider P (2007) Linking stress with macroscopic and microscopic leaf response in trees: New diagnostic perspectives. *Environ Pollut* 147(3):467–488.
40. Cooke JE, Eriksson ME, Junttila O (2012) The dynamic nature of bud dormancy in trees: Environmental control and molecular mechanisms. *Plant Cell Environ* 35(10):1707–1728.
41. Jibran R, A Hunter D, P Dijkwel P (2013) Hormonal regulation of leaf senescence through integration of developmental and stress signals. *Plant Mol Biol* 82(6):547–561.
42. Leuzinger S, Zotz G, Asshoff R, Körner C (2005) Responses of deciduous forest trees to severe drought in Central Europe. *Tree Physiol* 25(6):641–650.
43. Larcher W (2003) *Physiological Plant Ecology: Ecophysiology and Stress Physiology of Functional Groups* (Springer, New York), 4th Ed.
44. Carvalho HH, et al. (2014) The molecular chaperone binding protein BiP prevents leaf dehydration-induced cellular homeostasis disruption. *PLoS One* 9(1):e86661.
45. Naschitz S, Naor A, Wolf S, Goldschmidt EE (2014) The effects of temperature and drought on autumnal senescence and leaf shed in apple under warm, east Mediterranean climate. *Trees (Berl)* 28(3):879–890.
46. Xu Y, Huang B (2007) Heat-induced leaf senescence and hormonal changes for thermal bentgrass and turf-type bentgrass species differing in heat tolerance. *J Am Soc Hortic Sci* 132(2):185–192.
47. Rivero RM, et al. (2007) Delayed leaf senescence induces extreme drought tolerance in a flowering plant. *Proc Natl Acad Sci USA* 104(49):19631–19636.
48. Pääkkönen E, Vahala J, Holopainen T, Kärenlampi L (1998) Physiological and ultrastructural responses of birch clones exposed to ozone and drought stress. *Chemosphere* 36(4):679–684.
49. Hinckley TM, Dougherty PM, Lassoie JP, Roberts JE, Teskey RO (1979) A severe drought: Impact on tree growth, phenology, net photosynthetic rate and water relations. *Am Midl Nat* 102(2):307–316.
50. Caspersen JP, Kobe RK (2001) Interspecific variation in sapling mortality in relation to growth and soil moisture. *Oikos* 92(1):160–168.
51. Fu YSH, et al. (2014) Variation in leaf flushing date influences autumnal senescence and next year's flushing date in two temperate tree species. *Proc Natl Acad Sci USA* 111(20):7355–7360.
52. Keenan TF, Richardson AD (2015) The timing of autumn senescence is affected by the timing of spring phenology: Implications for predictive models. *Glob Chang Biol* 21(7): 2634–2641.
53. Diez JM, et al. (2012) Forecasting phenology: From species variability to community patterns. *Ecol Lett* 15(6):545–553.
54. PRISM Climate Group (2004) *Prism Climate Data*, Available at prism.oregonstate.edu. Accessed June 25, 2014.
55. Wilson AM, Silander JA, Jr (2014) Estimating uncertainty in daily weather interpolations: A Bayesian framework for developing climate surfaces. *Int J Climatol* 20(8): 1251–1263.
56. Richardson AD, Bailey AS, Denney EG, Martin CW, O'Keefe J (2006) Phenology of a northern hardwood forest canopy. *Glob Change Biol* 12(7):1174–1188.
57. Forsythe WC, Rykiel EJ, Stahl RS, Wu HI, Schoolfield RM (1995) A model comparison for day length as a function of latitude and day of year. *Ecol Modell* 80(1):87–95.
58. Duque AS, et al. (2013) Abiotic stress responses in plants: Unraveling the complexity of genes and networks to survive. *Abiotic Stress—Plant Responses and Applications in Agriculture*, eds Vahdati K, Leslie C (InTech, Rijeka, Croatia), pp 49–55.
59. Niinemets Ü (2010) Responses of forest trees to single and multiple environmental stresses from seedlings to mature plants: Past stress history, stress interactions, tolerance and acclimation. *For Ecol Manage* 260(10):1623–1639.
60. Bréda N, et al. (2006) Temperate forest trees and stands under severe drought: A review of ecophysiological responses, adaptation processes and long-term consequences. *Ann Sci* 63(6):625–644.
61. Primack RB, et al. (2009) Spatial and interspecific variability in phenological responses to warming temperatures. *Biol Conserv* 142(11):2569–2577.
62. Wilczek AM, et al. (2010) Genetic and physiological bases for phenological responses to current and predicted climates. *Philos Trans R Soc Lond B Biol Sci* 365(1555): 3129–3147.
63. Hwang T, et al. (2014) Divergent phenological response to hydroclimate variability in forested mountain watersheds. *Glob Change Biol* 20(8):2580–2595.
64. Dormann CF, et al. (2013) Collinearity: A review of methods to deal with it and a simulation study evaluating their performance. *Ecography* 36(1):27–46.
65. Hoerl AE, Kennard RW (1970) Ridge regression: Biased estimation for nonorthogonal problems. *Technometrics* 12(1):55–67.
66. Park T, Casella G (2008) The Bayesian LASSO. *J Am Stat Assoc* 103(482):681–686.
67. Zou H, Hastie T (2005) Regularization and variable selection via the elastic net. *J R Stat Soc, B* 67(2):301–320.
68. Sharma DB, Bondell HD, Zhang HH (2013) Consistent group identification and variable selection in regression with correlated predictors. *J Comput Graph Stat* 22(2): 319–340.
69. R Core Team (2015) *R: A Language and Environment for Statistical Computing* (R Foundation for Statistical Computing, Vienna, Austria).
70. Akaike H (1973) Information theory and an extension of the maximum likelihood principle. *Proceedings of the Second International Symposium on Information Theory*, eds Petrov BN, Caski S (Akademiai Kaido, Budapest, Hungary), pp 267–281.
71. Schwarz G (1978) Estimating the dimension of a model. *Ann Stat* 6(2):461–464.

Appendix 2.1

MODIS phenology product

The MODIS Land Cover Dynamics (MCD12Q2) Product (informally called the MODIS Global Vegetation Phenology Product) provides estimates of continuous variation in vegetation phenology at global scales. The raw data are satellite derived, Enhanced Vegetation Index (EVI) data from MODIS satellite surface-reflectance data obtained at 500m spatial resolution in each pixel of the earth globally. These data are summarized as 8-day composite EVI reflectance for each MODIS pixel as part of the MODIS Global Vegetation Phenology Product. Using the methodology developed by Zhang and colleagues (1) four key transition dates are estimated from the maximum rates of change in the curvature in EVI over time; these define the key phenological phases of vegetation dynamics at the landscape scale and annual time scales on the earth's surface: green-up (greenness starts to increase rapidly), maturity (greenness reaches maximum value), senescence (greenness starts to decrease rapidly), and dormancy (greenness reaches minimum value). See more details in the User Guide of this data product, http://www.bu.edu/lcsc/files/2012/08/MCD12Q2_UserGuide.pdf.

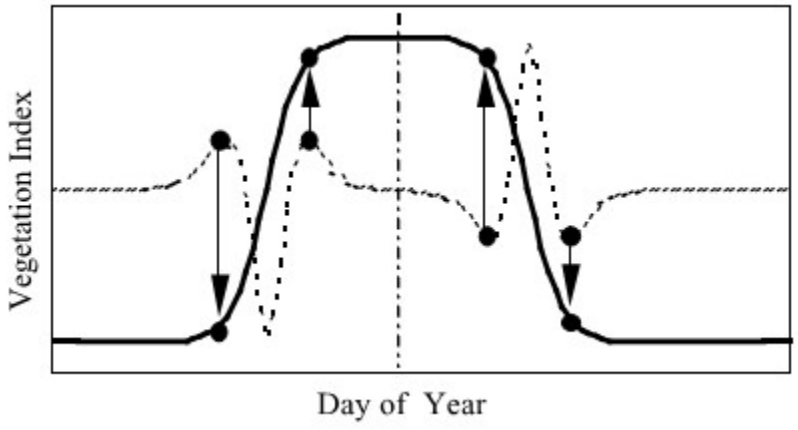

Figure 2.1-1 (Fig. 2 from ref. 1) A schematic showing how transition dates are calculated using minimum and maximum values in the rate of change in curvature. The solid line is an idealized time series of vegetation index data, and the dashed line is the rate of change in curvature from the VI data. The circles indicate transition dates. The extreme values located between each circle indicate the point at which the rate of change in curvature changes sign.

Dormancy dates derived from MODIS product are proxies of the timing of plant development stage (i.e. phenology) termed dormancy. Through comparisons among ground-based phenology observation, time series of color index from camera images, and remote sensing phenology (shown in Figure S2), dormancy dates indicate full plant dormancy, in which the greenness reaches the minimum values, shown as fully changed leaf colors to brown and leaf drop from trees. Besides Zhang's papers (1-4), many other published papers using remote sensing phenology data (also called as Land Surface Phenology) (5-6) also use the term 'dormancy' to define the final autumn phenological phase as derived from satellite data. This also corresponds to autumn dormancy in wood plants as defined by plant physiologists (8-10).

Table 2.1-1 Unstandardized coefficients of variables in eight models on deciduous forest fall dormancy dates in Northeastern Highlands from 2001 to 2010. AIC, BIC, and RMSE were calculated for 2001-2010 and 2011-2012, and yielded consistent results, so AIC, BIC, and RMSE only for 2011-2012 are shown. Smallest AIC, BIC, and RMSE are bold.

Variables	MLR	Ridge	Bayesian LASSO	Elastic Net	PACS	Spike&Slab	BMA	Posterior Median Model
Latitude	-4.206	-4.208	-4.215	-4.232	-4.211	-4.322	-4.238	-4.255
Elevation	-0.007	-0.007	-0.007	-0.007	-0.007	-0.006	-0.007	-0.007
$CDD20_{(Aug.1\text{-}Nov.15)}$	-0.022	-0.022	-0.022	-0.022	-0.022	-0.027	-0.022	-0.022
$FD_{(Sep.1\text{-}Nov.15)}$	-0.102	-0.100	-0.073	-0.030	-0.056	0	-0.024	0
$FD_{(Sep.1\text{-}Nov.15)}^2$	0.006	0.006	0.006	0.005	0.005	0.004	0.0004	0.004
$FD_{(Apr.1\text{-}Jun.30)}$	-0.052	-0.052	-0.052	-0.051	-0.052	0	-0.057	-0.059
$HD32_{(Jul.1\text{-}Aug.31)}$	1.124	1.113	1.085	0.912	1.025	1.250	0.111	1.111
$HD35_{(Jul.1\text{-}Aug.31)}$	-0.833	-0.830	-0.799	-0.762	-0.732	0	-0.824	-0.821
$GDR_{(May.1\text{-}Jun.30)}$	-0.058	-0.058	-0.055	-0.061	-0.045	0	-0.022	0
$GDR_{(Jul.1\text{-}Aug.31)}$	0.092	0.092	0.088	0.088	0.083	0	0.087	0.088
$GDR_{(Sep.1\text{-}Nov.15)}$	0.746	0.745	0.745	0.735	0.751	0.740	0.075	0.755
$GDR_{(Sep.1\text{-}Nov.15)}^2$	-0.028	-0.028	-0.028	-0.027	-0.028	-0.027	-0.029	-0.029
$RD_{(May.1\text{-}Jun.30)}$	-0.207	-0.207	-0.206	-0.208	-0.199	-0.177	-0.197	-0.192
$RD_{(Jul.1\text{-}Aug.31)}$	0.596	0.584	0.557	0.369	0.558	0.574	0.582	0.579
$RD_{(Jul.1\text{-}Aug.31)}^2$	-0.012	-0.012	-0.011	-0.007	-0.011	-0.011	-0.012	-0.012
$RD_{(Sep.1\text{-}Nov.15)}$	-0.065	-0.065	-0.062	-0.058	-0.062	0	-0.066	-0.067
$ECA_{(May.1\text{-}Jun.30)}$	-0.203	-0.203	-0.202	-0.208	-0.207	0	-0.204	-0.206
$ECA_{(Jul.1\text{-}Aug.31)}$	0.130	0.130	0.130	0.138	0.125	0	0.126	0.124
$ECA_{(Sep.1\text{-}Nov.15)}$	0.274	0.274	0.272	0.269	0.268	0	0.281	0.286
$HD32_{(Jul.1\text{-}Aug.31)}$ *$RD_{(Jul.1\text{-}Aug.31)}$	-0.057	-0.057	-0.055	-0.044	-0.051	-0.076	-0.057	-0.058
AIC(2011-2012)	49838	49841	49839	49886	49856	50026	51741	**49820**
BIC(2011-2012)	49981	49983	49983	50029	49999	50105	51884	**49949**
RMSE(2011-2012)	14.234	14.236	14.235	14.270	14.247	14.391	15.754	**14.223**

Table 2.1-2 Unstandardized coefficients of variables in eight models on deciduous forest fall dormancy dates in Northeastern Coastal Zone from 2001 to 2010. AIC, BIC, and RMSE were calculated for 2001-2010 and 2011-2012, and yielded consistent results, so AIC, BIC, and RMSE only for 2011-2012 are shown. Smallest AIC, BIC, and RMSE are bold.

Variables	MLR	Ridge	Bayesian LASSO	Elastic Net	PACS	Spike&Slab	BMA	Posterior Median Model
Latitude	-3.955	-3.956	-3.951	-3.925	-3.999	-4.054	-3.956	-3.953
Elevation	-0.017	-0.017	-0.017	-0.017	-0.017	-0.018	-0.017	-0.017
$CDD_{20(Aug.1\text{-}Nov.15)}$	-0.029	-0.029	-0.029	-0.029	-0.028	-0.027	-0.029	-0.029
$FD_{(Sep.1\text{-}Nov.15)}$	-0.269	-0.268	-0.267	-0.266	-0.269	-0.274	-0.268	-0.269
$HD_{32(Jul.1\text{-}Aug.31)}$	1.611	1.608	1.614	1.586	1.617	1.646	1.612	1.612
$HD_{35(Jul.1\text{-}Aug.31)}$	-1.706	-1.706	-1.708	-1.725	-1.720	-1.748	-1.706	-1.706
$GDR_{(May.1\text{-}Jun.30)}$	-0.079	-0.079	-0.079	-0.089	-0.084	0	-0.079	-0.078
$GDR_{(Jul.1\text{-}Aug.31)}$	0.050	0.050	0.050	0.055	0.048	0	0.049	0.050
$GDR_{(Sep.1\text{-}Nov.15)}$	0.111	0.111	0.111	0.112	0.111	0.103	0.111	0.111
$RD_{(Jul.1\text{-}Aug.31)}$	-0.099	-0.100	-0.099	-0.108	-0.101	-0.100	-0.099	-0.099
$RD_{(Sep.1\text{-}Nov.15)}$	0.743	0.737	0.722	0.529	0.587	1.002	0.744	0.742
$RD_{(Sep.1\text{-}Nov.15)}^2$	-0.019	-0.019	-0.019	-0.014	-0.015	-0.026	-0.019	-0.019
$ECA_{(May.1\text{-}Jun.30)}$	-0.243	-0.243	-0.242	-0.256	-0.255	-0.268	-0.243	-0.242
$ECA_{(Jul.1\text{-}Aug.31)}$	0.372	0.373	0.373	0.383	0.375	0.374	0.372	0.372
$ECA_{(Sep.1\text{-}Nov.15)}$	-0.795	-0.793	-0.779	-0.725	-0.768	-0.752	-0.795	-0.793
$ECA_{(Sep.1\text{-}Nov.15)}^2$	0.083	0.082	0.081	0.076	0.080	0.078	0.008	0.082
$FD_{(Sep.1\text{-}Nov.15)}$*elevation	0.002	0.002	0.002	0.002	0.002	0.002	0.002	0.002
$HD_{32(Jul.1\text{-}Aug.31)}$ *$RD_{(Jul.1\text{-}Aug.31)}$	-0.093	-0.092	-0.093	-0.090	-0.093	-0.095	-0.093	-0.093
AIC(2011-2012)	**36904**	36939	37198	36939	36927	36958	39493	36907
BIC(2011-2012)	**37034**	37068	37327	37068	37057	37073	39622	37036
RMSE(2011-2012)	**6.735**	6.747	6.838	6.747	6.743	6.755	7.700	6.736

Table 2.1-3 Mean relative biomass of top eight genera of woody plant in the two eco-regions of the study area. Values of mean relative biomass were calculated using data of 1103 plots from the Forest Inventory and Analysis (FIA) Program (http://fia.fs.fed.us/) during 2003-2010 for our spatial domain. Relative biomass of each genera of woody plant was calculated in each plot and then averaged for the two eco-regions.

Genus	Northeastern Highlands	Northeastern Coastal Zone
Acer	0.321	0.253
Betula	0.128	0.090
Carya	0.004	0.048
Fagus	0.034	0.013
Fraxinus	0.045	0.037
Populus	0.027	0.013
Prunus	0.021	0.026
Quercus	0.092	0.353

Figure 2.1-2 Growing season phenology of forest canopy trees at 3 spatial scales from observations in 2014: a) Observed percentage of leaf unfolding through to leaf drop among individuals of 6 deciduous forest species at one site (25m×50m) in one growing season (data from Xie); b) Time series of green color index extracted from digital time lapse cameras of the same site and two individual trees therein (11); c) Enhanced Vegetation Index (EVI) from MODIS (M*D13Q1) showing the 2014 canopy level phenology for the same location (250m resolution) as a & b (black points with spline curve) and 2000-2014 inter-annual variability (grey points and splines). These figures show the full annual phenological cycle for forest canopy trees (individuals to stands) at one site in a northeastern North American forest tract from leaf bud-break beginning around day 120 to fully expanded leaves around day 150, and leaf senescence beginning around day 250 and extending to leaf drop and dormancy by around day 300; compare these with idealized, yearly phenological schema shown in Figure S1.

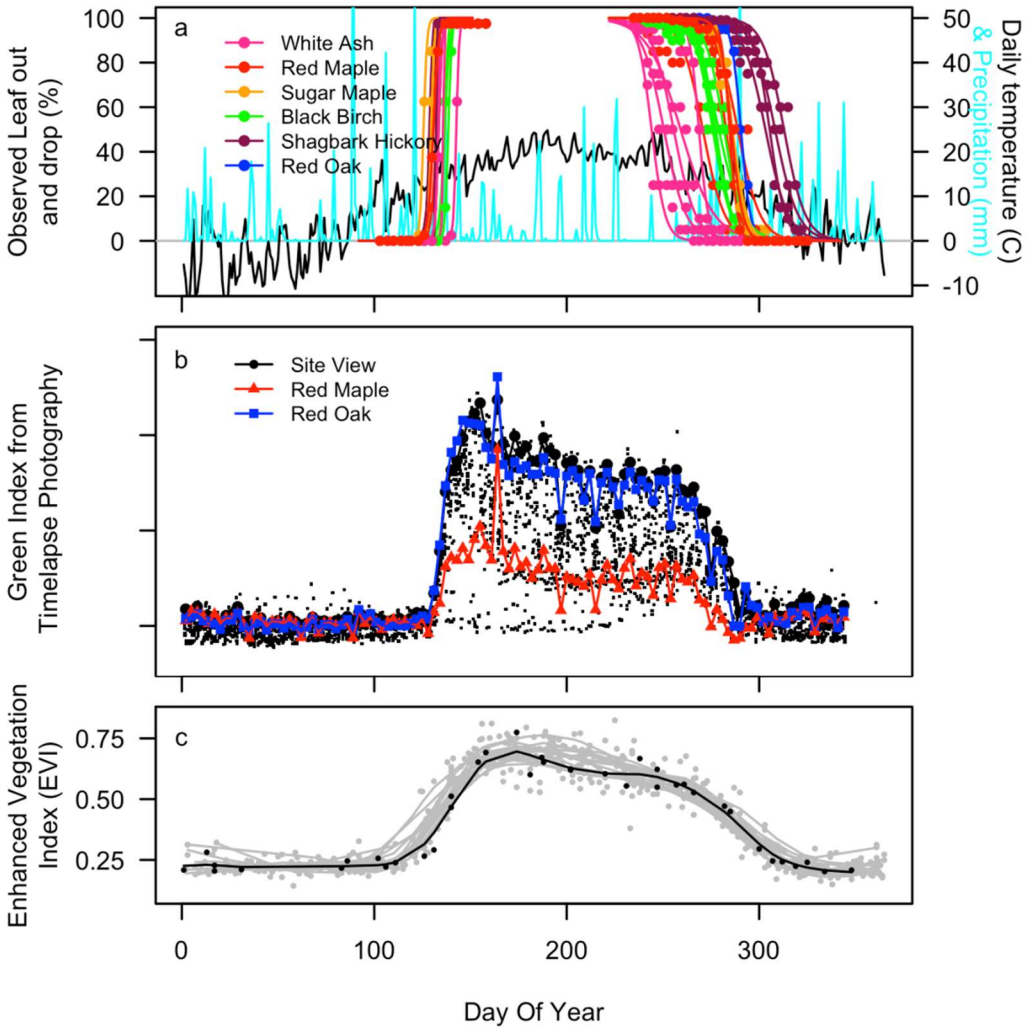

Figure 2.1-3 Added variable plots (partial regression) for four variables in the best models of two eco-regions. Variables are: latitude (lat), $CDD_{20(Aug.1\text{-}Nov.15)}$ (CDD820), $HD_{32(Jul.1\text{-}Aug.31)}$ (HD7832), and $GDR_{(Sep.1\text{-}Nov.15)}$ (GDR9d). Solid red lines are regression lines (p-value<0.001 for all lines).

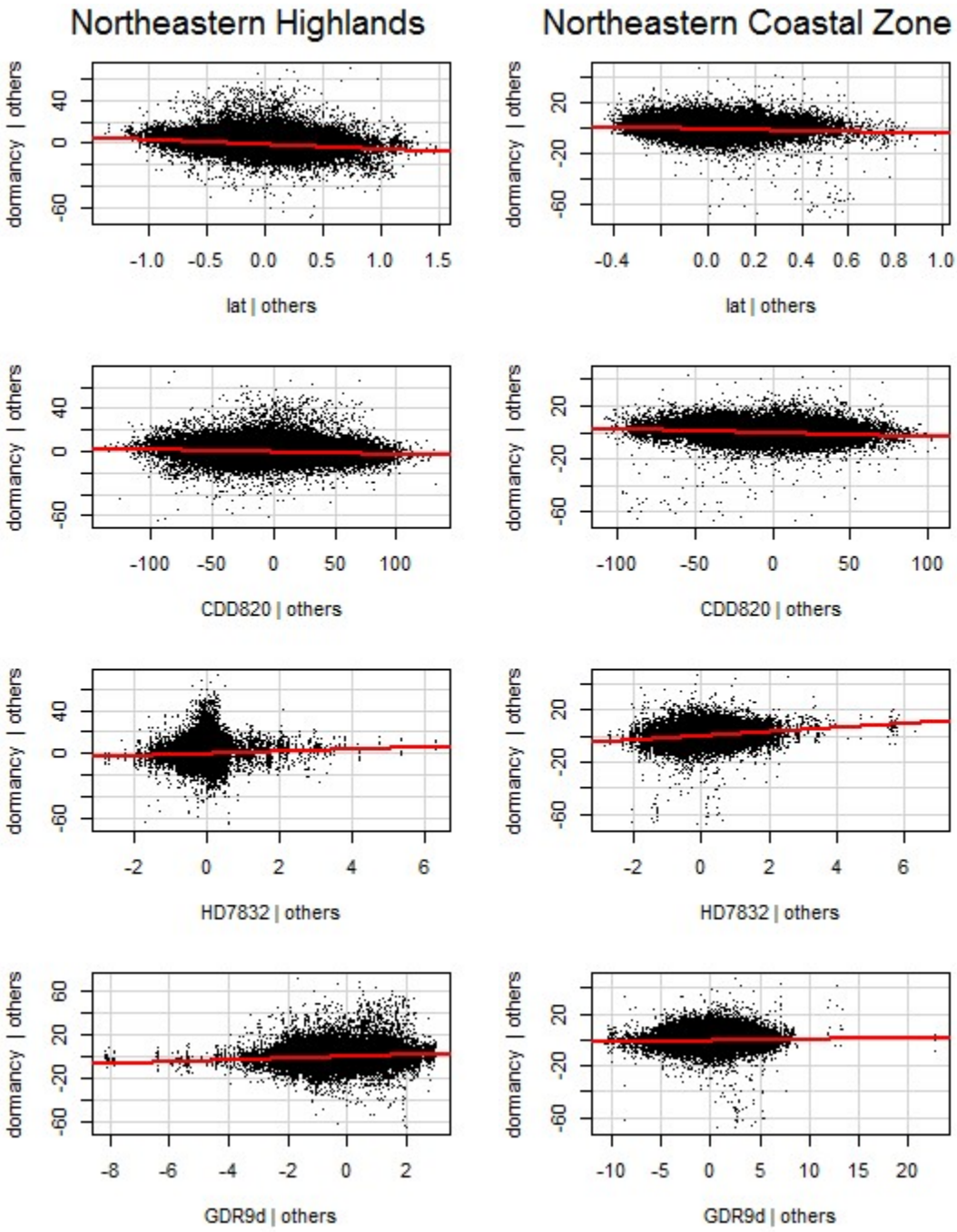

Figure 2.1-4 Boxplots of 10-year average values of climatic variables in Northeastern Highlands. The x-axis indicates different 10-year periods with climate change scenarios. L0: 2001-2010; L1: 2041-2050, RCP4.5; L2: 2090-2099, RCP 4.5; L3: 2041-2050, RCP8.5; L4: 2090-2099, RCP 8.5. Variables are: $CDD_{20(Aug.1\text{-}Nov.15)}$ (CDD820), $ECA_{(May.1\text{-}Jun.30)}$ (ECA56), $ECA_{(Jul.1\text{-}Aug.31)}$ (ECA78), $ECA_{(Sep.1\text{-}Nov.15)}$ (ECA9d), $FD_{(Sep.1\text{-}Nov.15)}^2$ (FDf_2), $FD_{(Apr.1\text{-}Jun.30)}$ (FDs), $GDR_{(Jul.1\text{-}Aug.31)}$ (GDR78), $GDR_{(Sep.1\text{-}Nov.15)}$ (GDR9d), $GDR_{(Sep.1\text{-}Nov.15)}^2$ (GDR9d_2), $HD_{32(Jul.1\text{-}Aug.31)}$ (HD7832), $HD32_{(Jul.1\text{-}Aug.31)}$*$RD_{(Jul.1\text{-}Aug.31)}$ (HD7832_RD78), $HD35_{(Jul.1\text{-}Aug.31)}$ (HD7835), $RD_{(May.1\text{-}Jun.30)}$ (RD56), $RD_{(Jul.1\text{-}Aug.31)}$ (RD78), $RD_{(Jul.1\text{-}Aug.31)}^2$ (RD78_2), and $RD_{(Sep.1\text{-}Nov.15)}$ (RD9d).

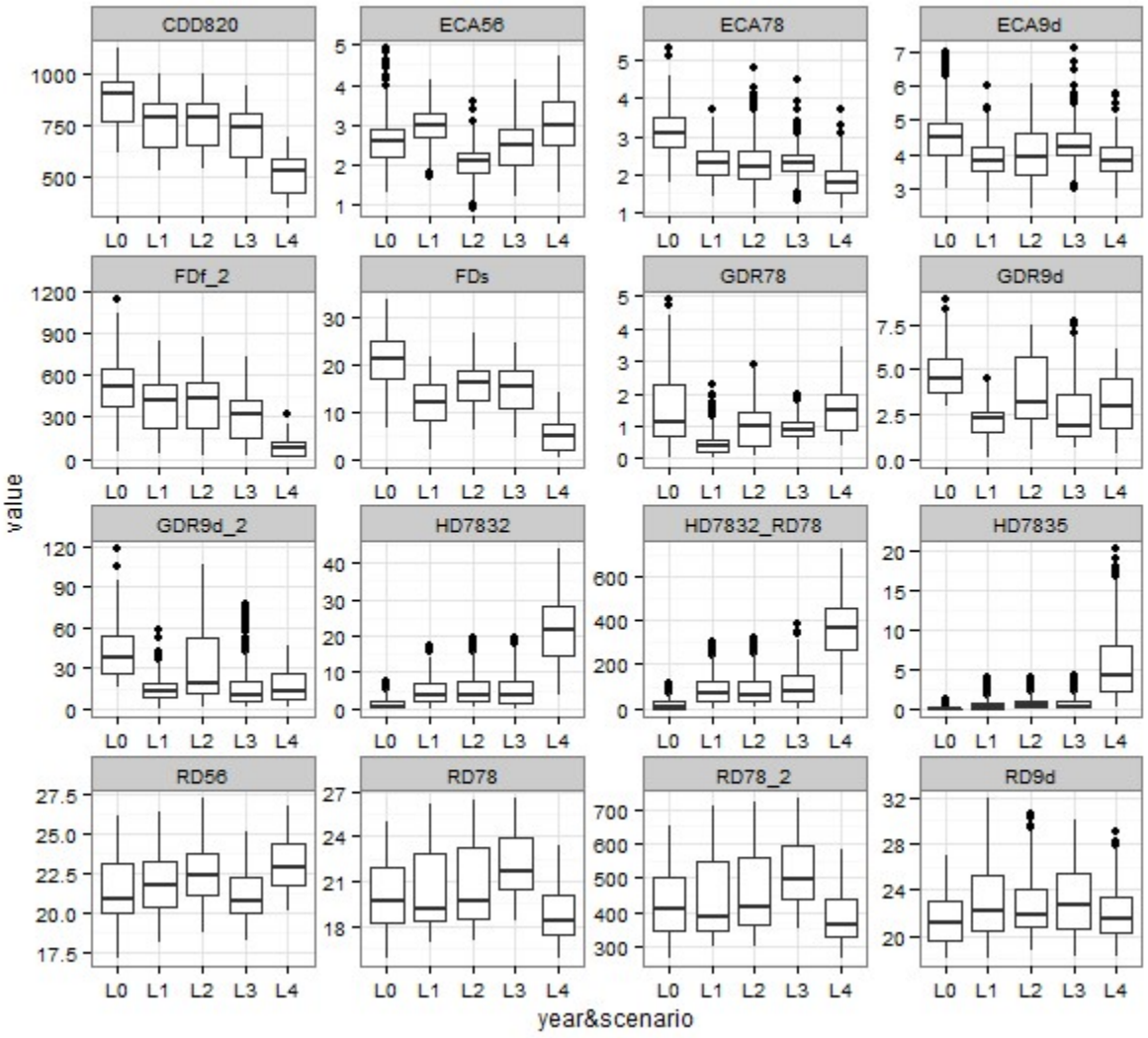

Figure 2.1-5 Boxplots of 10-year average values of climatic variables in Northeastern Coastal Zone. The x- axis indicates different 10-year periods with climate change scenarios. L0: 2001-2010; L1: 2041-2050, RCP4.5; L2: 2090-2099, RCP 4.5; L3: 2041-2050, RCP8.5; L4: 2090-2099, RCP 8.5. Variables are: $CDD_{20(Aug.1\text{-}Nov.15)}$ (CDD820), $ECA_{(May.1\text{-}Jun.30)}$ (ECA56), $ECA_{(Jul.1\text{-}Aug.31)}$ (ECA78), $ECA_{(Sep.1\text{-}Nov.15)}$ (ECA9d), $ECA_{(Sep.1\text{-}Nov.15)}^2$ (ECA9d_2), $FD_{(Sep.1\text{-}Nov.15)}$ (FDf), $FD_{(Sep.1\text{-}Nov.15)}$*elevation (FDf_elev), $GDR_{(May.1\text{-}Jun.30)}$ (GDR56), $GDR_{(Jul.1\text{-}Aug.31)}$ (GDR78), $GDR_{(Sep.1\text{-}Nov.15)}$ (GDR9d), $HD_{32(Jul.1\text{-}Aug.31)}$ (HD7832), $HD32_{(Jul.1\text{-}Aug.31)}$*$RD_{(Jul.1\text{-}Aug.31)}$ (HD7832_RD78), $HD35_{(Jul.1\text{-}Aug.31)}$ (HD7835, $RD_{(Jul.1\text{-}Aug.31)}$ (RD78), $RD_{(Sep.1\text{-}Nov.15)}$ (RD9d), and $RD_{(Sep.1\text{-}Nov.15)}^2$ (RD9d_2).

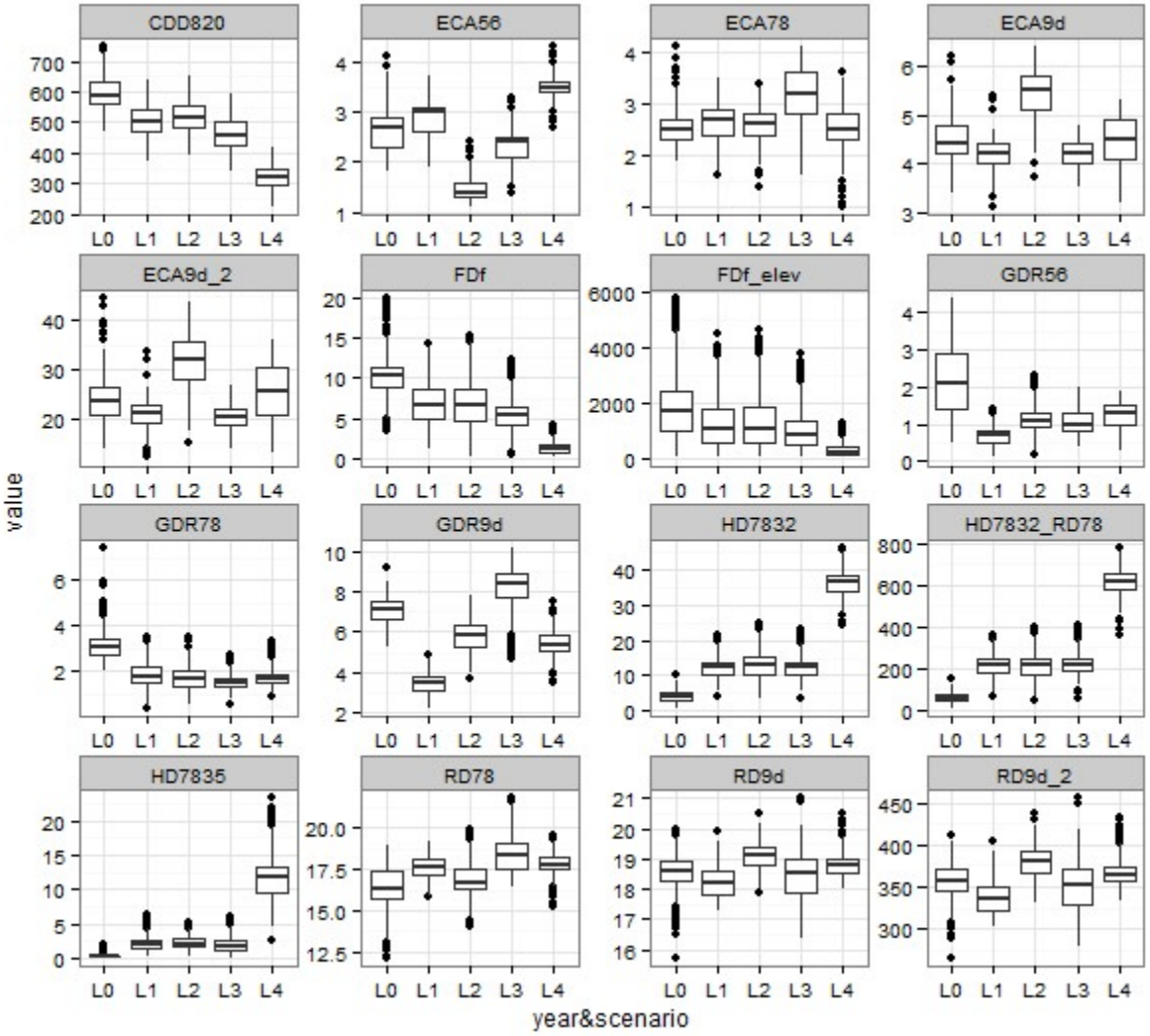

Figure 2.1-6 Values of four significant climatic factors (cf. Table 1 & 2) influencing autumn phenology across the landscape of the study domain from 2001 to 2012, showing temporal and spatial variation. (a) cumulative Cold Degree Day from Aug.1st to Nov. 15th, (b) number of frost days from Sep. 1st to Nov. 15th, (c) number of hot days with maximum temperature higher than 32°C from Jul. 1st to Aug. 31st, and (d) droughts from Sep. 1st to Nov. 15th. Data are calculated from PRISM daily weather data (http://www.prism.oregonstate.edu/). Black lines are New England states boundaries (cf. figure 1).

(a)

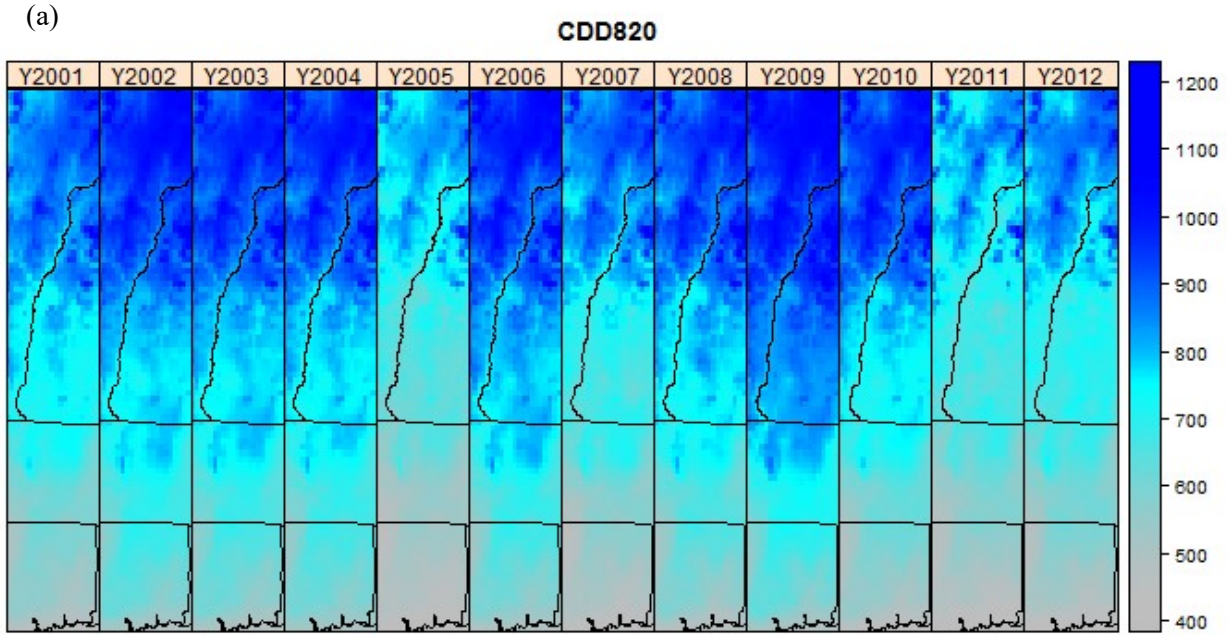

(b)

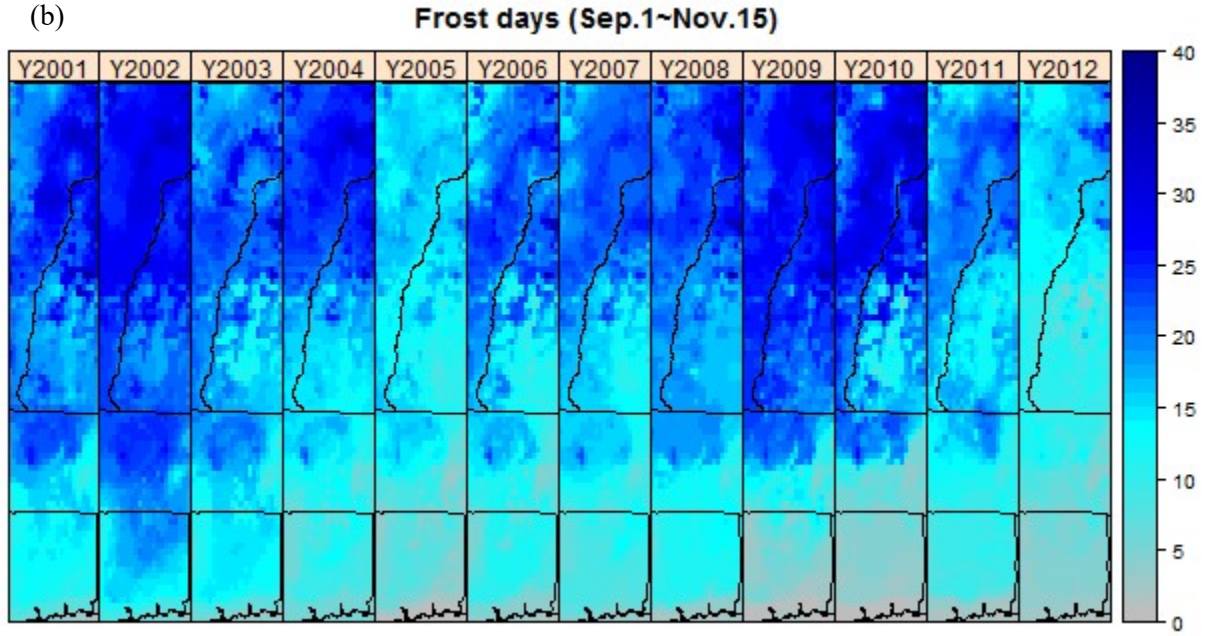

(c)

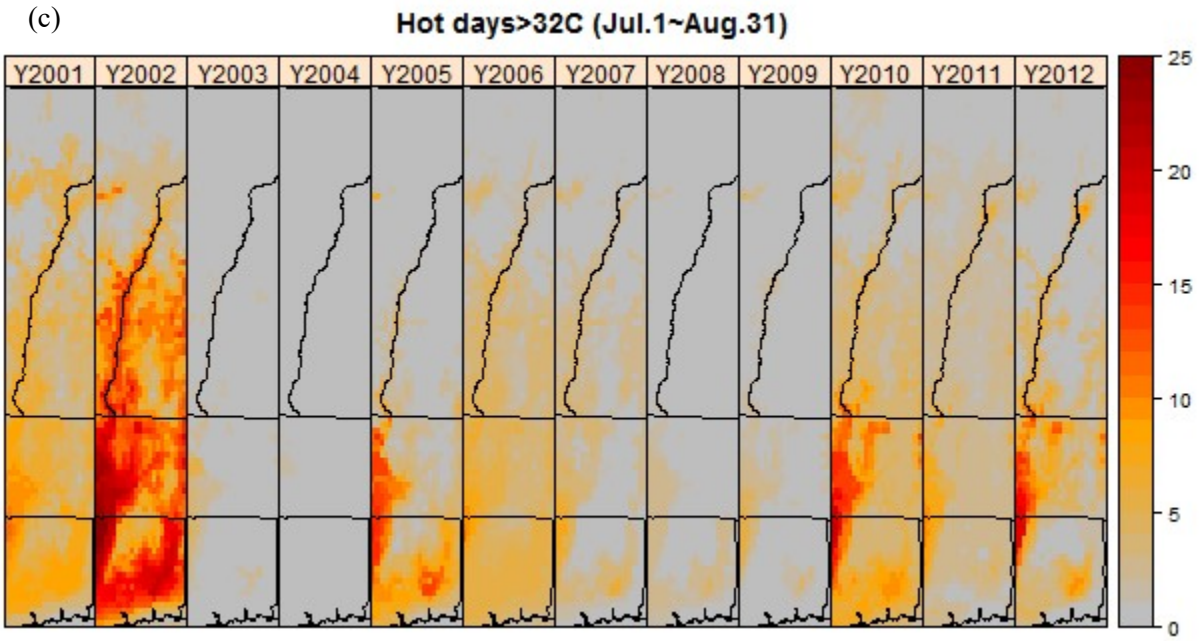
Hot days>32C (Jul.1~Aug.31)
Y2001
Y2002
Y2003
Y2004
Y2005
Y2006
Y2007
Y2008
Y2009
Y2010
Y2011
Y2012
25
20
15
10
5
0

(d)

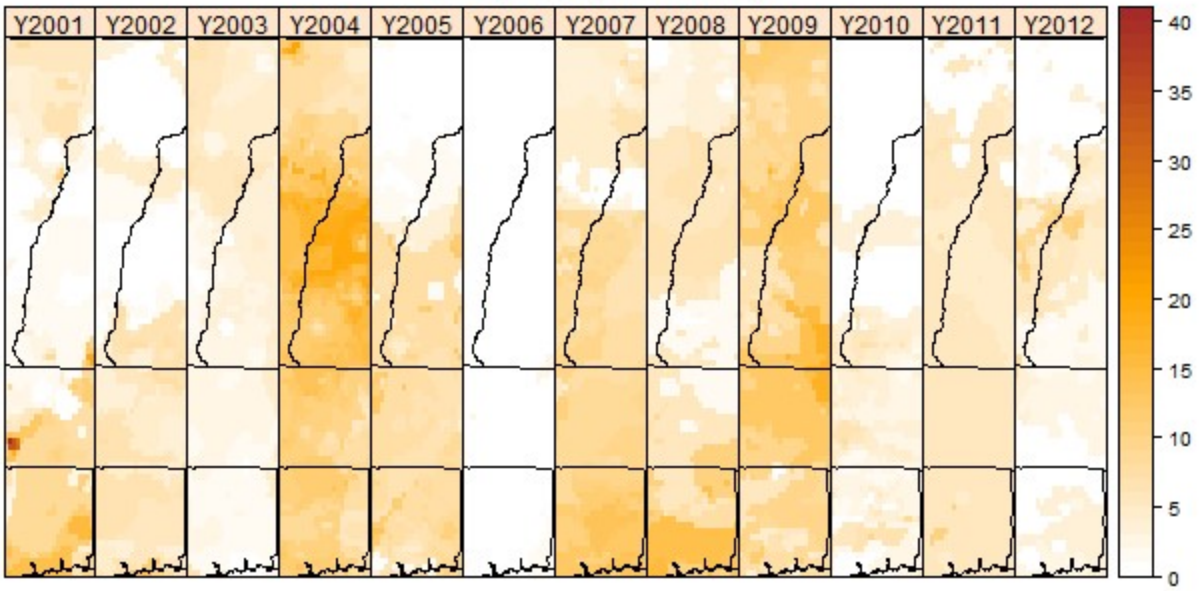
Drought (Sep.1~Nov.15)
Y2001
Y2002
Y2003
Y2004
Y2005
Y2006
Y2007
Y2008
Y2009
Y2010
Y2011
Y2012
40
35
30
25
20
15
10
5
0

References cited:

1. Zhang X, Friedl MA, Schaaf CB, Strahler AH, Hodges JCF, Gao F, Reed BC, Huete A (2003) Monitoring vegetation phenology using MODIS. *Remote Sens Environ*, 84, 471–475.

2. Zhang X., Friedl M.A., Schaaf CB, Strahler AH, Hodges JCF, Gao F (2002) Using MODIS data to study the relation between climatic spatial variability and vegetation phenology in northern high latitudes. *International Geoscience and Remote Sensing Symposium (IGARSS)*, 2, 1149-1151.

3. Zhang X, Friedl MA, Schaaf CB, Strahler AH (2004) Climate controls on vegetation phenological patterns in northern mid- and high latitudes inferred from MODIS data. *Global Change Biology*, 10(7), 1133-1145.

4. Zhang X, Friedl MA, Schaaf CB (2006) Global vegetation phenology from Moderate Resolution Imaging Spectroradiometer (MODIS): Evaluation of global patterns and comparison with in situ measurements. *Journal of Geophysical Research: Biogeosciences*, 111(4), art. no. G04017.

5. Liu L, Liang L, Schwartz MD, Donnelly A, Wang Z, Schaaf CB, Liu L (2015) Evaluating the potential of MODIS satellite data to track temporal dynamics of autumn phenology in a temperate mixed forest. *Remote Sensing of Environment*, 160,156-165.

6. Tang Q, Vivoni ER, MuñOz-Arriola F, Lettenmaier DP (2012) Predictability of evapotranspiration patterns using remotely sensed vegetation dynamics during the North American Monsoon. Journal of Hydrometeorology, 13(1), 103-121.

7. Yang Y, Guan H, Shen M, Liang W, Jiang L (2015) Changes in autumn vegetation dormancy onset date and the climate controls across temperate ecosystems in China from 1982 to 2010. *Global Change Biology*, 21(2), 652-665.

8. Pallardy SG (2008) *Physiology of Woody Plants 3rd edition*. Academic Press – Elsevier. Burlington, MA.

9. Hanninen H, Tanino K (2011) Tree seasonality in a warming climate. *Trends in Plant Science* 16(8): 412-416.

10. Paul KP, Rinne PH, van der Schoot C (2014) Shoot meristems of deciduous woody perennials: self-organization and morphogenetic transitions. *Curr Opin Plant Biol* 17:86-95.

11. Xie Y, Silander JA Jr. (2015) Species-specific leaf phenology of deciduous trees captured by digital cameras. Abstract for the Ecological Society of America 100th annual meeting, 9-14 August, 2015, Baltimore, MA, USA.

```
##############################################################################################
############## R codes for MODIS dormancy dates modeling ###################################

setwd("C:/~") # set path of data file
load("modeling_dataset.Rdata")              # all models use standardized dataset
data1.1s=as.data.frame(scale(data1.1))    # eco-region: Northeastern Highlands
data2.1s=as.data.frame(scale(data2.1))    # eco-region: Northeastern Coastal Zone

#### Multiple linear regression
lm1s=lm(dormancy~lat+elev+CDD820+FDf+FDf_2+FDs+HD7832+HD7835+GDR56+GDR78+GDR9d+GDR9
d_2 +RD56+RD78+RD78_2+RD9d+ECA56+ECA78+ECA9d+HD7832_RD78,data1.1s)
summary(lm1s)

lm2s=lm(dormancy~lat+CDD820+elev+FDf+HD7832+HD7835+GDR56+GDR78+GDR9d+RD78
      +RD9d+RD9d_2+ECA56+ECA78+ECA9d+ECA9d_2+FDf_elev+HD7832_RD78, data2.1s)
Summary(lm2s)

#### Penalized regressions
# ridge
library(MASS)
rg1=lm.ridge(dormancy~.,data1.1s,lambda=seq(0,50,by=0.1))
summary(rg1)
str(rg1)
select(lm.ridge(dormancy~.,data1.1s,lambda=seq(0,50,by=0.1)))  # find lambda for smallest GCV
rg1$coef[,51]

select(lm.ridge(dormancy~.,data2.1s,lambda=seq(0,50,by=0.1)))
rg2=lm.ridge(dormancy~.,data2.1s,lambda=seq(0,50,by=0.1))
rg2$coef[,19]

# Elastic Net
library(glmnet)
y1=data1.1s[,1]
X1=as.matrix(data1.1s[,-1])
fit_enet1=glmnet(X1,y1,alpha=0.5)
print(fit_enet1)
plot(fit_enet1)
coef(fit_enet1,s=0.00055)

y2=data2.1s[,1]
X2=as.matrix(data2.1s[,-1])
fit_enet2=glmnet(X2,y2,alpha=0.5)
print(fit_enet2)
plot(fit_enet2)
```

```
coef(fit_enet2,s=0.0004)

# Bayesian LASSO
library(lars)
library(monomvn)

bhs1 = blasso(X=data1.1s[,-1], y=data1.1s[,1], case="hs", RJ=FALSE, normalize=F) #already normalized
str(bhs1)
summary(bhs1)
beta1=apply(bhs1$beta[-1,], 2, mean)

bhs2 = blasso(X=data2.1s[,-1], y=data2.1s[,1], case="hs", RJ=FALSE, normalize=F) #already normalized
beta2=apply(bhs2$beta[-1,], 2, mean)

#### PACS
library(mvtnorm,MASS)
x=as.matrix(data1.1s[,-1])
y=data1.1s[,1]
betawt=lm(y~x-1)$coef
pacs1=PACS(y, x, lambda=1, betawt, type=3, rr=0.5)
rownames(pacs1)=colnames(data1.1)[-1]
str(pacs1)

x=as.matrix(data2.1s[,-1])
y=data2.1s[,1]
betawt=lm(y~x-1)$coef
pacs2=PACS(y, x, lambda=1, betawt, type=3, rr=0.5)
rownames(pacs2)=colnames(data2.1)[-1]
str(pacs2)

#### BMA
library(BAS)
M.ZSn1.s=bas.lm(dormancy~lat+elev+CDD820+FDf+FDf_2+FDs+HD7832+HD7835+GDR56+GDR78
        +GDR9d+GDR9d_2 +RD56+RD78+RD78_2+RD9d+ECA56+ECA78+ECA9d+HD7832_RD78,
        data1.1s,prior="ZS-null", n.models=NULL,
        modelprior=uniform(), initprobs="Uniform")
summary(M.ZSn1.s)
coef2=coef(M.ZSn1.s)

M.ZSn2.s=bas.lm(dormancy~ lat+CDD820+elev+FDf+HD7832+HD7835+GDR56+GDR78+GDR9d+RD78
        +RD9d+RD9d_2+ECA56+ECA78+ECA9d+ECA9d_2+FDf_elev+HD7832_RD78,
        data2.1s,prior="ZS-null", n.models=NULL,
        modelprior=uniform(), initprobs="Uniform")
summary(M.ZSn2.s)
```

```
coef2=coef(M.ZSn2.s)
plot(coef(M.ZSn2.s))

#### Bayesian posterior median model
library(bayesm)
library(coda)

Data1=list(y= as.matrix(data1.1s[,1]),X=as.matrix(data1.1s[,c(2:4,6:9,11:21)]))
Data2=list(y=as.matrix(data2.1s[,1]),X=as.matrix(data2.1s[,-1]))
Prior1 = list(betabar=rep(0,18),A=.01*diag(18))
R1 = 5000 # This is how many iterations to run the Gibbs sampler
keep1 = 1 # This is the thinning parameter. 1 means no thinning.
MCMC1 = list(R=R1,keep=keep1)
BLR1 = runiregGibbs(Data1,Prior1,MCMC1)
BLR2 = runiregGibbs(Data2,Prior1,MCMC1)
sum.blr1=summary(BLR1$betadraw)
sum.blr2=summary(BLR2$betadraw)

#### Spike and Slab
library(spikeSlabGAM)
spslG1.1s <- spikeSlabGAM(dormancy ~
lin(lat)+lin(elev)+lin(CDD820)+lin(FDf)+lin(FDf_2)+lin(FDs)+lin(HD7832)+lin(HD7835)+lin(GDR56)+lin(GDR
78)+lin(GDR9d)+lin(GDR9d_2)
+lin(RD56)+lin(RD78)+lin(RD78_2)+lin(RD9d)+lin(ECA56)+lin(ECA78)+lin(ECA9d)+lin(HD7832_RD78),
data=data1.1s)
summary(spslG1.1s)

spslG2.1s <- spikeSlabGAM(dormancy ~
lin(lat)+lin(elev)+lin(CDD820)+lin(FDf)+lin(HD7832)+lin(HD7835)+lin(GDR56)+lin(GDR78)+lin(GDR9d)
+lin(RD78)+lin(RD9d)+lin(RD9d_2)+lin(ECA56)+lin(ECA78)+lin(ECA9d)+lin(ECA9d_2)+lin(FDf_elev)+lin(HD
7832_RD78), data=data2.1s)
summary(spslG2.1s)

lm.spsl1=lm(dormancy~lat+elev+CDD820+FDf_2+HD7832+GDR9d+GDR9d_2+RD56+RD78+RD78_2
            +HD7832_RD78, data1.1s)
summary(lm.spsl1)
lm.spsl2=lm(dormancy~ lat+elev+CDD820+FDf+HD7832+HD7835+GDR9d+RD78+RD9d+RD9d_2
            +ECA56+ECA78+ECA9d+ECA9d_2+FDf_elev+HD7832_RD78,
            data2.1s)
summary(lm.spsl2)
```

Chapter 3

Species-specific autumn phenological responses to climatic factors suggest a complex mechanism and climate change impacts

Abstract

Shifts in autumnal phenology (leaf coloration and leaf drop) in temperate regions due to climate change bring substantial impacts on community and ecosystem processes (e.g. altered C and N cycling and biotic interactions) and the fall foliage ecotourism industry. However, our knowledge of the environmental control of autumn phenology has changed little over the past several decades. Using ground-based phenology observations in New England USA, we found several important weather/climatic factors to significantly affect autumn phenology of 12 dominant deciduous tree species. These patterns were revealed using linear mixed effects models. The significant weather/climate factors included not only autumn chill and frost, but also heat and drought stress plus precipitation. Species-specific sensitivities to those factors were also quantified for timing of leaf coloration and leaf drop. Positive relationship between spring and autumn phenology was confirmed by this study. Future changes in autumn phenology was predicted for all individual tree species from 2015 to 2099 based on future climate projections along with projected spring phenological changes. Our findings suggested climatic stresses are critical factors affecting autumn phenology, and divergent phenological responses by different tree species are important in predicting future impacts from climate change on forest community and ecosystem patterns and processes.

Introduction

Climate change to date has caused dramatic plant phenological changes including earlier spring phenology and delayed fall phenology in temperate regions around the world (Estrella and Menzel 2006, Körner and Basler 2010, Polgar and Primack 2014). However, the mechanism of autumn phenological responses in plants (i.e. leaf coloration and leaf drop) to environmental changes remains poorly understood (Gallinat et al. 2015). In contrast most phenology studies have focused on responses of bud burst, leafing out and flowering time to climate variation and weather. Changes in autumn phenology can influence ecological processes substantially, including C and N cycling, hydrology, demography, and biotic interactions (Weih 2009, Vitasse et al 2009, Jeong et al. 2011, Fridley 2012, Pépino et al. 2013, Estiarte and Peñuelas 2014). Delays in autumn phenology that lead to extended growing seasons, may increase the risk of freezing damage from early autumnal frosts or tree structural damage due to early snow events, preventing reabsorption of nutrients from leaves and altering nutrient cycles (Norby et al. 2003, Niinemets 2010, Richardson et al. 2012). Changes in the phenology of foliage coloring may also alter cues for animal behaviors such as avian migration (Ellwood et al. 2015), as well as impact the multi-billion dollar fall foliage ecotourism industry in the northeastern United States (Spencer and Holecek 2007, Rustad et al. 2011). However, those important, key environmental factors that affect plant fall phenology and the species-specific responses thereto, remain largely unknown.

Our knowledge of the interactions between plant autumn phenology and potential environmental factors has changed surprisingly little over the last 60 years (Samish 1954, Lim et al. 2007). Environmental variables that may affect the timing of leaf coloration and leaf drop as listed by Lim and colleagues (Lim et al. 2007), included day length, heat, cold, drought, wetness, nutrient and pathogen attack. But almost studies of environmental influences on autumn phenology published to date have focused only on the effects of autumn chilling, frost, and/or day length (Delpierre et al. 2009, Archetti et al. 2013, Jeong and Medvigy 2014); one exception is our own study of fall phenology based on satellite-derived data (Xie et al. 2015b). Although physiological experiments have reported the effects of a subset of these factors (i.e. temperature, day length, and drought) on plant leaf coloration and leaf drop

(Rosenthal and Camm 1997, Fracheboud et al. 2009, Naschitz et al. 2014), few studies have identified the most important factors or quantified the effects. Xie and colleagues (Xie et al. 2015b) found that other than decreasing temperature in autumn, moisture conditions and extreme weather events across the growing season (e.g. drought, heat stress and heavy rainfall) all have significant effects on the timing of autumn dormancy at the landscape scale (Xie et al. 2015b). However, few studies have investigated variations in autumn phenological responses at the species level to environmental changes (Archetti et al. 2013). Nothing is known prior to the study reported here about how these climate/weather factors may affect autumn phenological responses at the individual tree species. Though later autumn phenology in temperate regions has been reported in recent years (Estrella and Menzel 2006, Doi and Takahashi 2008), it is unclear which if any climatic stresses also affect autumn phenology of temperate forest tree species, or if these species have different phenological sensitivities to the environmental stresses.

It is critical to understand the mechanisms of autumn phenology and the species-specific phenological responses in order to predict future impacts from climate change. Two previous studies reported positive relationship between spring and autumn phenology (Fu et al. 2014, Keenan and Richardson 2015), which indicated a more complex mechanism of phenological responses of plants and point to our general lack of understanding of the phenological activities of plants across the entire growing season. Since both spring and autumn phenologies of plants are likely responding to climate change, the influences of phenological changes in the spring should also be included in building models to estimate phenological changes in autumn in response to climate change.

To improve our understanding of plant phenological responses to climate change, especially autumn phenology, the focus of the study reported here is on ground-based phenological observations in New England. We applied linear mixed effects models to investigate the relationship between environmental changes and leaf phenology of 12 dominant deciduous tree species of northeastern United States forest communities. The objectives of this study are to: 1) identify important climatic factors affecting timing of autumn phenology from the beginning of leaf coloration through to leaf drop in a suite of temperate deciduous tree species; 2) investigate species-specific autumn phenological responses to the important

climatic factors; 3) investigate variations of phenology among sites, species and individuals; 4) investigate relationships between spring and autumn phenology; and 5) predict future changes of autumn phenology based on future climate projections as well as spring phenological changes.

Methods

Data and processing

We established 5 plots (25m×50m) that stratified local site conditions (i.e. soil and soil moisture and species composition) in the natural forest landscapes in and around the University of Connecticut (UCONN) campus. We randomly selected 88 individuals of eight dominant tree species differentially present in five plots (Table 3.1-1). Eight species (with total number of replicates) were *Acer rubrum* (5), *Acer saccharum* (23), *Betula lenta* (5), *Carya glabra* (16), *Carya ovata* (17), *Fraxinus americana* (9), *Quercus alba* (10), and *Quercus rubra* (10). In total 88 individual adult trees were observed from 2012 to 2014. We directly observed leaf phenology for each individual, including bud burst, leaf unfolding, leaf coloration and leaf drop. Observations were conducted twice a week (See observation protocol in Appendix 3.1) in spring from late April when buds began to break to early June with full leaf out and in autumn from late August with initial leaf coloration to middle November ending with leaf drop. Hourly temperatures were recorded by temperature probe loggers at each plot. Daily precipitation data was available from the weather station in Storrs, Connecticut, USA.

Long-term phenology observation on 12 deciduous tree species (52 individual trees) and daily weather data (daily mean, maximum, and minimum temperatures, and precipitation) at Harvard Forest (http://harvardforest.fas.harvard.edu/data-archives) from 1993 to 2014 were used to provide a larger sample size to complement the data we collected in UConn Forest. Twelve species are: *A. pensylvanicum* (4), *A. rubrum* (5), *A. saccharum* (4), *B. alleghaniensis* (3), *B. lenta* (3), *B. papyrifera* (4), *B. populifolia* (4), *Fagus grandifolia* (6), *F. americana* (6), *Q. alba* (5), *Q. rubra* (4), and *Q. velutina* (4). Harvard Forest phenology observations used a very similar protocol (http://harvardforest.fas.harvard.edu) to that we used in Connecticut (see Appendix 3.1). The phenophases we used in this study included bud break,

leaf coloration and leaf drop. Since bud break in Harvard Forest observation protocol (buds on the tree that have broken open revealing leaves) and leaf unfolding in UConn observation protocol (one or more live unfolded leaves are visible) indicate similar life event of plants, we used leaf unfolding below for both of them for convenience.

Percentage values were observed for three phenophases (i.e. leaf unfolding, leaf coloration and leaf drop). We fitted logistic lines to the observation data (Fig. 3.1-1) analogous to that used in studying plant phenology from remotely-sensed satellite images (e.g. Zhang et al. 2003) to estimate three phenological transition dates (onset, peak and end date) for each individual tree. Onset and end dates of each phenophase were determined by points at where there was minimum change of curvature. They indicated the beginning and the end of the phenophases. The peak date was determined by the inflection point of fitted logistic lines, which was the timing when leaf unfolding, leaf coloration and leaf drop happened most quickly.

Multiple derived weather variables were developed from daily temperature (measured at each of our sites) and precipitation records (from the Storrs weather station) to explain the change of phenological transition dates spatially and temporally (Table 3-1). We first built a list of weather variables of potential environmental conditions that may affect fall phenology including: cold-stress, frost, heat-stress, rainfall, drought-stress, and flood events (Table 3-1) (Xie et al. 2015b). Previous studies have considered accumulating cold degree days (CDD) and decreasing day length that occur in fall as the primary triggers of leaf coloration and leaf drop (Richardson et al. 2006, Archetti et al. 2013). Considering the important effects from minimum temperature on autumn phenology (Kalcsits et al. 2009, Tanino et al. 2010), we developed a comparable index CDDi using minimum temperature as base temperature (Table 3-1) to measure chilling based on night temperatures in the autumn. We did not investigate the effect of day length effect since day length does not have year-to-year variation, and the small differences in day length between UCONN and Harvard Forest has a negligible effect relative to other variables including site random effects, and would be absorbed as a site random variable effect. We also developed other weather/climate variables in Table 1 to represent environmental stressors potentially affecting tree

performance (Niinemets 2010, Duque et al. 2013). Plant phenological responses to stresses may differ depending on when stresses occur in different seasons (Bréda et al. 2006). The physiological requirements of trees may also differ in different phenophases as well as across species (Primack et al. 2009, Wilczek et al. 2010, Hwang et al. 2014). Three sets of weather variables were calculated, growing season drought-stress (GDR), rainy days (RD), and heavy rainy days (ECA), for three periods that reference spring, summer and autumn intervals (May.1 to Jun.30, Jul.1 to Aug.31, and Sep.1 to Oct. 30). For our index of cold degree days (CDD and CDDi), we examined the effects of different base temperatures (daily mean and minimum temperature at 10°, 15°, and 20°C) for three months (August, September and October) to determine which period of CDD with what base temperature may best explain autumn phenology variation of the deciduous tree species. We used 35°C as the threshold temperatures for hot days (HD) indicating heat-stress, and we found HDs only occurred in July and August at the study sites. We calculated frost days (FD) in two months (September and October) indicating cold-stress that differs from CDD.

We obtained downscaled climate projection data for one global climate model (GCM, GFDL-ESM2G) with one future scenarios (RCP 8.5) from Multivariate Adaptive Constructed Analogs group for model predictions (Abatzoglou and Brown 2012). We used daily maximum and minimum temperature and daily precipitation at the location of Harvard Forest to calculate weather variables for future predictions from 2015 to 2099.

Statistical modeling

We used linear mixed effects models to explain the relationships between autumnal phenology and climatic variables from different species and sites. Linear mixed effects models considers heterogeneity and dependence from nested data structure with repeated measurements on individuals and sites. The advantages of linear mixed effect models are that they allow incorporation of random effects due to variations in phenology among individuals, species and sites levels while estimating the effects from climate/weather variables on leaf phenology.

We fitted linear mixed effects models using two datasets. One is combined dataset including observations on eight species from both UCONN and Harvard Forest during 2012 and 2014. Six phenological transition dates (3 of leaf coloration and 3 of leaf drop) were separately fitted as response variables in the models. Random intercept models with species and sites as random effects were used in the dataset. Potential climate/weather factors and spring phenology were set as fixed effects in the model. Important factors (variables) were identified for each transition dates of leaf coloration and leaf drop using AIC (Akaike 1973) and BIC (Schwarz 1978) as selection criteria. Whereas inter-annual variation in phenology were explained by climate/weather factors, variation in phenology among species and sites were indicated by random intercepts. One climatic factor with the highest contribution on explaining the response variables was selected from multiple climatic factors with high correlation ($r>0.5$) to avoid multicollinearity in the model. Top five best models were reported for each phenological transition date.

The relatively small sample size from our 3-year UConn Forest dataset cannot support complex model structures with random slope models to identify difference of sensitivity to climatic factors among species. Thus, we used the long-term dataset from Harvard Forest from 1993 to 2014 as the second dataset to fit random intercept and slope models with species and individuals as random effects. The data includes 933 observations on 12 species (52 individuals) over 22 years. We randomly selected 93 observations as validation data and used 840 observations as model training data. Climatic factors and spring phenology were used as fixed effects, and species and individuals were random effects in the model. Random slopes at the species level account for species-specific phenological responses in autumn to changes in climatic factors.

We used a top-down strategy (Diggle et al. 2002, West et al. 2007, Zurr et al. 2009) to build models and selected the best models using marginal AIC (mAIC) for fixed effects and conditional AIC (cAIC) for random effects (Greven and Kneib 2010) (see model selection procedures in Appendix 2). Data were analyzed using R software (R Core Team 2015). Best models were reported for six phenological transition dates (3 for leaf coloration and 3 for leaf drop). Using the best models identified by the above criteria we predicted six phenological transition dates for 93 observations in Harvard Forest across 12

species and 21 years. We compared predicted dates to the observed phenology dates and calculated r^2 and root mean square error (RMSE) to show the goodness of model fit as model validations.

Future predictions of autumn phenology of deciduous trees at Harvard Forest were based on future climate change and spring phenological changes. Thus, linear mixed effect models were also applied to estimate spring leaf unfolding dates (i.e. onset, peak and end dates) of 52 individual trees at Harvard Forest (1993-2014). Monthly mean temperature in March, April and May, cumulative growing degree day (GDD) and chilling units (CU) from January 1st to May 31st were used as fixed variables (Xie et al. 2015a), while species and individual trees were random effects in the models. Random slopes at the species level explain species-specific phenological responses in the spring to changes in these climate/weather factors. Best models for phenological dates were selected following the same procedure as for fall phenology (see Appendix 2) and were used to predict spring phenology changes in the future years in response to projected climate change (2015-2099) at the individual level. Then we used predicted spring phenological changes and future climate projection data to predict autumn phenology for future years for each individual tree (2015-2099).

Results

Based on phenology observations in and around UCONN Forest and at Harvard Forest, plant leaf color change and leaf drop in autumn is a slower biological process than spring phenology. In southern New England it typically takes a few months (September to November) to change leaf color and drop leaves for the suite of dominant deciduous tree species present in a community. This contrasts with a more rapid spring phenology (Fig. 3-1). During 1993 and 2014, the lengths between the start and the end date of leaf unfolding of 12 species in Harvard Forest were about 5-11 days, but for the leaf coloration and leaf drop, the lengths were about 19-25 days and 14-22 days respectively.

From the top five models for the six phenological transition dates from observations both in Connecticut and Harvard Forest during 2012 and 2014 (Table 3-2), it is clear that only one or two weather/climate variables were selected in each model. This is likely in part due to the relatively small

sample size and correlation among variables. For three phenological transition dates related to leaf coloration timing, CDDi and $RD_{(Jul.1\text{-}Aug.31)}$ were always included in the best model showing the important effects that chilling, based on minimum temperature in August or September, and summer rainfall have on the timing of leaf coloration processes (Table 3-2). In contrast, for onset, peak and end dates of leaf drop, the best models only included one weather variable ($CDDi_{Oct10}$ or $CDDi_{ASO10}$), showing the important effects of chilling in either just October or over three months (August, September, and October), based on minimum temperature at 10°C, on the timing of leaf drop processes (Table 3-2). The small difference in AIC and BIC among the top five models indicated the potential importance that drought-stress and precipitation, in addition to CDDi, may have on variation in autumn phenology. However the power of resolution, given the small dataset size, was insufficient to consistently support the inclusion of these other variables in the model. In addition, all models included onset or peak date of leaf unfolding as a significant predictor, indicating the important relationship between spring and autumn phenology. The magnitude of the random intercepts at species and site levels showed that variation in onset, peak and end dates of leaf coloration were respectively 9.0, 9.6, and 9.9 days among all eight species across all sites, and about 4.6, 4.5, and 4.8 days respectively among sites within species. These effects were not explained by climatic/weather factors in the models. For the leaf drop, the standard deviations of onset, peak and end dates among eight species across all sites were 9.5, 10.6, and 11.7 days, and the standard deviations among sites within species were 5.9, 5.3, and 5.2 days respectively. These results point to importance of species and site-level effects.

The best models (Table 3-3 and 3.1-2) for 12 species from Harvard Forest observations (1993-2014) suggested that timing of leaf coloration and leaf drop were significantly affected by temperature in autumn, precipitation in spring and summer, drought-stress in summer and autumn, and heavy rain in autumn. Generally, warming in autumn, more drought-stress in summer and autumn delayed leaf coloration and leaf drop, while more rainfall in the spring and more heavy rainy days in autumn lead to earlier leaf coloration and leaf drop. Specifically, each phenological transition date was affected by chilling-stress over a period one to two months prior to the particular phenological date. Onset of leaf

coloration was affected by CDD in August, but the peak dates of leaf coloration were affected by CDD in both August and September, while end of leaf coloration was affected by CDD in September and minimum temperature in October ($T_{min\text{-}Oct}$). For leaf drop, onset and peak dates were affected by CDD in both August and September, but the end of leaf drop was affected only by CDD in September.

Meanwhile, the coefficient values for the climatic variables in the random effects model at species level, suggested different sensitivities of autumn phenology among 12 species to changes of drought-stress and precipitation or heat-stress (Fig. 3-2). Overall, species with earlier autumn phenology, including white ash, maples, and birches, had higher sensitivities to drought-stress in the summer ($GDR_{(Jul.1\text{-}Aug.31)}$) and autumn ($GDR_{(Sep.1\text{-}Oct.31)}$), than those species with later autumn phenology (i.e. oaks and beech) (Fig. 3-2). In addition, the autumn phenology of paper birch had the largest absolute values across most of coefficients (16 out of 21 variables across 6 models) among the 12 species. This means that the autumn phenology of paper birch had higher sensitivities to weather variables, such as $RD_{(May.1\text{-}Jun.30)}$, $GDR_{(Jul.1\text{-}Aug.31)}$, $GDR_{(Sep.1\text{-}Oct.31)}$, and $ECA_{(Sep.1\text{-}Oct.31)}$, than any of the other species measured (Fig. 3-2).

For the timing of onset and peak of leaf coloration, all twelve species monitored at Harvard Forest had different responses to spring rainfall, drought-stress in summer and autumn, and heavy rainfall in autumn (Fig. 3-2a,b). For most species, spring rainfall ($RD_{(May.1\text{-}Jun.30)}$) and heavy rainfall in autumn ($ECA_{(Sep.1\text{-}Oct.31)}$) lead to earlier leaf coloration onset and peak dates. However, heavy rainfall in autumn ($ECA_{(Sep.1\text{-}Oct.31)}$) delayed leaf coloration onset dates of six of the species and peak dates of four of the species. While drought-stress in summer ($GDR_{(Jul.1\text{-}Aug.31)}$) and autumn ($GDR_{(Sep.1\text{-}Oct.31)}$) delayed leaf coloration onset dates for 6 and 11 species respectively and peak dates for 8 and 9 out of 12 species, summer drought-stress ($GDR_{(Jul.1\text{-}Aug.31)}$) advanced leaf coloration onset dates of six of the species and leaf coloration peak dates of four of the 12 species. Autumn drought-stress ($GDR_{(Sep.1\text{-}Oct.31)}$) advanced leaf coloration onset dates of American beech and leaf coloration peak dates of three of the species (black oak, red oak, and American beech). For leaf coloration end dates, all 12 species showed different sensitivities to minimum temperature in October ($T_{min\text{-}Oct}$), summer heat-stress (HD_{35}), and drought-stress in summer

($GDR_{(Jul.1\text{-}Aug.31)}$) and autumn ($GDR_{(Sep.1\text{-}Oct.31)}$) (Fig. 3-2c). Lower minimum temperature in October and more summer heat-stress lead to earlier leaf coloration end dates of most species, but had delayed effects for two and three species respectively. More drought-stress in summer and autumn delayed leaf coloration end dates of most species, but advanced timing of leaf coloration end dates for two and four species respectively.

In terms of the timing of leaf drop, all three transition dates showed species-specific response to three climatic conditions: spring rainfall, autumn drought-stress, and heavy rainfall in autumn (Fig. 3-2d-f). More spring rainfall and heavy rainfall in autumn lead to earlier leaf drop, and more autumn drought-stress delayed leaf drop of most species. However, the three transition dates associated with leaf drop for four species (white oak, black oak, red oak, and American beech) were advanced by autumn drought-stress and delayed by heavy rainfall in autumn, in contrast to the other 8 species.

Significant positive correlations between spring and autumn phenology were found in models for all species in both datasets. Coefficients of spring phenology in all models were consistent for every autumn phenological transition date. The models suggested that one day earlier in onset or peak of leaf unfolding lead to about 0.2~0.3±0.06 days earlier for all transition dates of leaf coloration and leaf drop of trees during 2012 and 2014. One day earlier for end of leaf unfolding lead to about 0.1±0.02 days earlier for three transition dates leaf coloration of trees at Harvard Forest over 1993- 2014 (Table 3-3).

For spring phenology, the best models of three transition dates of leaf unfolding all selected monthly mean temperatures in three months (March, April and May) as fixed predictors (Table 3.1-3). Higher monthly mean temperatures in spring lead to earlier leaf unfolding onset, peak and end dates for all species. The three best models also included a random slope for mean temperature in April at the species level, indicating species-specific responses to temperature changes in April. Using the best model, leaf unfolding end dates of each individual tree from 2015 to 2099 were predicted from the projected mean monthly temperatures.

Based on future climate change and predicted leaf unfolding end dates during 2015 and 2099, three transition dates of leaf coloration were predicted for all 52 individual trees. Three transition dates of leaf

drop were also predicted for all trees as well. To summarize the predicted phenological changes of each species through 85 years, we calculated mean and variance values of four time periods (1993-2014, 2015-2039, 2040-2069, and 2070-2099) for each species (Fig. 3-3 and 3-4). We found that the 12 species showed different changes in the phenological dates in the future. For the onset dates of leaf coloration, striped maple and American beech are projected to be 4.2-8.9 days earlier, while other species will likely be 0.8-12.8 days later by the end of this century (Fig. 3-3a). For the peak dates of leaf coloration, striped maple and American beech are projected to be 1.8-9.7 days earlier, while other species will likely be 0.4-14.7 days later by the end of this century (Fig. 3-3b). While striped maple (ACPE), yellow birch (BEAL), and American beech (FAGR) are projected to have 12.7-23.7 days earlier end dates of leaf coloration by the end of this century, red maple (ACRU), paper birch (BEPA), red oak (QURU), and black oak (QUVE) will likely have 8.3-29.9 days later leaf coloration end dates. The other five species, sugar maple (ACSA), black birch (BELE), grey birch (BEPO), white ash (FRAM) and while oak (QUAL), showed smaller changes (3.5 days earlier to 3.5 days later) for the end of leaf coloration compared to current years (Fig. 3-3c). By the end of this century, the onset of leaf drop for 10 of the 12 species will be 1.8-23.4 days later, while the two other species (American beech and white oak) will be 7.8 and 0.5 days earlier (Fig. 3-4a). For the changes in peak and end dates of leaf drop, all species showed 0.7-24.6 and 1.7-21.3 days delayed dates by the end of this century except American beech, 10.2 days earlier of leaf drop peak date and 13.2 days earlier of leaf drop end date (Fig. 3-4b, c).

Discussion

This study identified multiple important weather/climatic factors affecting autumn phenology of deciduous tree species in New England forest systems. Autumn phenology of deciduous trees significantly responded not only to cold condition in autumn, but also to variation in precipitation, drought-stress and extreme weather events (e.g. heat-stress and heavy rainfall) across the growing season. These results are consistent with our findings based on remotely-sensed land surface phenology in

community and landscape levels (Xie et al. 2015b), and also provides some insight into autumn phenological mechanisms at the species and individual levels as well as local site effects.

The best models suggest that all 12 species examined had consistent phenological responses to chilling in autumn. Focusing on Cold Degree Days (CDD), our models consistently selected CDDi that is indexed to daily minimum temperature as an important explanatory variable (Table 3-2). This indicates that changes in night-time temperatures had more effects on triggering autumn phenology than temperatures in the day time temperatures. Kalcsits et al. (2009) and Tanino et al. (2010) also reported that night-time temperatures had a greater impact on temperate deciduous woody plant growth cessation and bud set than day-time temperatures. While climate change to date and projections for the future point to increasing night-time temperatures, the effects on autumn phenology could be larger than what would be expected based on changes in mean temperatures alone (Way 2011). In addition, more spring rainfall leads to earlier autumn phenological dates for all species. This could be related to more likely early fungal infection of leaves under higher moisture conditions and earlier leaf drop (Hepting 1963, Chabot and Hicks 1982, Huber and Gillespie 1992).

Our models also suggest that while timing of leaf coloration and leaf drop of deciduous tree species respond to heat-stress, drought-stress and rainfall amounts across the whole growing season, different species have contrasting phenological sensitivities to these factors. These differences could be related to species-specific variation in physiological requirements and adaptations to environmental variation among these tree species. Paper birches perform better in colder environment, for example while performing poorly under heat-stress, as well as very wet or dry conditions (Prasad and Iverson 2003, Climate change atlas 2014). This may explain why paper birch showed the highest sensitivities to drought and precipitation (He et al. 2005), but the smallest response to minimum temperature in October among the 12 species modeled.

Species that are less drought tolerant, including white ash, maples and birches (Pääkkönen et al. 1998, Prasad and Iverson 2003, Climate change atlas 2014) showed higher sensitivities to drought than species with greater drought tolerance, such as oaks and beech (Abrams 1990, Climate change atlas

2014). In addition, they had opposite responses to drought-stress in summer and autumn, which delayed autumn phenology of ash, maples and birches and advanced autumn phenology of oaks and beech. One reason of this difference may be molecular and physiological responses to moderate drought-stress by gene regulation on plant hormones and stress-shock proteins (Carvalho et al. 2014). This mechanism may increase drought tolerance in ashes, maples and birches, and also reduce the risk of cell death in leaves (i.e. leaf senescence) (Rivero et al. 2007, Naschitz et al. 2014). However, the details of the mechanisms and how these may operate have not been examined in any of our study species (Xu et al. 2007, Paul et al. 2014). This should be a focus for future research efforts: understanding mechanistically how Northeastern forest systems may respond to variation in climate and weather now and in the future. Another explanation for differential sensitivities among species to weather/climate variables could be the heterogeneity among micro-environments in our forest study system. White ash, maples and birches prefer higher soil moisture, whereas oaks and beech tend to tolerate drier soil condition (Prasad and Iverson 2003). Natural drought may induce different levels of drought (moderate or severe drought) for these species depending on soil and site conditions. Although oaks and beech are less sensitive to drought, they can also avoid severe drought-stress by entering leaf senescence earlier, preventing loss of resources and nutrients by drought-induced leaf death (Hinckley et al. 1979).

Environmental stresses affect both the timing and the length of leaf coloration for our 12 common forest tree species. Several of these are iconic elements of the fall foliage ecotourism industry. In investigating the relationship between climatic/weather variables and the length of leaf coloration process (i.e. the length between onset and end dates of leaf coloration), we found that summer heat-stress had the greatest effect on the length of leaf coloration. One more hot day (HD_{35}) on average reduces by 4.2 days the length of leaf coloration across our 12 species. Increasing one unit of chilling in autumn ($CDDi_{ASO10}$) and summer drought ($GDR_{(Jul.1\text{-}Aug.31)}$) also reduces on average the length of the fall color season by only 0.02 and 0.1 days, and increasing one heavy rainy days ($ECA_{(Sep.1\text{-}Oct.31)}$) tends to increase the season length by 0.9 days. Given the increased heat-stress predicted for future years based on climate projection

data for New England, the length of leaf coloration season is predicted to be strongly reduced by about 20-40 days across all species.

Our best models on spring leaf unfolding dates did not include GDD or CU as we expected. One reason is we do not have any specific information to set accumulation time period and base temperatures of GDD or CU for each species in the model, although we are aware of the differences among species on the requirements of GDD and CU from previous studies (Polgar et al. 2014, Allen et al. 2014). Additionally, we do not have large sample sizes to fit species-specific models based on only 3 to 6 individuals of each species. Thus, the best models selected monthly mean temperatures as best predictors, which represent general mechanisms of spring phenology among all dominant species. The random slope for monthly mean temperature in April at species level indicate the species specific responses to temperatures in spring.

This study is the first time that linear mixed effects models have been used to estimate plant phenological dates. The advantage of including random effects at individual, species and site levels is that it points to the importance of variations in phenological timing among individuals, species and sites. By calculating the marginal and conditional R^2 of our best models, we found that the fixed variables in the models explained much less variation in phenological dates than what the random effects explained (Table 3.1-4). We also found that predictions of phenology had poorer performances in model validations when random effects at individual or species levels in the model were lacking. These findings suggested that it is critical to include the information of variation among individuals and species to get more accurate phenological predictions. It is noteworthy that these sources of variation have not been considered in previous phenology modeling studies, even though they have been observed (Crawley and Akhteruzzaman 1988, Ne'Eman 1993). We observed that some individuals always had earlier or later phenologies than other individuals from same species at the same site (see one example in Fig. 3.1-3). This consistent difference among individual trees within species and sites could be caused by variation in health condition of the individual tree (e.g. pests, pathogens or other stresses), local hydrological conditions due to ontogeny and micro-environment conditions (e.g. soil texture and nutrients) in the

particular location in the forest, or the genotypic effects (Crawley and Akhteruzzaman 1988, Ne'Eman 1993). Thus, we encourage further research and experiments to investigate the factors that affect individual phenological variations within species.

Future predictions on the timing of autumn phenology show species-specific phenological responses to projected climate change. Though more than one species were predicted to have later autumn phenology in the future, their magnitudes of changes vary considerably among species, from no more than 1 day to more than 20 days. These differences match the variation in sensitivities to climatic/weather factors among the species. For example, paper birch with the highest sensitivities to drought-stress, heat-stress and heavy rainfall always showed largest changes in the future (12.8-24.6 days later across all dates of leaf coloration and leaf drop) in response to projected climate change among 12 species. We projected seven species to show earlier leaf coloration end dates, which was more than other phenological transition dates (i.e. 2 species for onset and peak coloration), which reflects the likelihood that there will be reduced length of the leaf senescence processes in the future. This change is caused by more heat-stress (more than 10 HD_{35} compared to 1 HD_{35} in current years) in the future, especially towards the end of this century (2070-2099). In the model validations of our best models for the Harvard Forest dataset, comparisons between predicted and observed dates of six transition dates showed that our model prediction uncertainties was about 5 to 7 days, and r^2 were about 0.7 (Fig. 3.1-2). The observations on some individuals (2 sugar maples, 4 American beeches, 4 white ashes, and 2 white oaks) had replicates less than 22 years, which caused not all individuals and species had the same number of replicated observations over the same time period (i.e. the unbalanced dataset). Thus, it may not accurately provide information of individual phenological variations within species. This unbalanced dataset may cause larger uncertainties in random effects in the mixed effects models. Thus, we emphasize the importance of keeping long-term phenology observations on the same individuals and multiple individuals per species.

This study significantly enhances our understanding of the complex mechanisms affecting the autumn phenology of deciduous tree species. More environmental factors, such as extreme weather events (e.g. drought, heat and heavy rain), should be taken into account in explaining or predicting the timing of

leaf coloration and leaf drop of deciduous trees. Our findings regarding the positive relationship between spring and autumn phenology confirm the results from previous studied (Fu et al. 2014, Keenan and Richardson 2015). While projected climate change will likely bring increased intensity and frequency of extreme weather events (e.g. drought, heat and heavy rain) (Garcia et al. 2014), and significant changes of spring phenology are predicted (Cleland et al. 2007, Allen et al. 2014, Xie et al. 2015a), the impact of these changes on autumn phenology will be more complicated than previously thought. Our results point to the need for phenology observations on more species and sites with greater replication over a greater spatial-temporal scale. Physiological experiments will also be necessary to help understand the physiological as well as molecular genetic mechanisms behind autumn phenology patterns and processes. These efforts can inform us how to predict how autumn phenology of deciduous trees in response to climate change now and in the future as well as predict the ecological and economic consequences.

Acknowledgements

This study was supported in part by NSF grant DEB 0842465 to JAS. We thank R. Primack, R. Chazdon, E. Adams, and D. Civco for helpful comments to improve this manuscript.

Reference

Abatzoglou JT and Brown TJ (2012) A comparison of statistical downscaling methods suited for wildfire applications. Int J Climatol 32(5): 772–780.

Abrams, M. D. (1990). Adaptations and responses to drought in Quercus species of North America. Tree physiology, 7, 227-238.

Akaike H (1973) *Information theory and an extension of the maximum likelihood principle.* B. N. Petrovand S. Caski, editors. Proceedings of the Second International Symposium on Information Theory. Akademiai Kaido, Budapest, Hungary. pp. 267–281.

Allen JM, Terres MA, Katsuki T et al. (2014) Modeling daily flowering probabilities: expected impact of climate change on Japanese cherry phenology. Global Change Biology 20: 1251-1263.

Archetti, M., Richardson, A. D., O'Keefe, J. & Delpierre, N. (2013) Predicting Climate Change Impacts on the Amount and Duration of Autumn Colors in a New England Forest. 8, e57373.

Bréda N, et al. (2006) Temperate forest trees and stands under severe drought: a review of ecophysiological responses, adaptation processes and long-term consequences. Ann For Sci 63(6): 625-644.

Carvalho HH, et al. (2014) The Molecular Chaperone Binding Protein BiP Prevents Leaf Dehydration-Induced Cellular Homeostasis Disruption. PloS one 9(1): e86661.

Cleland EE, Chuine I, Menzel A, Mooney HA, Schwartz MD (2007) Shifting plant phenology in response to global change. Trends Ecol Evol 22(7):358–365.

Chabot BF and Hicks DJ (1982) The ecology of leaf lift spans. Annual Review of Ecology and Systematics, 13: 229-259.

Crawley MJ and Akhteruzzaman M (1988) Individual Variation in the Phenology of Oak Trees and Its Consequences for Herbivorous Insects. Functional Ecology, 2: 409-415.

Delpierre, N. et al. (2009) Modelling interannual and spatial variability of leaf senescence for three deciduous tree species in France. Agricultural and Forest Meteorology 149: 938-948.

Diggle, P.J., Heagerty, P., Liang, K.Y. & Zeger, S.L. (2002). *Analysis of longitudinal data*. 2nd edn. New York, Oxford.

Doi H, Takahashi M (2008) Latitudinal patterns in the phenological responses of leaf colouring and leaf fall to climate change in Japan. *Global Ecol Biogeogr* 17(4): 556-561.

Duque AS, et al (2013) Abiotic stress responses in plants: unraveling the complexity of genes and networks to survive. Abiotic Stress - Plant Responses and Applications in Agriculture, eds Vahdati K, Leslie C (InTech) pp 49-55.

Ellwood, E. R., Gallinat, A., Primack, R. B., & Lloyd-Evans, T. L. (2015) in Autumn migration of North American landbirds.

Estiarte, M. & Peñuelas, J. (2014) Alteration of the phenology of leaf senescence and fall in winter deciduous species by climate change: effects on nutrient proficiency. Global Change Biology. 21(3):1005-1017.

Estrella, N. & Menzel, A. (2006) Responses of leaf colouring in four deciduous tree species to climate and weather in Germany. Climate Research 32, 253-267.

Fracheboud, Y. et al. (2009) The Control of Autumn Senescence in European Aspen. Plant Physiology 149: 1982-1991.

Fridley, J. D. (2012) Extended leaf phenology and the autumn niche in deciduous forest invasions. Nature 485: 359-362.

Fu YSH, et al. (2014) Variation in leaf flushing date influences autumnal senescence and next year's flushing date in two temperate tree species. Proc Natl Acad Sci 111(20): 7355-7360.

Gallinat, A. S., Primack, R. B. & Wagner, D. L. (2015) Autumn, the neglected season in climate change research. Trends in Ecology and Evolution 30: 169-176.

Garcia RA, Cabeza M, Rahbek C, Araújo MB (2014) Multiple dimensions of climate change and their implications for biodiversity. *Science* 344(6183):1247579.

Greven, S. & Kneib, T. (2010). On the behaviour of marginal and conditional AIC in linear mixed models. Biometrika, doi: 10.1093/biomet/asq042.

He, J. S., Zhang, Q. B., & Bazzaz, F. A. (2005). Differential drought responses between saplings and adult trees in four co-occurring species of New England. Trees, 19(4), 442-450.

Hepting GH (1963) Climate and forest diseases. Annu. Rev. Phytopathol. 1:31-50.

Hinckley TM, Dougherty PM, Lassoie JP, Roberts JE, Teskey RO (1979) A severe drought: impact on tree growth, phenology, net photosynthetic rate and water relations. Am Midl Nat 102(2): 307-316

Huber L and Gillespie TJ (1992) Modeling leaf wetness relation to plant disease epidemiology. Annu. Rev. Phytopathol. 30:553-577.

Hwang T, et al. (2014) Divergent phenological response to hydroclimate variability in forested mountain watersheds. Glob Chang Biol. 20(8):2580–2595.

Jeong, S., Ho, C., Gim, H. & Brown, M. E. (2011) Phenology shifts at start vs. end of growing season in temperate vegetation over the Northern Hemisphere for the period 1982–2008. Global change biology 17: 2385–2399.

Jeong, S. & Medvigy, D. (2014) Macroscale prediction of autumn leaf coloration throughout the continental United States. Global Ecology and Biogeography 23: 1245-1254.

Kalcsits, L., S. Silim and K. Tanino. (2009) Warm temperature accelerates short photoperiod-induced growth cessation and dormancy induction in hybrid poplar (*Populus x spp.*). Trees 23:973–979.

Keenan TF, Richardson AD (2015) The timing of autumn senescence is affected by the timing of spring phenology: implications for predictive models. Glob Chang Biol 21(7): 2634-2641.

Körner C, Basler D (2010) Phenology under global warming. Science 327(5972):1461-1462.

Landscape Change Research Group. (2014) Climate change atlas. Northern Research Station, U.S. Forest Service, Delaware, OH. http://www.nrs.fs.fed.us/atlas.

Lim, P. O., Kim, H. J. & Nam, H. G. (2007) Leaf senescence. Ann Rev Plant Biol 58, 115-136.

Naschitz S, Naor A, Wolf S, Goldschmidt EE (2014) The effects of temperature and drought on autumnal senescence and leaf shed in apple under warm, east mediterranean climate. Trees 28(3):879–890.

Ne'Eman G. (1993) Variation in Leaf Phenology and Habit in Quercus Ithaburensis, a Mediterranean Deciduous Tree. Journal of Ecology, 81: 627-634.

Niinemets Ü (2010) Responses of forest trees to single and multiple environmental stresses from seedlings to mature plants: Past stress history, stress interactions, tolerance and acclimation. Forest Ecol Manag260(10): 1623–1639.

Norby, R. J., Hartz-Rubin, J. S. & Verbrugge, M. J. (2003) Phenological responses in maple to experimental atmospheric warming and CO2 enrichment. Global Change Biology 9: 1792-1801.

Pääkkönen E, Vahala J, Holopainen T, Kärenlampi L (1998) Physiological and ultrastructural responses of birch clones exposed to ozone and drought stress. Chemosphere 36(4):679-684.

Paul, L. K., Rinne, P. & van der Schoot, C. (2014) Shoot meristems of deciduous woody perennials: self-organization and morphogenetic transitions. Current Opinion in Plant Biology 17: 86-95.

Pépino, M., Proulx, R. & Magnan, P. (2013) Fall synchrony between leaf color change and brook trout spawning in the Laurentides Wildlife Reserve (Québec, Canada) as potential environmental integrators. Ecological Indicators 30: 16-20.

Polgar, C. A. & Primack, R. B. (2014) Leaf-out phenology of temperate woody plants: from trees to ecosystems. New Phytologist 191: 926–941.

Polgar C, Gallinat A and Primack RB (2014) Drivers of leaf-out phenology and their implications for species invasions: insights from Thoreau's Concord. New Phytologist, 202: 106-115.

Prasad AM, Iverson LR (2003) Little's Range and FIA Importance Value Database for 135 Eastern US Tree Species. Delaware, OH: Northeastern Research Station, USDA Forest Service.

Primack RB, et al. (2009) Spatial and interspecific variability in phenological responses to warming temperatures. Biol Conserv 142(11):2569–2577.

R Core Team (2015). *R: A language and environment for statistical computing.* R Foundation for Statistical Computing, Vienna, Austria.

Rivero RM, et al. (2007) Delayed leaf senescence induces extreme drought tolerance in a flowering plant. Proc Natl Acad Sci USA 104(49): 19631–19636.

Rosenthal, S. I. & Camm, E. L. (1997) Photosynthetic decline and pigment loss during autumn foliar senescence in western larch (Larix occidentalis). Tree Physiol. 17: 767-775.

Richardson, A. D. et al. (2012) Climate change, phenology, and phenological control of vegetation feedbacks to the climate system. Agricultural and Forest Meteorology 169: 156–173.

Richardson AD, Bailey AS, Denney EG, Martin CW, O'Keefe J (2006) Phenology of a northern hardwood forest canopy. *Glob Chang Biol.* 12(7):1174–1188.

Rustad, L. et al. (2011) Changing Climate, Changing Forests: The Impacts of Climate Change on Forests of the Northeastern United States and Eastern Canada. USDA Forest Service Northern Research Station General Technical Report NRS-99, 48.

Samish, R. M. (1954) Dormancy in woody plants. Annual Review of Plant Physiology 5: 183–204.

Schwarz G (1978) Estimating the dimension of a model. *Ann Stat*, 6: 461–464.

Spencer, D. M. & Holecek, D. F. (2007) A profile of the fall foliage tourism market. Journal of Vacation Marketing 13: 339-358.

Tanino, K.K., L. Kalcsits, S. Silim, E. Kendall and G.R. Gray. (2010) Temperature-driven plasticity in growth cessation and dormancy development in deciduous woody plants: a working hypothesis suggesting how molecular and cellular function is affected by temperature during dormancy induction. Plant Mol. Biol. 73:49–65.

Vitasse, Y., Porté, A. J., Kremer, A., Michalet, R. & Delzon, S. (2009) Responses of canopy duration to temperature changes in four temperate tree species: relative contributions of spring and autumn leaf phenology. Oecologia 161, 187-198.

Way, D. A. (2011). Tree phenology responses to warming: spring forward, fall back? Tree physiology, 31(5), 469-471.

Weih, M. (2009) Genetic and environmental variation in spring and autumn phenology of biomass willows (Salix spp.): effects on shoot growth and nitrogen economy. Tree Physiol. 29, 1479-1490.

West, B.T., Welch, K.B. & Galecki, A.T. (2007). *Linear mixed models: a practical guide using statistical software.* CRC Press, pp. 39-41.

Wilczek AM, et al. (2010) Genetic and physiological bases for phenological responses to current and predicted climates. Philos T Roy Soc B: Biological Sciences 365(1555): 3129-3147.

Xie Y, Ahmed KF, Allen JM, Wilson AM, Silander JA (2015a) Green-up of deciduous forest communities of northeastern North America in response to climate variation and climate change. Landscape Ecology, 30: 109-123.

Xie, Y., Wang, X. & Silander, J. A. (2015b) Deciduous forest responses to temperature, precipitation, and drought imply complex climate change impacts. Proceedings of the National Academy of Sciences (USA). doi: 10.1073/pnas.1509991112

Xu Y, Huang B (2007) Heat-induced leaf senescence and hormonal changes for thermal bentgrass and turf-type bentgrass species differing in heat tolerance. J Amer Soc Hort Sci 132(2):185–192.

Zhang X, et al. (2003) Monitoring vegetation phenology using MODIS. Remote Sens Environ 84(3):471–475.

Zuur, A., Ieno, E.N., Walker, N., Saveliev, A.A. & Smith, G.M. (2009). *Mixed effects models and extensions in ecology with R.* Springer Science & Business Media, pp. 105-122.

Figure 3-1 Observed leaf phenology of 6 deciduous tree species in spring and autumn in 2013 at the RMP site in UCONN Forest (a) and at Harvard Forest (b). Each color indicates one species. Each dot is one observation. Each curve line is fitted logistic line fitted to the observations. Daily temperatures and precipitation are shown as black and light blue lines respectively. Spring phenology is leaf unfolding, and autumn phenology includes leaf coloration and leaf drop.

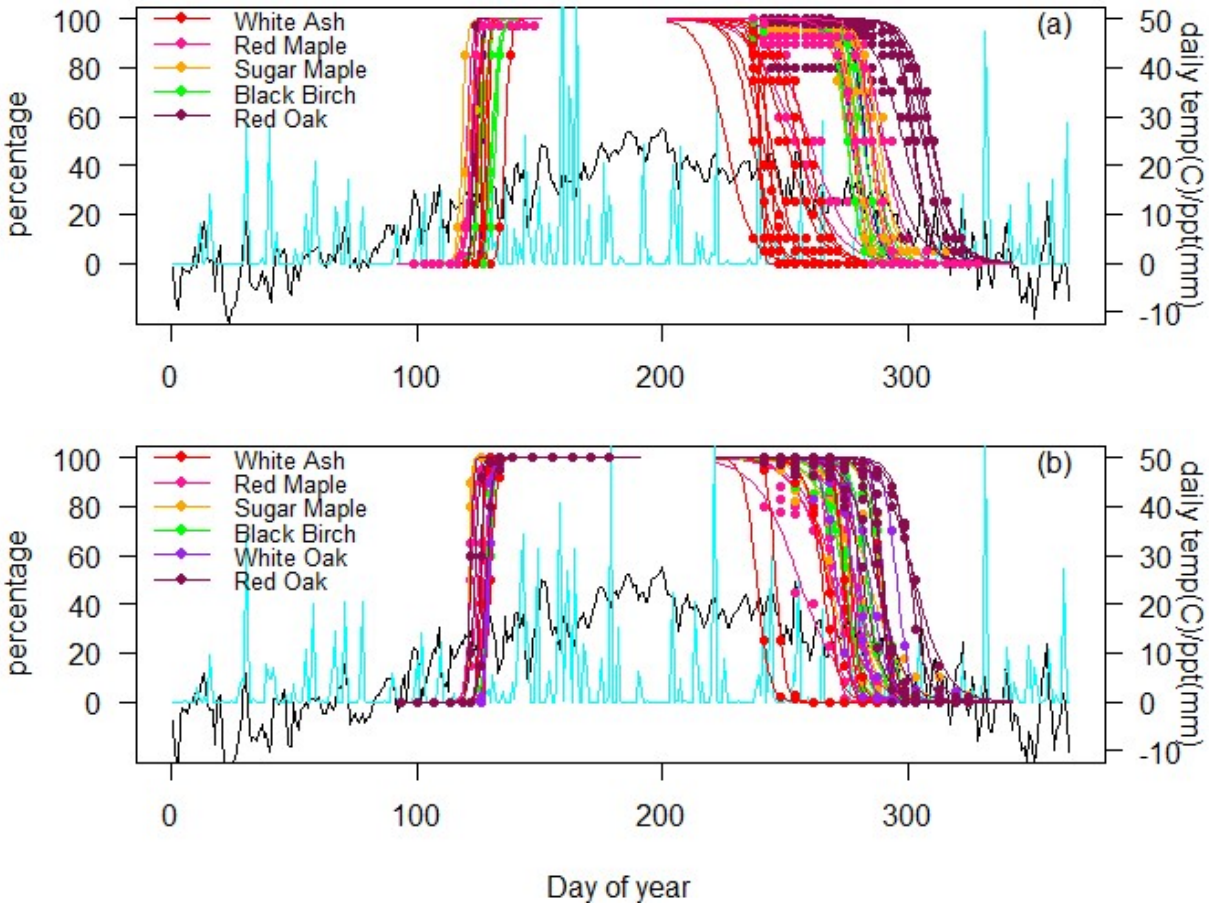

Figure 3-2 Coefficient values of predictors as deviation from random slopes in the best models for autumn phenology of 12 deciduous tree species at Harvard Forest (1993-2014). X axis displays the 12 tree species. 1: ACRU, 2: FRAM, 3: BEAL, 4: BEPO, 5: BELE, 6: BEPA, 7: ACPE, 8: ACSA, 9: QUAL, 10: QUVE, 11: QURU, 12: FAGR. Each set of bar plots represent one phenological transition date: (a) leaf coloration onset date; (b) leaf coloration peak date; (c) leaf coloration end date; (d) leaf drop onset date; (e) leaf drop peak date; (f) leaf drop end date. RD56: $RD_{(May.1- Jun.30)}$; GDR78: $GDR_{(Jul.1- Aug.31)}$; GDR90: $GDR_{(Sep.1- Oct.31)}$; ECA90: $ECA_{(Sep.1- Oct.31)}$; Tmin10: $T_{min-Oct}$; HD35: HD_{35}.

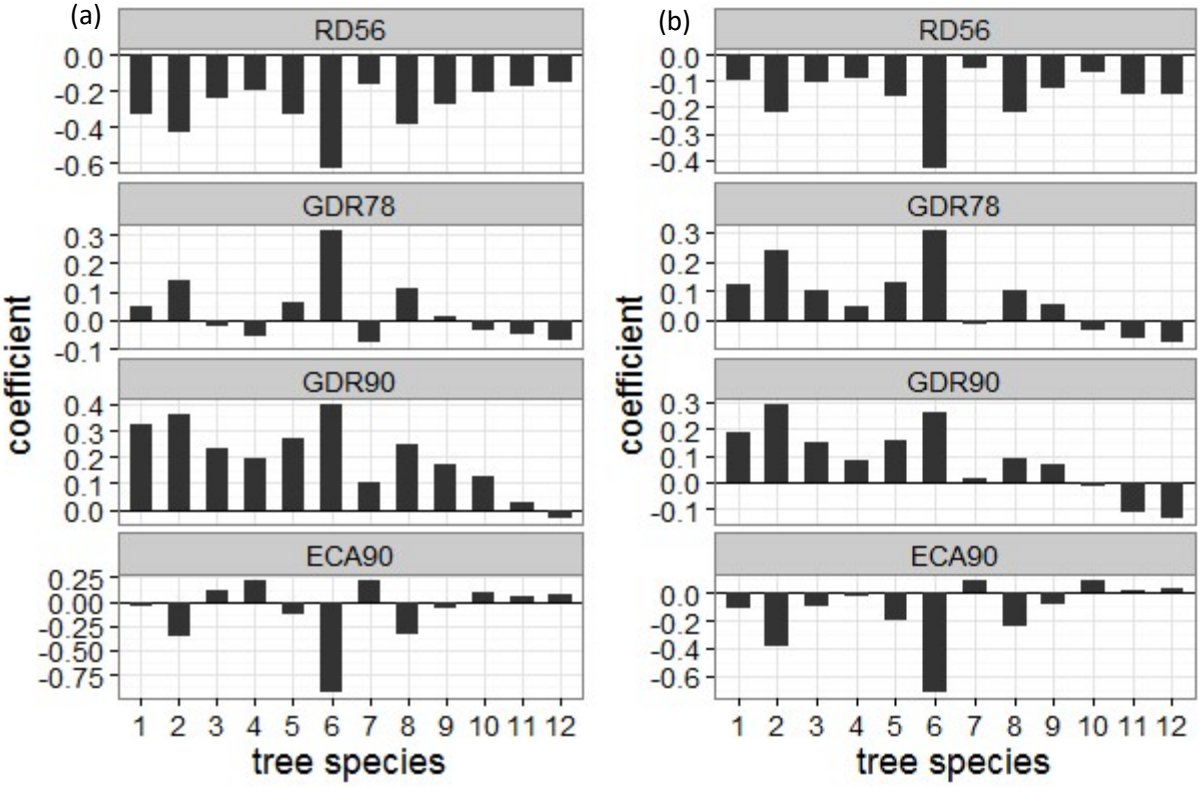

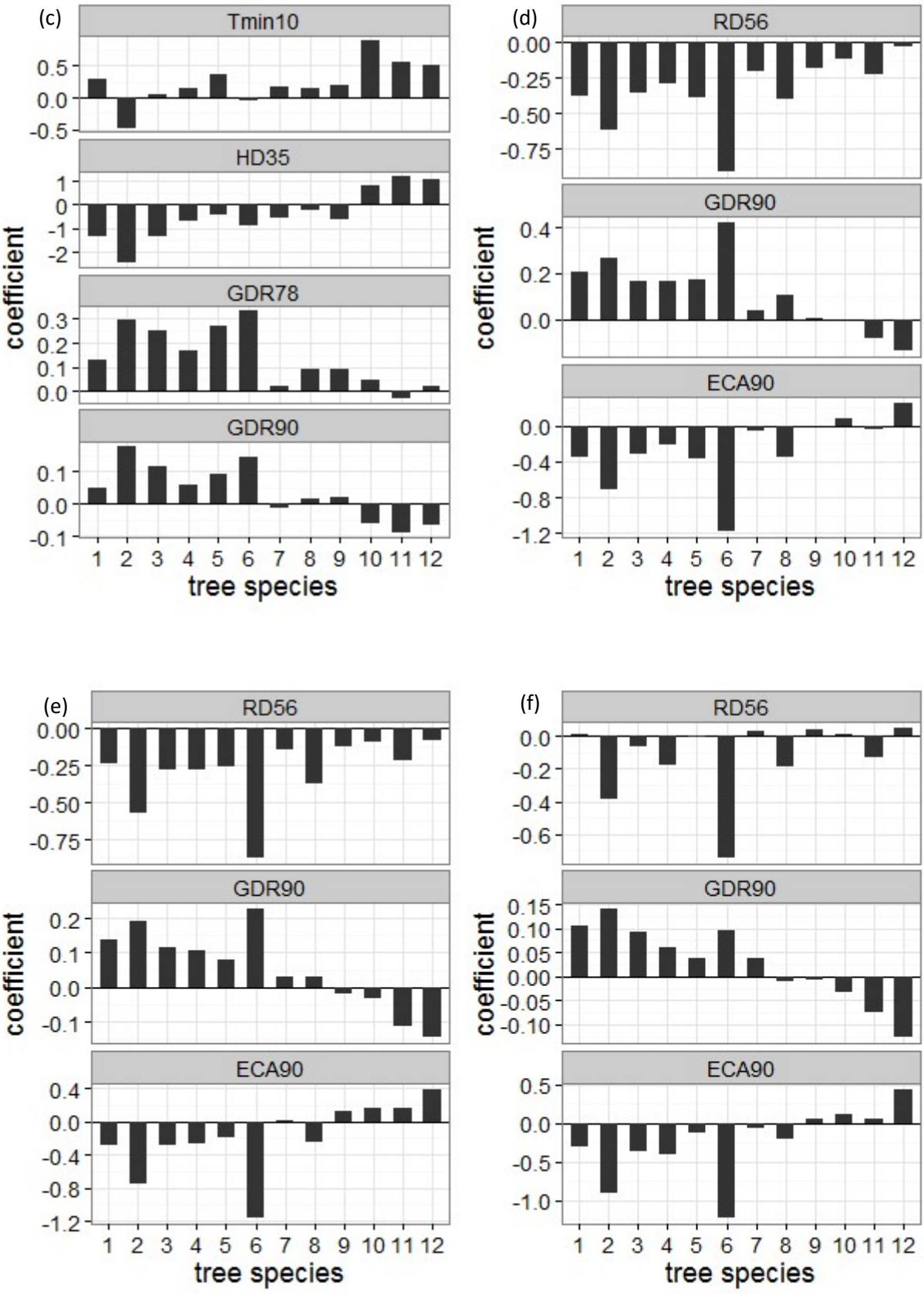
(c)
Tmin10
HD35
GDR78
GDR90
coefficient
tree species
(d)
RD56
GDR90
ECA90
coefficient
tree species
(e)
RD56
GDR90
ECA90
coefficient
tree species
(f)
RD56
GDR90
ECA90
coefficient
tree species

Figure 3-3 Boxplot of phenological transition dates of leaf coloration of 12 species over four time periods. X axis shows time periods: 0: 1993-2014; 1: 2015-2039; 2: 2040-2069; 3: 2070-2099. (a), leaf coloration onset date; (b), leaf coloration peak date; (c), leaf coloration end date.

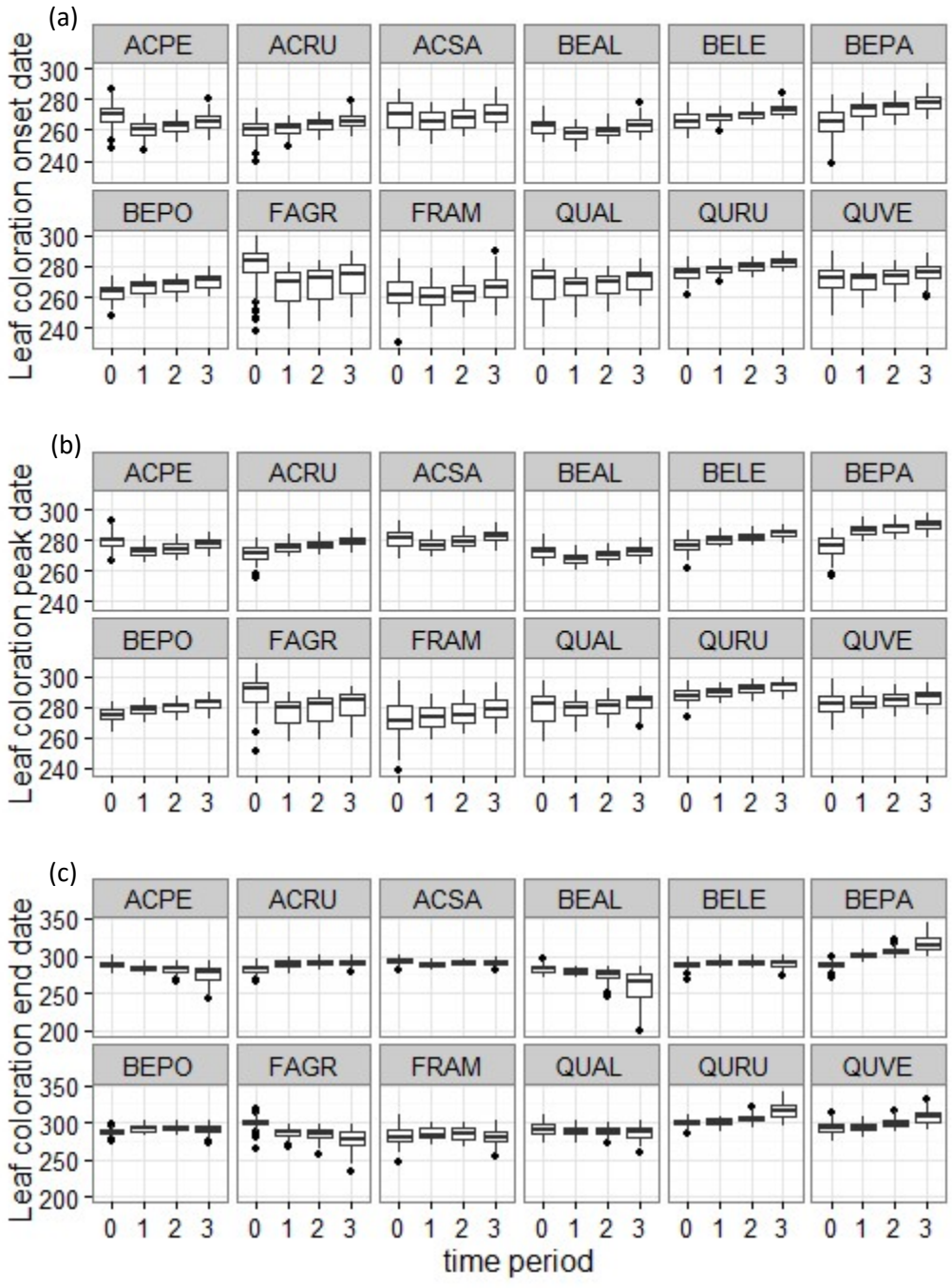

Figure 3-4 Boxplot of phenological transition dates of leaf drop of 12 species in four time periods. X axis shows time periods: 0: 1993-2014; 1: 2015-2039; 2: 2040-2069; 3: 2070-2099. (a), leaf drop onset date; (b), leaf drop peak date; (c), leaf drop end date.

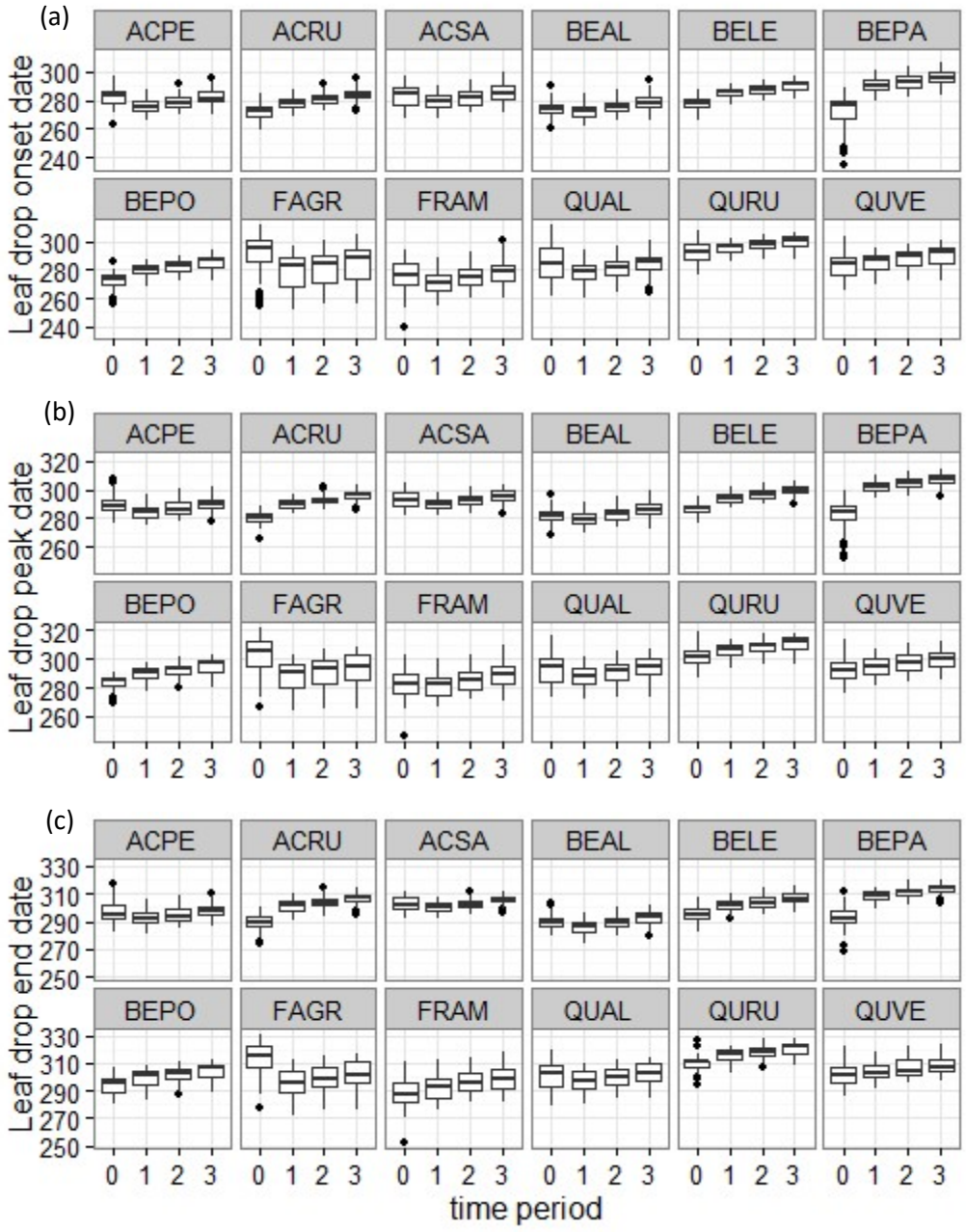

Table 3-1 Weather/climate variables developed to represent and summarize different conditions.

Name	**Description**
Cold degree day (CDD)	$\sum(T_b - T_i)$
Cold degree day (CDDi)	$\sum(T_b - T_{min})$
$T_{min\text{-}Oct}$	Monthly mean minimum temperature in October
Hot days (HD_{35})	number of days with $T_{max} \geq 35°C$
Frost days (FD)	number of days with $T_{min} \leq 0$ °C
Growing season drought (GDR)	number of events when ≥ 7 consecutive days without precipitation
Rainy days (RD)	number of days with precipitation ≥ 2mm
Heavy rainy days (ECA)	number of days with precipitation ≥ 20mm

T_b: base temperature; T_i: daily mean temperature; T_{max}: daily maximum temperature; T_{min}: daily minimum temperature

Table 3-2 Top five best mixed effects models for each phenophase of autumn phenology of 8 species in Connecticut and Harvard Forest from 2012 to 2014. Random effects include intercepts at both species and site levels. Variables in included in the models are all statistically significant. Bold numbers are smallest AIC and BIC. For variables names refer to Table 1. Subscript in each variable indicates the time period for each variable or the base temperature in calculations. LUs is leaf unfolding onset date, and LUp is leaf unfolding peak date.

Phenological transition date	Fixed effects in models	AIC	BIC
Leaf coloration onset date	$CDDi_{Aug10}$+$RD_{(Jul.1-Aug.31)}$+LUs	**2192.189**	**2218.277**
	$CDDi_{Aug10}$+$ECA_{(Sep.1- Oct.31)}$+LUs	2195.407	2221.495
	$CDDi_{Aug10}$+$GDR_{(Sep.1- Oct.31)}$+LUs	2202.934	2229.022
	$FD_{(Sep.1- Oct.31)}$+$GDR_{(Sep.1- Oct.31)}$+LUs	2203.426	2229.513
	$CDDi_{Aug10}$+$RD_{(Sep.1- Oct.31)}$+LUs	2205.532	2231.62
Leaf coloration peak date	$CDDi_{Aug10}$+$RD_{(Jul.1-Aug.31)}$+LUs	**2109.631**	**2135.719**
	$CDDi_{Aug10}$+$ECA_{(Sep.1- Oct.31)}$+LUs	2113.983	2140.071
	$FD_{(Sep.1- Oct.31)}$+$RD_{(Jul.1-Aug.31)}$+LUs	2114.41	2140.497
	$CDDi_{Aug10}$+$GDR_{(Sep.1- Oct.31)}$+LUs	2118.605	2144.693
	$CDDi_{Aug10}$+$RD_{(Sep.1- Oct.31)}$+LUs	2120.757	2146.844
Leaf coloration end date	$CDDi_{Aug10}$+$RD_{(Jul.1-Aug.31)}$+LUp	**2105.148**	**2131.235**
	$CDDi_{Aug10}$+$ECA_{(Sep.1- Oct.31)}$+LUp	2106.533	2132.621
	$FD_{(Sep.1-Nov.31)}$+$RD_{(Jul.1-Aug.31)}$+LUe	2106.811	2132.899
	$CDDi_{Sep10}$+$GDR_{(Sep.1- Oct.31)}$+LUp	2108.318	2134.406
	$CDDi_{Sep10}$+$RD_{(Sep.1- Oct.31)}$+LUp	2109.556	2135.644
Leaf drop onset date	$CDDi_{Oct10}$+LUs	**2132.261**	**2154.622**
	$CDDi_{ASO10}$+LUs	2132.822	2155.183
	$T_{min-Oct}$ +LUs	2133.921	2156.282
	$RD_{(Sep.1- Oct.31)}$+LUs	2135.763	2158.124
	$GDR_{(Sep.1- Oct.31)}$+LUs	2136.861	2159.222
Leaf drop peak date	$CDDi_{Oct10}$+LUs	**2075.138**	**2097.499**
	$CDDi_{ASO10}$+LUs	2075.239	2097.6
	$T_{min-Oct}$ +LUs	2076.001	2098.363
	$RD_{(Sep.1- Oct.31)}$+LUs	2080.033	2102.394
	$GDR_{(Sep.1- Oct.31)}$+LUs	2081.735	2104.096
Leaf drop end date	$CDDi_{ASO10}$+LUs	**2147.761**	**2170.122**
	$CDDi_{Oct10}$+LUs	2148.689	2171.05
	$T_{min-Oct}$ +LUs	2148.304	2170.665
	$RD_{(Sep.1- Oct.31)}$+LUs	2153.082	2175.443
	$GDR_{(Sep.1- Oct.31)}$+LUs	2154.381	2176.742

Table 3-3 Fixed variables from the best linear mixed effects models of autumn phenology for 12 deciduous tree species at Harvard Forest (1993-2014). For variables names refer to Table 1. Subscript in each variable indicates the time period for each variable or the base temperature in calculations. LUe is leaf unfolding end date.

Phenophase	Predictor	Coefficient	SE	p-value
leaf coloration onset date	$CDDi_{Aug20}$	-0.055	0.005	<0.001
	$RD_{(May.1\text{-}Jun.30)}$	-0.258	0.067	<0.001
	$GDR_{(Sep.1\text{-}Oct.31)}$	0.183	0.056	<0.001
	LUe	0.070	0.031	0.011
leaf coloration peak date	$CDDi_{Aug20}$	-0.028	0.005	<0.001
	CDD_{Sep20}	-0.043	0.006	<0.001
	$RD_{(May.1\text{-}Jun.30)}$	-0.114	0.051	0.013
	LUe	0.104	0.022	<0.001
leaf coloration end date	CDD_{Sep20}	-0.076	0.005	<0.001
	$T_{min\text{-}Oct}$	0.369	0.126	<0.001
	$GDR_{(Jul.1\text{-}Aug.31)}$	0.095	0.041	0.011
	LUe	0.126	0.022	<0.001
leaf drop onset date	$CDDi_{Aug20}$	-0.036	0.006	<0.001
	CDD_{Sep20}	-0.031	0.008	<0.001
	$RD_{(May.1\text{-}Jun.30)}$	-0.173	0.072	0.008
	$RD_{(Jul.1\text{-}Aug.31)}$	0.331	0.071	<0.001
leaf drop peak date	$CDDi_{Aug20}$	-0.019	0.005	<0.001
	CDD_{Sep20}	-0.059	0.007	<0.001
	$RD_{(May.1\text{-}Jun.30)}$	-0.194	0.065	0.002
	$RD_{(Jul.1\text{-}Aug.31)}$	0.309	0.057	<0.001
leaf drop end date	CDD_{Sep20}	-0.077	0.005	<0.001
	$RD_{(Jul.1\text{-}Aug.31)}$	0.334	0.062	<0.001
	$GDR_{(Jul.1\text{-}Aug.31)}$	0.165	0.037	<0.001

Appendix 3.1

1. Autumn phenology ground observation protocol

Observation frequency: Twice a week.

Environmental record: Cloudness (1-10) and temperature condition (40s, 50s, …, 80s F°) are recorded in every observation.

Phenophase: Budburst
One or more breaking leaf buds are visible on the plant. A leaf bud is considered "breaking" once a green leaf tip is visible at the end of the bud, but before the first leaf from the bud has unfolded to expose the leaf stalk (petiole) or leaf base.

Phenophase: Leaves unfolding
One or more live unfolded leaves are visible on the plant. A leaf is considered "unfolded" once the leaf stalk (petiole) or leaf base is visible. New small leaves may need to be bent backwards to see whether the leaf stalk or leaf base is visible. Do not include dried or dead leaves.

Phenophase: Leaf coloration
One or more leaves (including any that have recently fallen from the plant) have turned to their late-season colors.

Phenophase: Leaf drop
One or more leaves are falling or have recently fallen from the plant.

Table 3.1-1 Phenology ground observation protocol for four phenophases.

Stage	Score	Status	Meaning
Bud burst	01	Less than 3	How many buds are breaking
	02	3 to 10	
	03	More than 10	
Leaf unfolding	11	Less than 5%	What proportion of the canopy is full with leaves
	12	5-24%	
	13	25-49%	
	14	50-74%	
	15	75-94%	
	16	95% or more	
Leaf coloration	99% 98% 97% 95% 93% 90% 85% 80% 75% 70% 60% 50% 25% 10% 5%		What proportion of the canopy is full with green leaves
Leaf drop	99% 98% 97% 95% 93% 90% 85% 80% 75% 70% 60% 50% 25% 10% 5%		What proportion of the canopy is still with leaves

2. Linear mixed effects models and model selection procedure

The linear mixed effects model is written in equation 2.1.

$$Y_i=X_i\beta + Z_i\gamma_i + \varepsilon_i \qquad (2.1)$$

In equation 2.1, Y_i represents response variable for the i-th subject. $X_i\beta$ is the fixed component of the model, and $Z_i\gamma_i$ is the random component of the model. X_i is matrix including fixed variables. β contains fixed parameters of fixed variables. Z_i is a design matrix that represents the known values, which have effects on the continuous response variable that vary randomly across subjects. γ_i and ε_i are assumed to be independent and normally distributed (West et al. 2007; Zurr et al. 2009; Greven and Kneib 2010). In this study, the response variable is phenological date for each individual tree. The fixed variables are climatic/weather variables and spring phenological date. The random components include random intercept at individual or species or site levels, and random slopes at species level.

The model selection procedure used in this study is top-down strategy, which is recommended by Diggle et al. (2002) and discussed by Zurr et al. (2009) and West et al. (2007). The strategy contains a few steps. 1. Start with a model where the fixed component contains as many explanatory variables as possible to make sure the response variables is well explained. This is called the beyond optimal or loaded model. 2. Select an optimal structure for random effects in the model. In this step, we tested a set of random effects, and we applied condition AIC (cAIC) (Greven and Kneib 2010) as a selection criteria. Residual maximum likelihood estimation (REML) was used. The goal is to select important random slopes to contribute to explain variations of response variables that are not explained by fixed component. 3. Select an optimal structure for fixed variables. Using the optimal random structure selected in previous step, we tested the covariance in fixed component to select significant variables. In this step, we applied marginal AIC (mAIC) (Greven and Kneib 2010) as a selection criteria. Maximum likelihood estimation (ML) was used. 4. Report the best model using REML.

References:

Diggle, P.J., Heagerty, P., Liang, K.Y. & Zeger, S.L. (2002). *Analysis of longitudinal data*. 2nd edn. New York, Oxford.

Greven, S. & Kneib, T. (2010). On the behaviour of marginal and conditional AIC in linear mixed models. Biometrika, doi: 10.1093/biomet/asq042.

West, B.T., Welch, K.B. & Galecki, A.T. (2007). *Linear mixed models: a practical guide using statistical software.* CRC Press, pp. 39-41.

Zuur, A., Ieno, E.N., Walker, N., Saveliev, A.A. & Smith, G.M. (2009). *Mixed effects models and extensions in ecology with R.* Springer Science & Business Media, pp.105-122.

Table 3.1-2 Coordinates and altitude of five plots and observed 8 species in each site in UConn Forest and 12 species in Harvard Forest.

Site name	Latitude	Longitude	Elevation (m)	Species
ASP	41.821	-72.250	198	*Acer saccharum* (5), *Carya glabra* (5), *Carya ovata* (4), *Fraxinus americana* (5)
CRP	41.795	-72.202	166	*Carya glabra* (5), *Carya ovata* (3), *Quercus alba* (5), *Quercus rubra* (5)
HBP	41.822	-72.249	186	*Acer saccharum* (4), *Carya glabra* (6), *Carya ovata* (5), *Quercus alba* (2), *Quercus rubra* (1)
RMP	41.816	-72.238	155	*Acer rubrum* (5), *Acer saccharum* (4), *Betula lenta* (5), *Carya ovata* (1), *Quercus alba* (3), *Quercus rubra* (5), *Fraxinus americana* (4)
SMP	41.832	-72.246	115	*Acer saccharum* (10), *Carya ovata* (3)
Harvard Forest	42.535	-72.185	335~365	*Acer pensylvanicum (4), Acer rubrum (5), Acer saccharum (4), Betula alleghaniensis (3), Betula lenta (3), Betula papyrifera (4), Betula populifolia (4), Fagus grandifolia (6), Fraxinus americana (6), Quercus alba (5), Quercus rubra (4), Quercus velutina (4).*

Table 3.1-3 Random effects from the best linear mixed effects models of autumn phenology of 12 deciduous tree species in Harvard Forest (1993-2014). Intercept_spp and intercept_id are random intercepts at species and individual levels. Variables names refer Table 1. Subscript in each variable indicates the time period for each variable or the base temperature in calculations.

Phenophase	Random effects	Standard deviation*
leaf coloration onset date	Intercept_spp	4.60
	$RD_{(May.1\text{-}Jun.30)}$	0.15
	$GDR_{(Jul.1\text{-}Aug.31)}$	0.13
	$GDR_{(Sep.1\text{-}Oct.31)}$	0.14
	$ECA_{(Sep.1\text{-}Oct.31)}$	0.38
	Intercept_id	6.99
leaf coloration peak date	Intercept_spp	6.31
	$RD_{(May.1\text{-}Jun.30)}$	0.12
	$GDR_{(Jul.1\text{-}Aug.31)}$	0.14
	$GDR_{(Sep.1\text{-}Oct.31)}$	0.16
	$ECA_{(Sep.1\text{-}Oct.31)}$	0.28
	Intercept_id	5.80
leaf coloration end date	Intercept_spp	5.90
	$T_{min\text{-}Oct}$	0.41
	HD_{35}	1.23
	$GDR_{(Jul.1\text{-}Aug.31)}$	0.15
	$GDR_{(Sep.1\text{-}Oct.31)}$	0.10
	Intercept_id	3.92
leaf drop onset date	Intercept_spp	4.78
	$RD_{(May.1\text{-}Jun.30)}$	0.30
	$GDR_{(Sep.1\text{-}Oct.31)}$	0.20
	$ECA_{(Sep.1\text{-}Oct.31)}$	0.48
	Intercept_id	5.37
leaf drop peak date	Intercept_spp	5.87
	$RD_{(May.1\text{-}Jun.30)}$	0.26
	$GDR_{(Sep.1\text{-}Oct.31)}$	0.13
	$ECA_{(Sep.1\text{-}Oct.31)}$	0.48
	Intercept_id	4.36
leaf drop end date	Intercept_spp	6.98
	$RD_{(May.1\text{-}Jun.30)}$	0.27
	$GDR_{(Sep.1\text{-}Oct.31)}$	0.09
	$ECA_{(Sep.1\text{-}Oct.31)}$	0.52
	Intercept_id	4.24

*Values of standard deviation of random effects indicates variability of random intercepts and slopes at species and individual levels.

Table 3.1-4 Best models of the onset, peak and end dates of leaf unfolding of 12 species in Harvard Forest from 1993 to 2014. T_{mean3}, T_{mean4}, and T_{mean5} are monthly mean temperature in March, April and May. Coefficients of fixed variables include mean values and standard deviations. Intercept_spp and intercept_id are random intercepts at species and individual levels.

Transition date	Fixed variable	Coefficient	Random effects	Standard Deviation
onset date	T_{mean3}	-0.53(0.09)	T_{mean4}	0.81
	T_{mean4}	-1.74(0.27)	Intercept_spp	4.76
	T_{mean5}	-1.18(0.12)	Intercept_id	2.79
peak date	T_{mean3}	-0.43(0.09)	T_{mean4}	0.76
	T_{mean4}	-1.41(0.25)	Intercept_spp	4.87
	T_{mean5}	-1.54(0.12)	Intercept_id	2.69
end date	T_{mean3}	-0.27(0.10)	T_{mean4}	0.70
	T_{mean4}	-1.01(0.25)	Intercept_spp	5.77
	T_{mean5}	-1.90(0.13)	Intercept_id	2.71

Table 3.1-5 Marginal and conditional R-squared of the best linear mixed effects models for autumn phenology of 12 deciduous tree species in Harvard Forest (1993-2014).

Transition date	$R_{(m)}^2$	$R_{(c)}^2$
leaf coloration onset date	0.044	0.73
leaf coloration peak date	0.064	0.82
leaf coloration end date	0.110	0.82
leaf drop onset date	0.040	0.78
leaf drop peak date	0.050	0.84
leaf drop end date	0.055	0.85

Marginal $R_{(m)}^2$ represents the variance explained by fixed factors. Conditional $R_{(c)}^2$ is interpreted as variance explained by both fixed and random factors (i.e. the entire model).

Figure 3.1-1 Demonstration on determining three phenological transition dates for observed leaf unfolding (solid dots), leaf coloration (solid triangles) and leaf drop (solid squares). The solid curve lines are fitted logistic lines based on observed data. Red arrows indicate three phenological transition dates: onset, peak and end date.

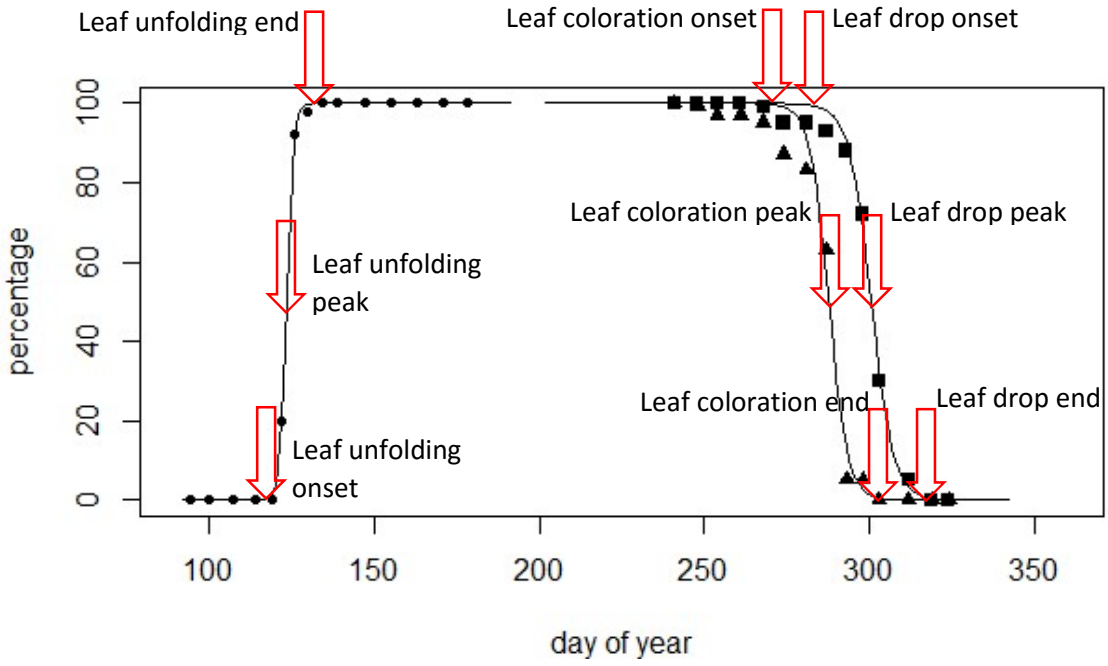

Figure 3.1-2 Observed phenological dates and predicted dates from the best models for 12 tree species autumn phenology in Harvard Forest (1993-2014). Root mean square error and r^2 values indicate goodness of model predictions. Smaller RMSE and higher r^2 indicate better model predictions. Black lines are 1:1 lines.

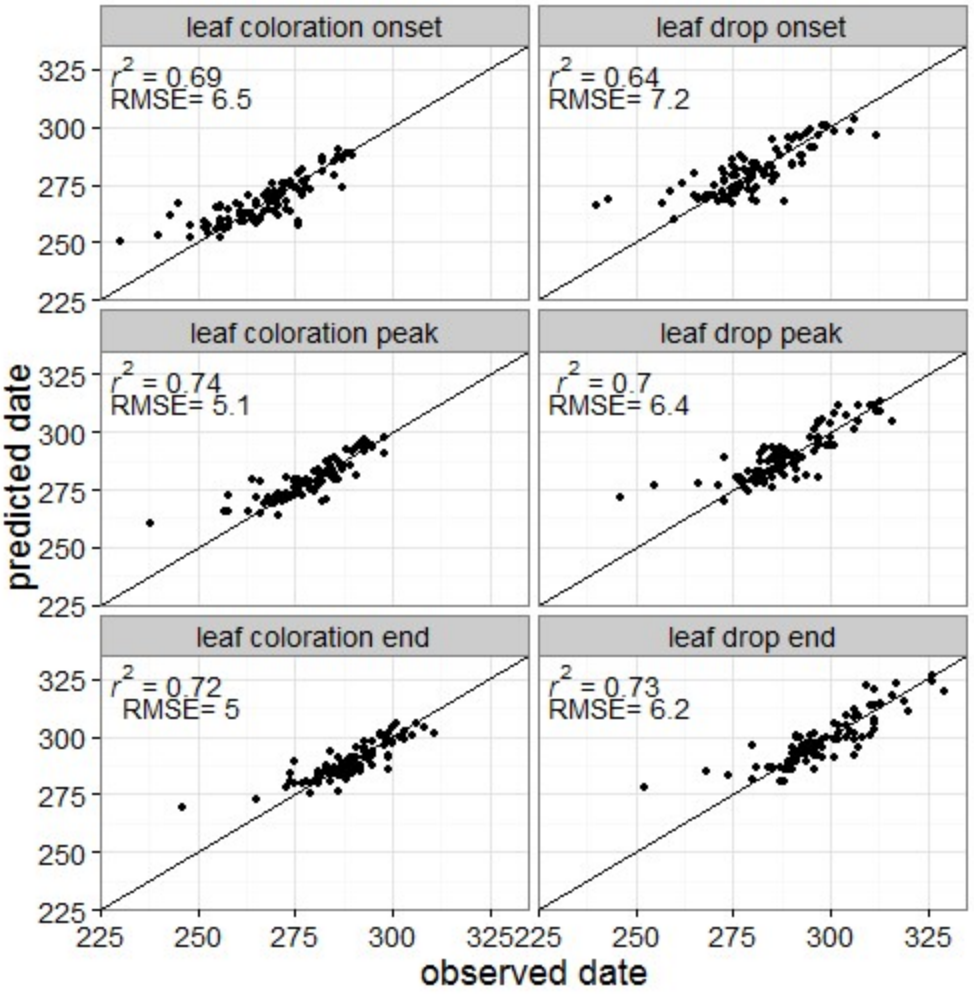

Figure 3.1-3 Boxplots of leaf coloration peak dates of 52 trees of 12 species in Harvard Forest during 1993 and 2014. Different colors indicate species. Each boxplot is for one individual tree. Variations of leaf coloration peak dates among individual trees with each species is clear from this plot. Similar patterns are found in other phenological transition dates as well.

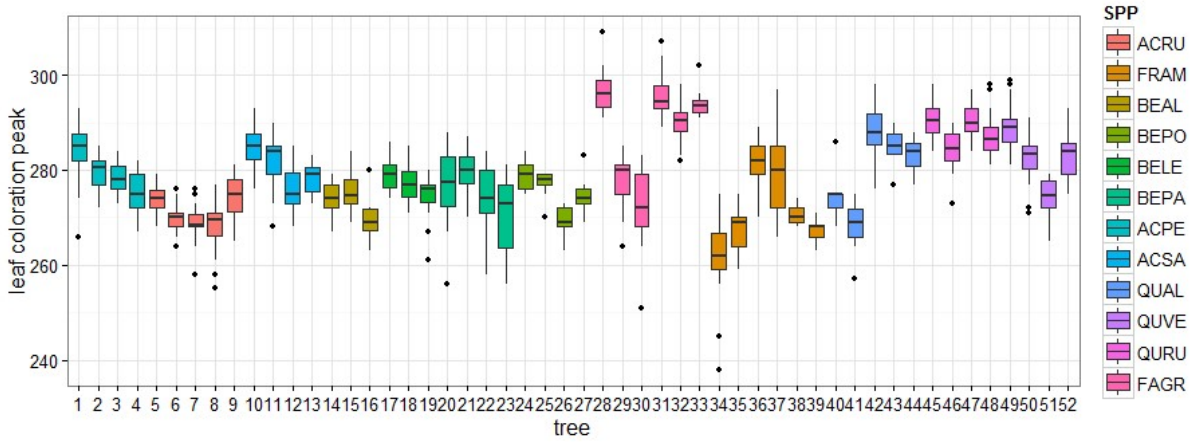

Chapter 4

Species-specific leaf phenology captured by digital cameras

Abstract

Plant leaf phenology is typically observed either via ground-based visual observations on individuals or via remote sensing of land surface vegetation. But the challenge exists in interpreting phenological information from both data sources, collected at different spatial scales using different observational protocols. As an intermediate step, digital cameras are employed, that span an area with enough spatial resolution to identify temporal changes in individual deciduous tree species canopies with continuous observations. But it was unknown how these camera images relate to field observations, and how the metrics from those images provide comparable species-specific phenological responses to the environment. We set a suite of digital time-lapse cameras to take continuous photos of deciduous tree canopies in Connecticut from 2012 to 2014. Color indices were derived from three color channels from the images, focusing on green and red, and phenological transition dates were determined from time series of color indices for each tree canopy at each site. Comparisons between image derived dates and observed phenological dates showed that both green and red color indices could be matched to ground observations, and red color indices had better performance in match autumn phenology across our group of 8 dominant tree species. New phenological transition dates were developed based on the red color index. Linear mixed effects models were applied to investigate the relationships between climatic/weather conditions and the timing of peak and intensity of red color in fall foliage for each species. Model results suggested that temperature, precipitation in autumn, drought-stress in summer and autumn, and heat-stress in summer are all important factors of the timing of peak fall foliage color. This study improves our understanding of temporal and spatial variation in the phenology of deciduous trees as captured by digital cameras. This study also provides insights into linking information on phenology from field to remote sensing and emphasize the need for further research on autumn phenology using the change in redness of tree canopies.

Introduction

Plant leaf phenology in temperate deciduous forests, the study of annual life-cycle events in plants from bud-bust and leaf expansion in the spring through to leaf coloration and drop in the fall, is typically observed through ground-based observation on individuals in the field or remote sensing of land surface vegetation from satellites. We know that species differ in their phenological responses to environmental cues (Richardson et al. 2006, Primack et al. 2009, Polgar et al. 2014). As a consequence, community-level phenology as observed remotely will vary spatially and temporally as species and environmental conditions vary. Large spatiotemporal variation of phenology provides challenges in analyzing and summarizing community-level phenogical patterns (Diez et al. 2012, Xie et al. 2015). Moreover, the different observation scales and protocols make the integration of ground-based observations and remotely sensed data difficult. New methodology is needed to build a bridge linking ground-based species phenology to multi-species land surface phenology viewed remotely.

Digital cameras have been used as a near-surface remote sensing tool to record seasonal change in forest canopy phenology (Richardson et al. 2007, 2009, Ide and Oguma 2010, Sonnentag et al. 2012). These "pheno-cameras" may provide the necessary tool to bridge ground-based and satellite-based phenological observations and modeling. One advantage of digital "pheno-cameras" is that they may compensate for time-consuming and necessarily periodic field observations, and the large spatial extent of satellite remote sensing. Moreover, digital pheno-cameras cover areas with enough spatial resolution to identify temporal changes in individual species tree canopies as well as groups of individuals forming a continuous canopy with unbroken daily observations. Phenological time series metrics can be derived from digital camera images for the whole growing season at local stand scales. Comparisons between vegetation indices from satellite remote sensing and color indices from digital cameras suggest significant agreement of these two metrics (Hufkens et al. 2012, Keenan et al. 2014). However, it is not known how near-surface remote sensing relates to field observations. More specifically, it is unclear whether

phenological information is adequately captured by digital camera images, and whether the metrics from pheno-camera images can be compared to ground-based metrics.

Pheno-camera images typically report out three color channels (red, green and blue), which allows the detection of changes in greenness and redness of tree canopies across the growing season (Richardson et al. 2007), that is difficult to measure simply using ground-based visual phenological observations. However, previous studies using digital cameras have only focused on the changes in greenness (Ide and Oguma 2010, Sonnentag et al. 2012, Keenan et al. 2014). The changes in leaves during autumn senescence include greenness declining and the accumulation of red pigments (primarily anthocyanins and some carotenoids) (Sanger 1971, Archetti et al. 2011). Although chlorophyll is the visually dominant pigment in leaves, carotenoids are present as well. In the fall with the beginning of leaf senescence chlorophyll is degraded (chlorophyll *a* to *b* forms that give leaves a darker green color tone) and carotenoids are uncovered (various forms expressing yellow, orange and sometimes reddish colors in the senescent leaves) (Lee et al. 2003, Field et al. 2011). At the same time anthocyanins concentrations may build up in leaves typically in response to various abiotic and biotic stresses (e.g. nutrient deficiency, low pH, drought-stress, insect damage, high UV light, etc.) (Dixon and Paiva 1995, Chalker-Scott 1999). To date we know more about role of anthocyanins in leaf coloration in the autumn, because of more extensive work on the physiology, genetic regulation, biosynthesis and basic biology of red anthocyanin pigments (Close and Beadle 2003, Viña and Gitelson 2011, Misyura et al. 2012). Different forms of anthocyanins tend to be intensely red or even purple in color. These pigments also breakdown as leaves continue to senesce, nutrients are reabsorbed and leaves turn brown with just tannins remaining as leaves drop (Close and Beadle 2003). Good correlations have recently been found between redness derived from camera images and anthocyanin indices (Yang et al. 2014). The striking color of leaves displayed in autumn is the key element of fall foliage ecotourism (Rustad et al. 2011, Archetti et al. 2013, Morse and Smith 2015). Although how climate and weather variation affects the leaf colors and the timing of fall foliage gets considerable attention from the public, few studies have focused on quantifying the colors

and the effects of environmental conditions on the timing or intensity of color. Thus, it is important to explore the capability of using the change of redness as observed via phenol-cameras to collect information on fall foliage in autumn for different species to help understand how environmental factors affect the autumn leaf senescence and coloration.

This study aims to: 1) capture seasonal phenological changes in a suite of canopy trees using digital 'pheno-cameras'; 2) examine the relationship between signals caught by digital cameras compared with ground-based visual observation on leaf phenology; 3) examine different patterns of phenological change among different species and individuals within species using digital camera images; 4) investigate the relationships between climatic/weather conditions and the peak date and value of fall foliage color) derived from camera images across species and sites.

Methods

We set up time-lapse cameras (Wingscapes, http://www.wingscapes.com/) that we term "pheno-cameras" to take photos of deciduous forest tree species canopies in nine sites in and around the forested landscapes of University of Connecticut campus and Mansfield, CT, USA. Cameras faced west or north avoiding direct sun light in the camera lens. Photos are taken hourly during the daytime across the whole growing season. The resolution of the images, containing 4 to 6 canopy trees in the field of view, was 2560×1920 pixels. This resolution allows identification of tree species canopies and their associated phenophases (bud burst, leafing out, leaf coloration and leaf dropping) for each individual in the image (see a video showing seasonal change of tree canopies at one site in 2013, https://www.youtube.com/watch?v=riRznj2kfw0). Images were processed using PhenoCam GUI, software developed by Andrew Richardson's research group in Harvard University (http://phenocam.sr.unh.edu/webcam/tools/, Richardson et al. 2007, 2009). Foggy or dark images due to poor weather (fog, rain and snow) and light conditions were excluded from analyses. Regions of interest (ROI) in each image series were designed to include specific areas for image processing, such as the

whole canopy of the forest in the image, or individual canopies of specific trees (Fig. 4.1-1). Sky and shadow areas were avoided from including in ROI, and the region with the most homogeneous canopy was chosen as the ROI for each individual tree in the image. Reflectance information in the images were represented by three color channels (Red, Green, and Blue) digital numbers (DN). DN of each color channel was calculated using the PhenoCam software and averaged for all the pixels within the ROI for each image. Three color chromatic coordinates of red, green and blue (r_{cc}, g_{cc} and b_{cc}) were calculated in each ROI in each image over time (Gillespie et al. 1987; Sonnentag et al. 2012) to represent relative brightness of three color channels. The equations are:

$$r_{cc} = \text{R\_DN}/(\text{R\_DN} + \text{G\_DN} + \text{B\_DN}),$$

$$g_{cc} = \text{G\_DN}/(\text{R\_DN} + \text{G\_DN} + \text{B\_DN}),$$

$$b_{cc} = \text{B\_DN}/(\text{R\_DN} + \text{G\_DN} + \text{B\_DN}).$$

We calculated time series of visible atmospherically resistant vegetation index (VARI) for each ROI in images. It has been shown that VARI, defined as: $\text{VARI} = (\text{G\_DN} - \text{R\_DN})/(\text{R\_DN} + \text{G\_DN} - \text{B\_DN})$, has a strong linear relationship with the relative content of anthocyanin in plant leaves and that this may be used to detect plant phenological change over time in the autumn (Viña and Gitelson 2011).

Time series of color indices from the pheno-camera images were analyzed for eight dominant tree species of southern New England forests at nine sites (Table 4-1). Eight species (with total number of replicates) were *Acer rubrum* (6)*, Acer saccharum* (7)*, Betula lenta* (3)*, Carya glabra* (3)*, Carya ovata* (3)*, Fraxinus americana* (4)*, Quercus alba* (2)*,* and *Quercus rubra* (14). Based on the time series of g_{cc}, both the start and the end of season were determined for each canopy tree. The start of season (SOS) was determined as the day on which g_{cc} started to increase in spring (Fig. 4-1a). The end of season (EOS) was determined as the day on which g_{cc} reached the minimum value in autumn (Fig. 4-1a). To capture more information of changes of tree foliage color in autumn, we used time series of r_{cc} to determine the day on which r_{cc} reached to the maximum value, which indicates the timing of the peak of redness of fall foliage

(POR) (Fig. 4-1b). We also used the day on which r_{cc} stopped decreasing from the maximum value and reaching the minimum value in late autumn to indicate the end of redness (EOR) (Fig. 4-1b). We calculated the deviation of redness (DOR), which is the maximum minus the minimum value of r_{cc}, to represent how much redness was expressed (i.e intensity of redness) in each tree in each year. The value of VARI is negatively correlated to relative content of anthocyanins, which means VARI decreases during autumn when anthocyanins are produced. To extract the day on which the relative content of anthocyanin was highest, we used the minimum value of VARI in autumn to determine the day of the peak of relative anthocyanin (PORA) in tree canopies (Fig. 4-1c). PORA is an alternative metric to POR for scoring peak autumn foliage redness.

We had parallel, ground-based visual observations on leaf phenology for each of these eight tree species measured twice a week in spring and autumn replicated at four sites (Table 4.1-1). Phenological transition dates (i.e. onset, peak and end dates) of leaf unfolding, leaf coloration and leaf drop of each tree were determined based on our visually observed data. We compared the visually observed leaf phenology of each tree in the field with the phenological dates derived from pheno-camera images to help us understand how ground-based visual observations relate to the dates derived from pheno-camera monitoring of the same canopy trees. Observed leaf phenology dates included the onset, peak, and end dates for each of: leaf unfolding, leaf coloration and leaf drop. Image derived dates included SOS, EOS, POR, and EOR. Comparison for spring phenology was between three phenological transition dates of leaf unfolding and SOS. For autumn phenology we conducted comparisons between the onset, peak, and end date of leaf coloration and EOS and POR, and between the onset, peak, and end date of leaf drop and EOS and EOR. PORA was not used in comparison since we found that POR was highly correlated to PORA. For each pair of comparison, r^2 and root mean square error were calculated between visually scored observations and image derived dates to show how comparable the dates were for all tree species and sites sampled.

To investigate how climatic/weather factors affect the timing of the peak of fall foliage color of canopy trees, we applied similar statistical methods used in Chapter 3 to two image derived dates: POR and PORA. We set HOBO® loggers to record hourly temperature at the nine sites, then calculated daily mean, minimum, and maximum temperatures. Daily precipitation data was obtained from the weather station in Storrs, Connecticut from the United States Historical Climatiology Network (http://cdiac.ornl.gov/epubs/ndp/ushcn/ushcn_map_interface.html). Climatic/weather variables across three seasons (spring, summer and autumn) were calculated to represent chill, frost, wet conditions and extreme weather events (e.g. heat-, drought-stress, and heavy rainfall events) (cf. Table 3-1).

We used linear mixed effects models to identify and quantify the important climatic/weather factors affecting the timing of the peak of fall foliage. POR and PORA were separately fitted as response variables in the models. Random intercept and slopes models, with species and sites as random intercept, were used in the modeling. Potential climate/weather factors and spring phenology were set as fixed effects or random slopes. While inter-annual variation in phenology was explained by climate/weather factors, variation in phenology among species and sites were modeled by random intercepts. Random slopes at the species level explained species-specific phenological responses in autumn to variation in climate/weather factors. We used a top-down strategy (Diggle et al. 2002, West et al. 2007, Zurr et al. 2009) to build models and selected the best models using marginal AIC (mAIC) for fixed effects and conditional AIC (cAIC) for random effects (Greven and Kneib 2010) (see model selection procedures in Appendix of Chapter 3). Data were analyzed using R software (R Core Team 2015). Best models based on AIC criteria were reported for two dates, POR and PORA. We also applied linear mixed effects models to DOR to investigate the relationships between climatic/weather factors and how red each tree canopy was (i.e. DOR). We used random intercept at the individual tree level in the linear mixed effect models for DOR, and used climatic/weather factors as fixed variables. Models were fitted for eight species together and three species separately (red maple, sugar maple and red oak) that had most replicate trees in the dataset, and are known to display red-hued foliage in the autumn (Coder 2008).

Results

Color indices generated from pheno-camera images represent seasonal changes of deciduous trees species over the growing season. Across the whole growing season from spring to autumn, the change of g_{cc} represented the seasonal change of greenness of tree canopies. All tree species had similar patterns of change in g_{cc} (Fig. 4-2). Increasing g_{cc} in spring indicated the development stages of canopy tree leaves from bud burst and leaf unfolding to full leaf expansion, while the decrease in g_{cc} in autumn indicated the process of leaf coloration change associated with leaf senescence through to leaf drop. During the summer, g_{cc} deceasing slightly with the green color of leaves became darker as they matured. Among eight dominant deciduous tree species, their Start of Seasons (SOSs) had small differences (within 0-9 days), but the differences in End of Seasons (EOSs) were much larger, varying from 3 to 30 days (Table 4-2). The period between SOS and EOS can be used as proxies of growing season length for these deciduous tree species. Consistent differences of growing season length among deciduous tree species (e.g. shorter growing season length of maples (158-162 days on average) than oaks (164-169 days on average)) were found. Interestingly these differences were mostly attributed to the larger differences among species in the end of growing season (EOS).

All tree species showed similar patterns in change of r_{cc} across the growing season. While r_{cc} started to increase in spring matching the increasing of g_{cc}, r_{cc} increased most dramatically in the fall reached to the maximum value corresponding to the peak of red color of fall foliage. After the peak, r_{cc} decreased while leaves dropped. The changes of r_{cc} during the growing season also reflect species-specific differences (Fig. 4-3). In our eight species, PORs and EORs of maples, white ash and black birch were always earlier than oaks and hickories. Similar patterns were also found in the time series of VARI and PORAs of eight species (Fig. 4.1-2). We found that PORs and PORAs had a high positive correlation (r=0.92).

Comparisons of spring phenology using leaf unfolding based on visual scoring and SOS based on phenol-camera g_{cc} metrics, showed that SOS were later on average than the onset date of leaf unfolding,

but were earlier on average than the peak date of leaf unfolding across all tree species (Fig. 4.1-3). In comparisons of autumn phenology, we found that dates derived from time series of r_{cc} (POR and EOR) had a better match (relative high values of r^2 and low values of RMSE) to visually observed end dates of leaf coloration and end dates of leaf drop than the EOS derived from g_{cc} metrics (Fig. 4-4 and 4-5). Both EOS and POR match well with the end date of leaf coloration, but POR had more data points falling on the 1:1 line than EOS based on the distributions of data in the figures (Fig. 4-4c and 4-4f). Compared to EOS, EOR had better matches to onset, peak and end dates of leaf drop based on values of r^2 and RMSE (Fig. 4-5). While EOS matched well with the peak date of leaf drop, EOR matched well with the end of leaf drop (Fig. 4-5b and 4-5f).

Linear mixed effects models for POR and PORA suggested that chill, frost, and rainfall in autumn, and drought in summer and autumn were most important factors affecting the timing of peak of red color in fall foliage. The best models of POR and PORA suggested that more frost in October (FD_{Oct}) and rainfall in autumn ($RD_{(Sep.1\text{-}Oct.31)}$) caused earlier peak of red color in fall foliage (Table 4-3). But different species showed different responses in POR and PORA to drought in autumn ($GDR_{(Sep.1\text{-}Oct.31)}$) and summer ($GDR_{(Jul.1\text{-}Aug.31)}$) (Fig. 4-6). More autumn drought delayed POR for two species (ACRU and QUAL), but lead to earlier POR for five other species (ACSA, BELE, CAOV, FRAM and QURU). The effect from autumn drought on POR for pignut hickory (CAGL) was minimal (coefficient is 0.002). More summer drought delayed PORA for six species (ACRU, ACSA, BELE, CAGL, FRAM, and QUAL), but lead to earlier PORA for the other two species (CAOV and QURU).

Large variation in Deviation of Redness (DOR) was found among species and individual replicate trees. DOR is a measure of the intensity of redness in autumn foliage. Black birch, maples and oaks had larger DORs than other species, and within each species the variation of DOR among years is much smaller than among replicate trees in different sites (Table 4-4). Linear mixed effects models did not find any significant results except in the models for sugar maple. Only CDDi (Cold Degree Day) and monthly minimum temperatures in September and October ($T_{min\text{-}Sep;}$ $T_{min\text{-}Oct}$), and frost days in October (FD_{Oct}) had

significant effects on DOR for sugar maples (Table 4.1-2). The coefficients in the models suggested that lower CDDi or higher minimum temperatures in September and October lead to higher value of DOR in sugar maples, and more frosts in October decreased DOR in sugar maples.

Discussion

This study focused on the use of digital "pheno-cameras" to monitor seasonal changes of deciduous tree canopies foliage color from spring through autumn. The objective was to investigate how foliage color indices derived from digital camera images match with ground-based visual observations of phenology on multiple tree species and quantify how these may vary spatially and temporally. We also investigated how climatic/weather factors affect the timing and intensity of peak red color in fall foliage across species and sites. We found the seasonal changes in greenness (g_{cc}) and redness (r_{cc}) seen in time series across the growing season, match what has been found in changes in leaf chlorophyll, carotenoids and anthocyanin pigments measured overtime in some of these same species elsewhere (Sanger 1971, Dixon and Paiva 1995, Lee et al. 2003, Coder 2008). The slight decrease in g_{cc} during summer may be related to the changes in chlorophyll *a* and *b* concentrations and the associated reflectance differences that change over the growing season (Shull 1929, Sanger 1971, Lee et al. 2003). The increasing in r_{cc} in spring may be mainly caused by the synthesis of reddish carotenoids (Garcia-Plazaola et al. 1997, Sanger 1971). But the most dramatic increases in redness occurred in the fall, with elevated anthocyanin levels in response to environmentally driven gene up-regulation of anthocyanin biosynthesis (Dixon and Paiva 1995, Coder 2008). We found that color indices and phenological dates derived from digital camera images can be used to determine plant phenological stages across different species. The time series of green and red color indices reflect the differences in timing of development stages in spring and autumn among species (Inoue et al. 2014). For example, white ash always had the shortest growing season, with later spring leafing out and earlier leaf coloration and leaf drop, than other species.

Our comparisons between image derived dates and observed phenological dates provided insights in to how digital camera monitoring relates to ground-based visual observations. The findings will also help relate phenology observations from visual scoring in the field to remotely sensed, phenological analyses across large spatial scales in satellite images. We found that phenological dates derived from time series of and greenness (g_{cc}) and redness (r_{cc}) were well matched wtih ground observations on phenology of multiple species, but there is some temporal offset. In spring, SOS (i.e. increase in g_{cc} values form a minimum level in early spring) correspond to the development stage of trees between the onset and the peak of leaf unfolding. The reason for this temporal offset could be that digital cameras can only detect the change of greenness above some threshold. The onset of leaf unfolding and bud burst probably does not provide large enough change of greenness for the cameras to detect. Another reason could be the uncertainties from ground observations. With only two observations per week, one may not adequately capture the fast changes in bud burst and leaf unfolding in spring. This may cause deviations from the real phenological dates that may be better captured via continuous digital monitoring.

For autumn phenology, we developed a set of new color indices (POR, EOR and PORA) to capture the change of redness of tree foliage canopies over time. As we found that POR (Peak of Redness) from r_{cc} time series data was highly correlated to PORA (Peak of Relative Anthocyanins) from VARI, it suggests that r_{cc} and POR can be good proxies of changes of anthocyanins in leaves as VARI and PORA. But note that there is an offset (about 2 days) between POR and PORA. The reason for the offset could be that the time series of r_{cc} and VARI were measuring slightly different colors, though both of them can be proxy of relative content of anthocyanins. Data uncertainties could also be one reason leading to the offset. In comparisons with ground-based visual observation, we found that both POR and EOS matched well with visually scored observations on the end of leaf coloration, and EOS matched well with the peak of leaf drop, while EOR matched well with the end of leaf drop. In autumn, when onset of leaf coloration was detected visually, most leaves on tree canopies were still green. The visually observed peak of leaf coloration represented the timing when leaves changed color most quickly. However, POR

and EOS measured the timing of fully changed leaf color with the highest proportion of redness and lowest proportion of greenness present. These factors likely caused the temporal offset between the onset and peak of leaf coloration versus POR and EOS (Fig. 4-4). In terms of leaf drop, when leaves started to drop (onset of leaf drop), color changes in greenness and redness were probably not large enough to be captured by the cameras, but when visually about half of canopy lost leaves (peak of leaf drop), this corresponded to the end of season (EOS) with the lowest proportion of greenness. When visually the canopy trees dropped almost all leaves (end of leaf drop), this corresponded to the timing of EOR since very low quantities of red colored leaves would be detected. These are probably the main reasons for the temporal offset showed in Fig. 4-5. Moreover, this provides a direct means of comparison between visual observations of phenological changes in forest tree species over the course of the growing season and corresponding changes detected with remotely sensed images. These findings point out the potentially valuable application of redness measures in autumn phenology, that the change of redness in tree canopies may provide an informative measure of the biological processes of autumn phenology. This has not been mentioned, to our knowledge, in previous phenology studies using digital cameras (Ide and Oguma 2010, Sonnentag et al. 2012, Keenan et al. 2014). Thus while we suggest using g_{cc}-based SOS and EOS indices as proxy of the start and end of growing season, we also encourage the use of r_{cc} -based, POR and EOR indices to investigate autumnal changes of foliage in temperate deciduous trees.

The linear mixed effects models of POR and PORA may not have included all the potentially important climatic/weather or other explanatory factors that affect these response variables. In part there is the problem of high correlations among the variables we had available. In model selection procedures, we found a few models had very similar values of AIC and BIC with difference smaller than 2 (Table 4.1-3), which means these models had similar performance in explaining the peak date of fall foliage color. This suggested that all variables in these models can be important. Thus, summer heat, minimum temperature in September and CDDi in September may also be significant factors affecting the timing of peak color in fall foliage. More summer heat, lower minimum temperature in September or more chill in

September lead to earlier peak of color in fall foliage. The random intercepts at site levels in the models point to the potential importance of site effect explanatory variables not included in the model such as soils (e.g. site variation in soil pH values, nitrogen and phosphorous levels, and soil moisture variation, etc.) and biotic effects (e.g. pest and pathogen levels) (Dixon and Paiva 1995, Close and Beadle 2003). Clearly, further research needs to be focused on understanding the effects of these variables on the timing and color expression of fall foliage.

Large variation in DOR (Deviation of Redness) as a measure of the intensity of redness in the autumn foliage was found among species as well as individual replicate trees. The reason could be the differences in foliage color expression among species in fall. Black birch, white ash and hickories usually have yellow leaves, showing less redness than other species, such as maples and oaks (Coder 2008). Large variations among individuals within species may be due to several different factors. It could reflect different nutrient conditions in leaves affecting anthocyanin biosythesis, including pH, N and P levels, which in turn reflect differences in local soil conditions (Close and Beadle 2003, Outchkourov et al. 2014). It also can be wound responses by leaves caused by pathogen and pests (Dixon and Paiva 1995, Close and Beadle 2003). Additionally, genetic variations among individuals may lead to different metabolism pathway of anthocyanins production that influence color expressions in leaves (Albert et al. 2011, Misyura et al. 2012).

The inter-annual variations of DOR of each tree may be related to temporal changes of climatic/weather conditions (e.g. temperature and drought stress). However, we had only three-year dataset for each tree with relatively little year-to year variations, and this may partially explain why we did not find significant results for DOR for most species. In addition, although concentrations of anthocyanin in leaves are related to cool but non-freezing temperature, high light, low nutrient conditions and environmental stresses (e.g. drought and frost) (Dixon and Paiva 1995, Chalker-Scott 1999), the mechanism of accumulating red pigments (e.g. anthocyanin) in leaves could be different from the timing of leaf coloration and leaf drop. To our knowledge, no study has provided any more specific findings

about how various environmental factors may affect anthocyanin accumulation and expression in leaves other than a general list of leaf-level cellular factors including pH, P, N, and osmotic effects. Another reason for our poor resolution in explaining spatio-temporal variation in DOR values is that this index does not represent the accumulation of only anthocyanin, but also describes the quantity of all red pigments in leaves, including some carotenoids and other flavinoids (Sanger 1971, Field et al 2001, Lee et al. 2003). This is because we set the value of redness in winter as the baseline of the DOR, however carotenoids are produced from the spring, which then decline in late autumn, while anthocyanins are produced mainly during the autumn (Sanger 1971, Coder 2008). Further work is necessary to evaluate the relationship between DOR and the concentration of anthocyanin (along with other red pigments) in leaves. How climate change may affect the timing of fall foliage color and intensity is important to foliage ecotourism industry with its broad interests from both the public and scientists. Thus, we encourage long-term monitoring on fall foliage and further investigates on the mechanism of affecting color change of fall foliage via controlled physiological experiments (e.g. transplants, soil nutrient treatment, drought and temperature treatments) and observations, along with the interacting effects of climate/weather conditions.

Digital camera images provide useful information for continuous monitoring of seasonal changes of tree canopy phenology. But we did find that the weather conditions affect the time series of color indices shown in individual daily images. Rainy and cloudy days showed very low values of digital colors metrics, which produces spikes in the time series (Fig. 4.1-4). Although we used 3-day smoothed data to reduce the effect, the uncertainty of determining dates could be large when consecutive rainy and cloudy days happened during a time when canopy color (g_{cc} or r_{cc}) is rapidly changing.

In this study, we compared and contrasted image-derived phenological dates to visual, ground-based observational dates to investigate how phenological information is captured using different methods. This in turn provides insights into relating the information on phenology derived from field visual observation to data derived via remote sensing. We found that SOS digitally derived from a green

color index (g_{cc}) matched with the visually observed timing between onset and peak of leaf unfolding in spring. In the autumn POR (Peak of Redness) and EOR (End of Redness) derived digitally from a red color index (r_{cc}) matched well with the visually scored end of leaf coloration and leaf drop. We developed new autumn phenological date metrics (POR and EOR) and DOR (Deviation of Redness) to help extract information of the timing and intensity of redness in fall foliage. Moreover, this is the first application of linear mixed effects models to investigating the interactions between autumn phenology and climatic/weather factors. Our findings identified and quantified the important effects from chill and minimum temperatures in autumn, heat-stress in summer and drought-stress in autumn on the timing and intensity of redness in fall foliage of deciduous tree canopies. Different coefficients of autumn drought in models of timing of peak fall foliage color of eight species suggested species-specific phenological responses to drought conditions, which has been rarely examined in previous studies. Long term monitoring on tree canopies by digital cameras can be easily and inexpensively expanded in future research to capture more extensive spatial and temporal data on phenology. In order to understand and predict how climate change affects colors in fall foliage, we encourage studies focusing on the physiological mechanisms of the color change of fall foliage and the effects from spatial and temporal variation in environmental factors on the expression of color hue and saturation or intensity in fall foliage.

Acknowledgements

This study was supported in part by NSF grant DEB 0842465 to JAS. We thank R. Primack, R. Chazdon, E. Adams, and D. Civco for helpful comments to improve this manuscript.

References

Albert NW, Lewis DH, Zhang H, Schwinn KE, Jameson PE, Davies KM (2011) Members of an R2R3-MYB transcription factor family in Petunia are developmentally and environmentally regulated to control complex floral and vegetative pigmentation patterning. The Plant Journal, 65(5):771-784.

Archetti M, Döring TF, Hagen SB, Hughes NM, Leather SR, Lee DW, et al. (2009) Unravelling the evolution of autumn colours: an interdisciplinary approach. Trends in Ecology & Evolution, 24(3):166-173.

Archetti M, Richardson AD, O'Keefe J, Delpierre N (2013) Predicting Climate Change Impacts on the Amount and Duration of Autumn Colors in a New England Forest. PLoS ONE 8(3): e57373. doi:10.1371/journal.pone.0057373.

Chalker-Scott L (1999) Environmental significance of anthocyanins in plant stress responses. Photochemistry and photobiology, 70:1-9.

Close DC, Beadle CL (2003) The ecophysiology of folia anthocyanin. The Botanical Review 69(2): 149–161.

Coder KD (2008) Primer On Autumn Tree Leaf Colors. Outreach Monograph WSFNR08, 28, 1-52.

Diez MJ, Ibanes I, Miller-Rushing AJ, Mazer SJ, Crimmins MA, Bertelsen CD, Inouye DW (2012) Forecasting phenology: from species variability to community patterns. Ecol Lett 15:545–553.

Diggle, P.J., Heagerty, P., Liang, K.Y. & Zeger, S.L. (2002). Analysis of longitudinal data. 2nd edn. New York, Oxford.

Dixon RA, Paiva NL (1995) Stress-induced phenylpropanoid metabolism. The Plant Cell, 7:1085–1097.

Feild TS, Lee DW, Holbrook NM (2001) Why leaves turn red in autumn. The role of anthocyanins in senescing leaves of red-osier dogwood. Plant physiology, 127(2):566-574.

Greven, S. & Kneib, T. (2010). On the behaviour of marginal and conditional AIC in linear mixed models. Biometrika, doi: 10.1093/biomet/asq042.

Gillespie AR, Kahle AB, Walker RE (1987) Color enhancement of highly correlated images. II. Channel ratio and “chromaticity” transformation techniques. Remote Sensing of Environment, 22:343-365.

Hufkens K, Friedl M, Sonnentag O, Braswell BH, Milliman T, Richardson AD (2012) Linking near-surface and satellite remote sensing measurements of deciduous broadleaf forest phenology. Remote Sens. Environ. 117:307–321.

Ide R, Oguma H (2013) A cost-effective monitoring method using digital time-lapse cameras for detecting temporal and spatial variations of snowmelt and vegetation phenology in alpine ecosystems. Ecological Informatics 16:25–34.

Inoue T, Nagai S, Saitoh TM, Muraoka H, Nasahara KN, Koizumi H (2014) Detection of the different characteristics of year-to-year variation in foliage phenology among deciduous broad-leaved tree species by using daily continuous canopy surface images. Ecological Informatics, 22:58-68.

Keenan TF, Darby B, Felts E, Sonnentag O, Friedl MA, Hufkens K, et al. (2014) Tracking forest phenology and seasonal physiology using digital repeat photography: a critical assessment. Ecological Applications, 24(6):1478-1489.

Lee DW, O'keefe J, Holbrook NM, Feild TS (2003) Pigment dynamics and autumn leaf senescence in a New England deciduous forest, eastern USA. Ecological Research, 18(6): 677-694.

Misyura M, Colasanti J, Rothstein SJ (2012) Physiological and genetic analysis of Arabidopsis thaliana anthocyanin biosynthesis mutants under chronic adverse environmental conditions. Journal of experimental botany, doi:10.1093/jxb/ers328.

Morse SC, Smith EM (2015) Hotel Revenue Management Strategies during Fall Foliage Travel Season. J Hotel Bus Manage, 4(111):2169-0286.

Outchkourov NS, Carollo CA, Gomez-Roldan V, de Vos RCH, Bosch D, Hall RD, Beekwilder J (2014) Control of anthocyanin and non-flavonoid compounds by anthocyanin-regulating MYB and bHLH transcription factors in Nicotiana benthamiana leaves. Frontiers in Plant Science, 5: 1-9, doi: 10.3389/fpls.2014.00519.

Polgar C, Gallinat A and Primack RB (2014) Drivers of leaf-out phenology and their implications for species invasions: insights from Thoreau's Concord. New Phytologist, 202: 106-115.

Primack RB, et al. (2009) Spatial and interspecific variability in phenological responses to warming temperatures. Biol Conserv 142(11):2569–2577.

R Core Team (2015). R: A language and environment for statistical computing. R Foundation for Statistical Computing, Vienna, Austria.

Richardson AD, Bailey AS, Denney EG, Martin CW, O'Keefe J (2006) Phenology of a northern hardwood forest canopy. Glob Chang Biol. 12(7):1174–1188.

Richardson AD, Jenkins JP, Braswell BH, Hollinger DY, Ollinger SV, Smith M-L (2007) Use of digital webcam images to track spring green-up in a deciduous broadleaf forest. Oecologia, 152: 323-334.

Richardson AD, Braswell BH, Hollinger DY, Jenkins JP, Ollinger SV (2009) Near-surface remote sensing of spatial and temporal variation in canopy phenology. Ecological Applications, 19:1417-1428.

Rustad, L. et al. (2011) Changing Climate, Changing Forests: The Impacts of Climate Change on Forests of the Northeastern United States and Eastern Canada. USDA Forest Service Northern Research Station General Technical Report NRS-99, 48.

Sanger JE (1971) Quantitative investigations of leaf pigments from their inception in buds through autumn coloration to decomposition in falling leaves. Ecology, 52:1075-1089.

Sonnentag O, Hufkens K, Teshera-Sterne C, Young AM, Friedl M, Braswell BH, Milliman T, O'Keefe J, and Richardson AD (2012) Digital repeat photography for phenological research in forest ecosystems. Agric. For. Meteorol., 152:159–177.

Viña A, Gitelson A (2011) Sensitivity to foliar anthocyanin content of vegetation indices using green reflectance. Geoscience and Remote Sensing Letters, IEEE, 8(3):464-468.

Xie Y, Ahmed KF, Allen JM, Wilson AM, Silander JA (2015) Green-up of deciduous forest communities of northeastern North America in response to climate variation and climate change. Landscape Ecology, 30: 109-123.

Yang X, Tang J, Mustard JF (2014) Beyond leaf color: Comparing camera-based phenological metrics with leaf biochemical, biophysical, and spectral properties throughout the growing season of a temperate deciduous forest. Journal of Geophysical Research: Biogeosciences, 119(3):181-191.

Figure 4-1 Demonstration on determining of EOS (end of season), SOS (start of season) from time series of g_{cc} (a), POR (peak of redness) and EOR (end of redness) from r_{cc} (b), and PORA (peak of relative anthocyanin) from VARI (c). Data were from one red maple tree at site, Turf1, in 2013.

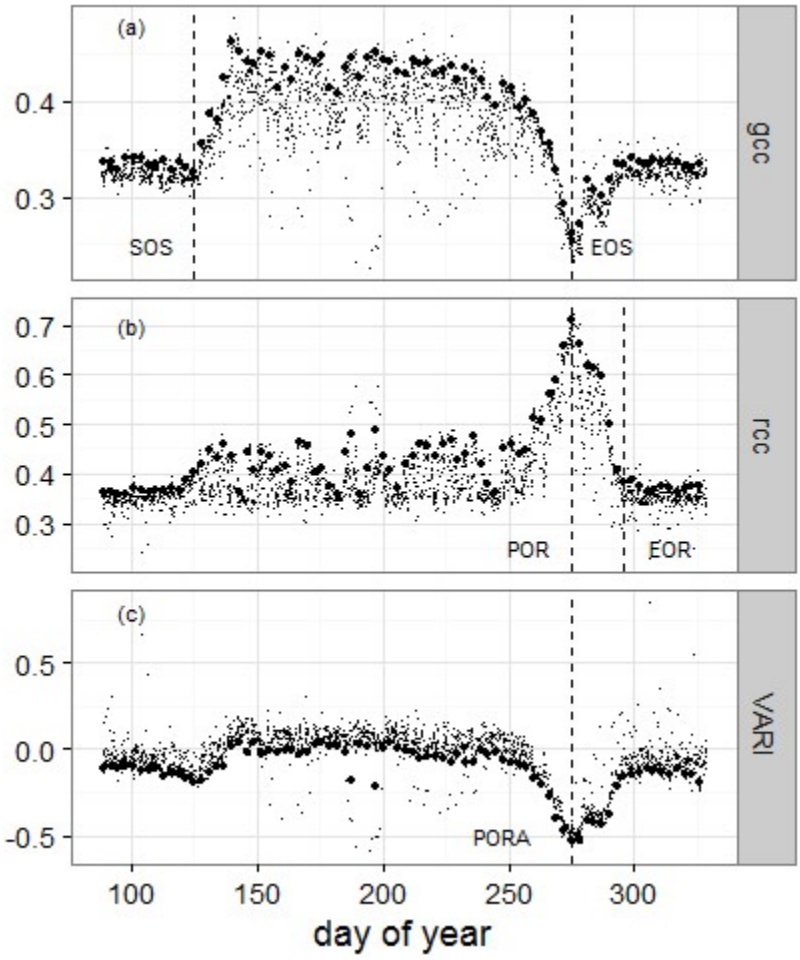

Figure 4-2 Time series of g_{cc} of eight species in one growing season. a: red maple, b: sugar maple, c: white oak, d: red oak, e: pignut hickory, f: shagbark hickory, g: white ash, h: black birch. Small dots are hourly raw data, and big dots are 3-day smoothed data. Two dashed lines and the numbers indicate the date of SOS and EOS.

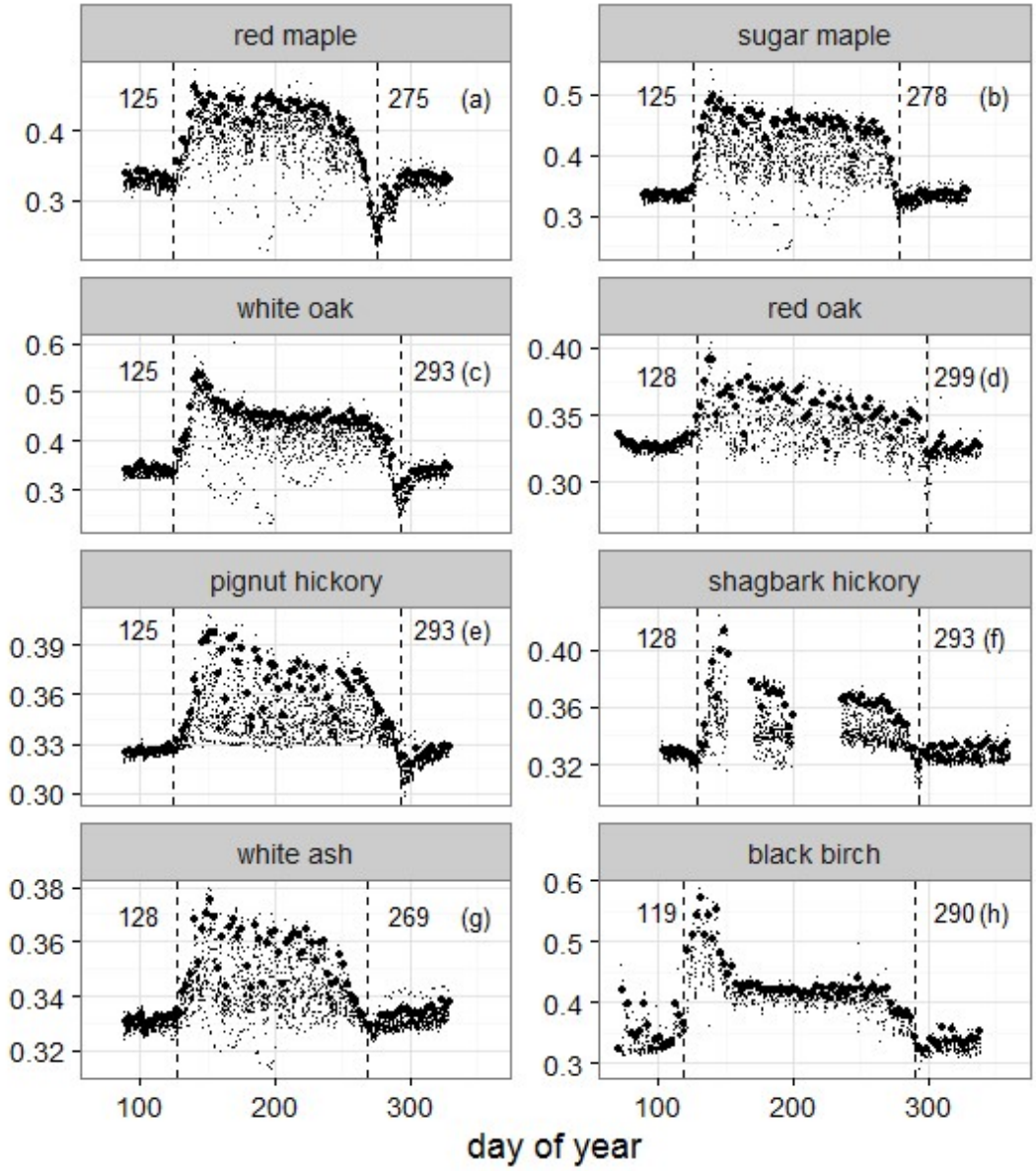

Figure 4-3 Time series of r_{cc} of eight species in one growing season. a: red maple, b: sugar maple, c: white oak, d: red oak, e: pignut hickory, f: shagbark hickory, g: white ash, h: black birch. Small dots are hourly raw data, and big dots are 3-day smoothed data. Two dashed lines and the numbers indicate the date of POR and EOR.

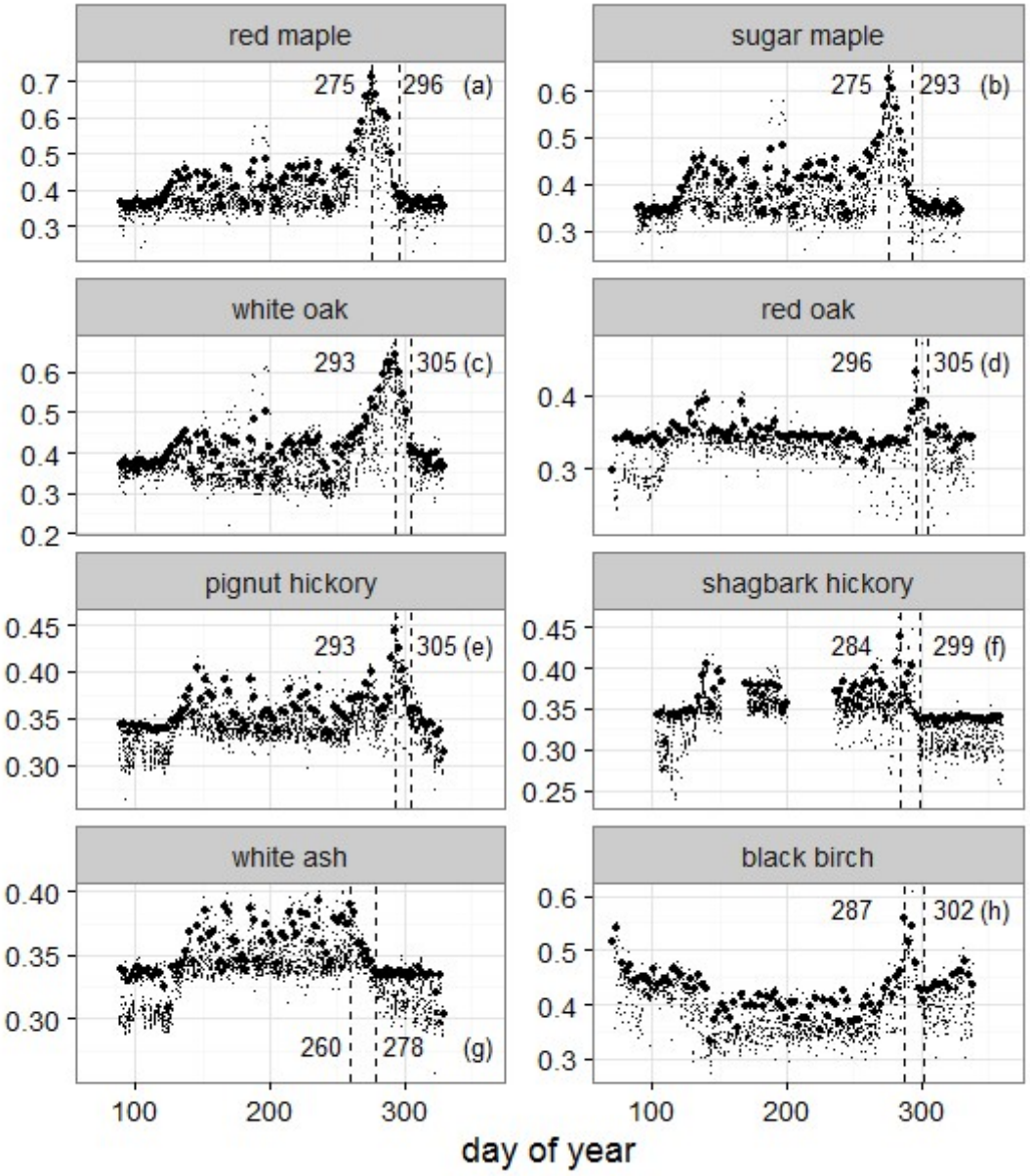

Figure 4-4 Comparison plots between three phenological transition dates of leaf coloration and EOS and POR. The solid line is 1:1 line. X axis is EOS or POR, and y axis is observed leaf coloration dates. a: EOS vs. the onset date of leaf coloration, b: EOS vs. the peak date of leaf coloration, c: EOS vs. the end date of leaf coloration, d: POR vs. the onset date of leaf coloration, e: POR vs. the peak date of leaf coloration, f: POR vs. the end date of leaf coloration.

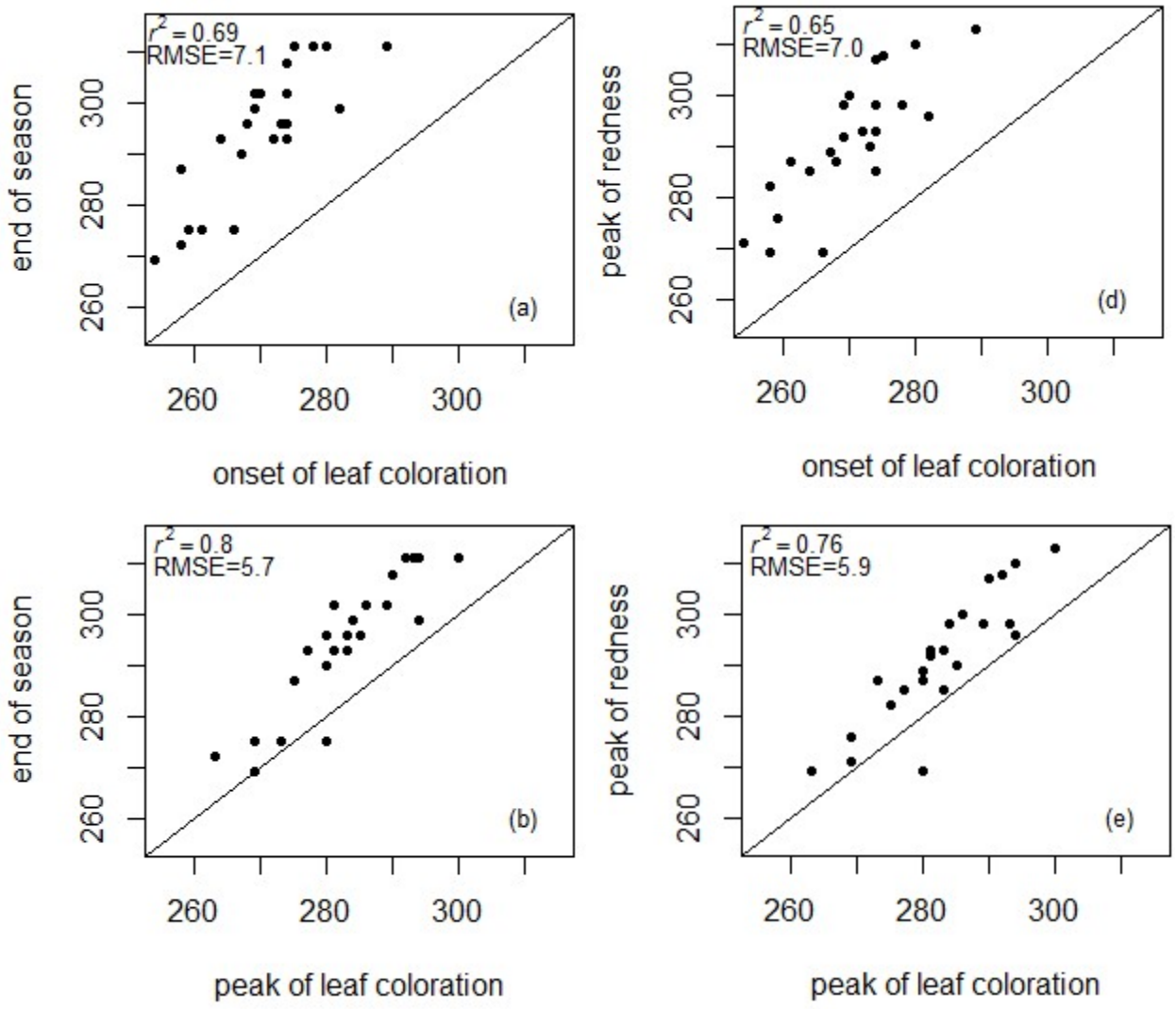

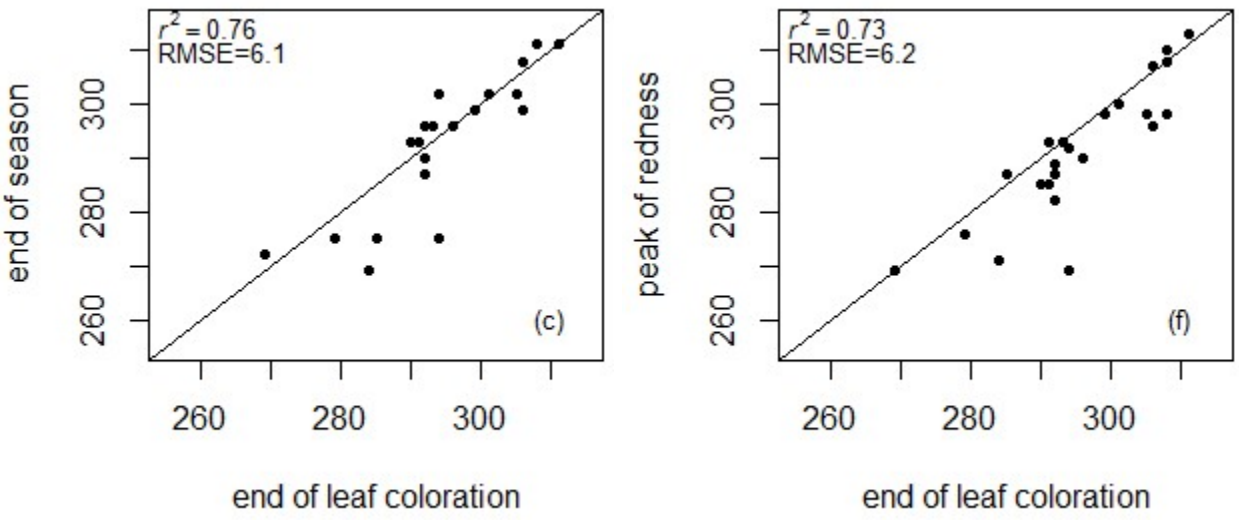
r^2 = 0.76
RMSE=6.1
(c)
end of season
260
280
300
end of leaf coloration
r^2 = 0.73
RMSE=6.2
(f)
peak of redness
260
280
300
end of leaf coloration

Figure 4-5 Comparison plots between three phenological transition dates of leaf drop and EOS and EOR. The solid line is 1:1 line. X axis is EOS or EOR, and y axis is observed leaf drop dates. a: EOS vs. the onset date of leaf drop, b: EOS vs. the peak date of leaf drop, c: EOS vs. the end date of leaf drop, d: POR vs. the onset date of leaf drop, e: POR vs. the peak date of leaf drop, f: POR vs. the end date of leaf drop.

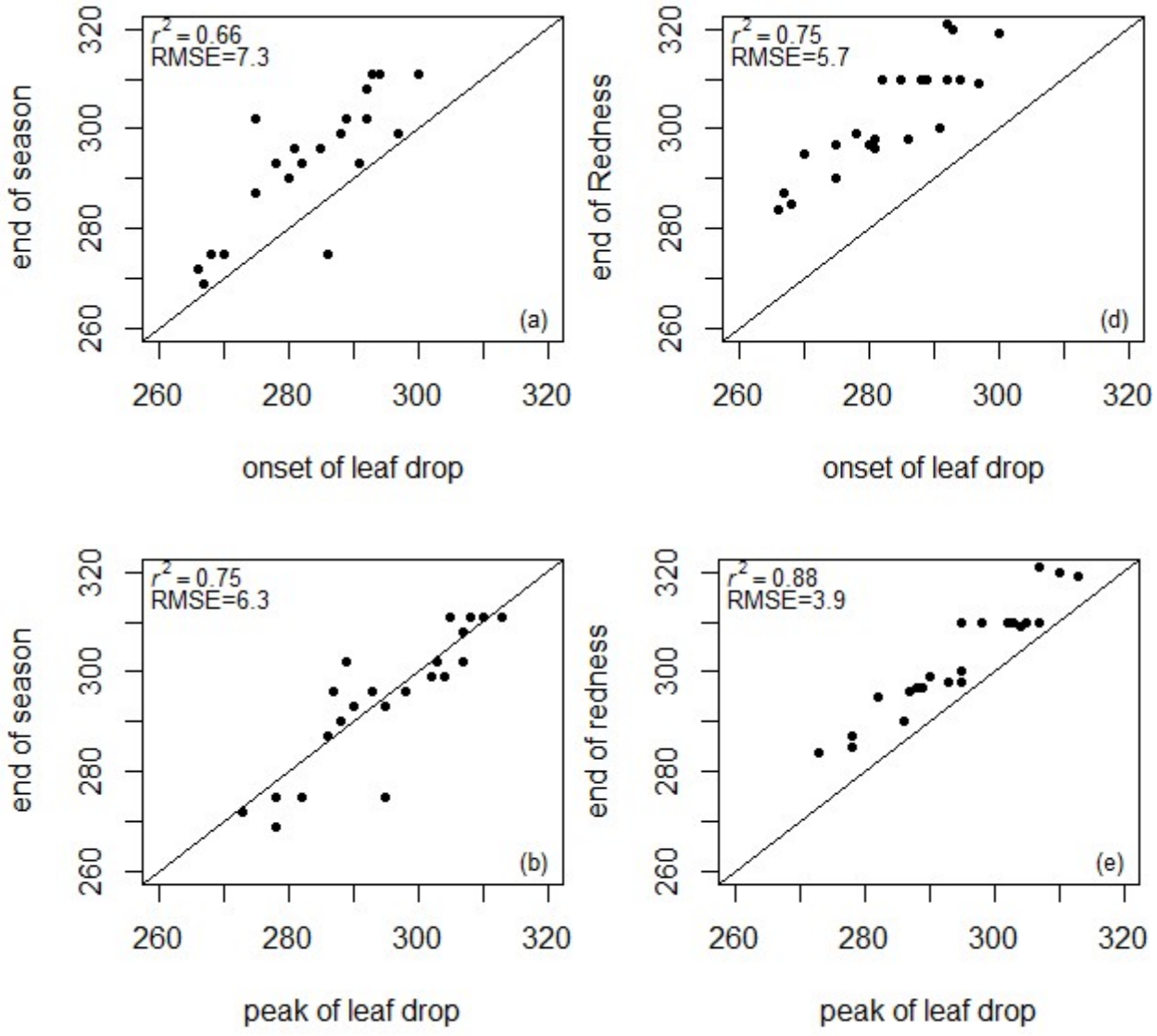

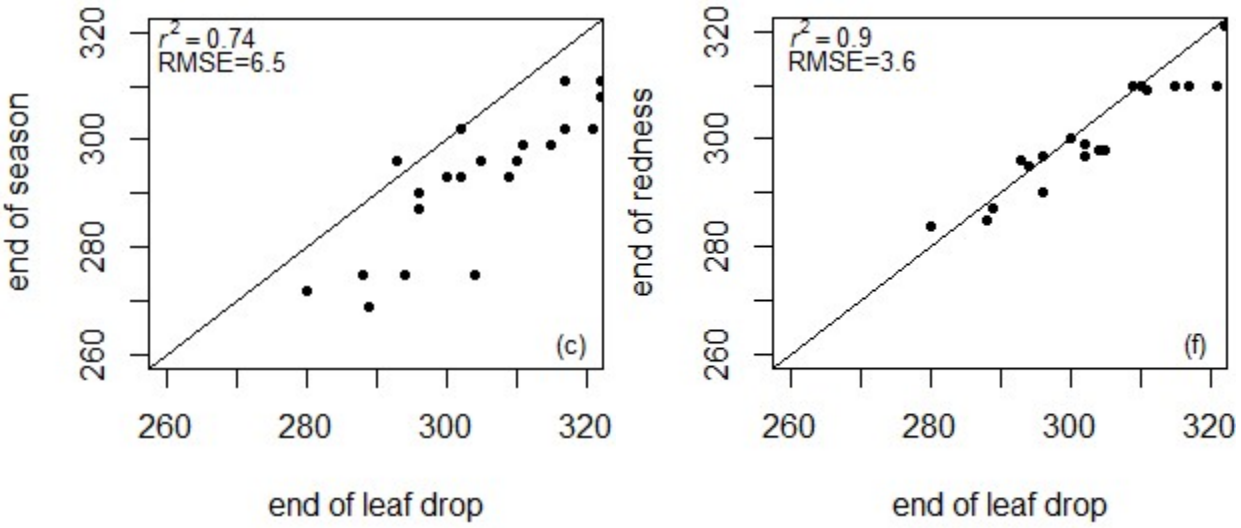
r^2 = 0.74
RMSE=6.5
(c)
end of season
end of leaf drop
260
280
300
320
r^2 = 0.9
RMSE=3.6
(f)
end of redness
end of leaf drop

Figure 4-6 Coefficient values of (a) $GDR_{(Sep.1- Oct.31)}$ and (b) $GDR_{(Jul.1- Aug.31)}$ as deviation from random slopes in the best models for (a) POR and (b) PORA. X axis displays the 8 tree species. 1: ACRU, 2: ACSA, 3: BELE, 4: CAGL, 5: CAOV, 6: FRAM, 7: QUAL, 8: QURU.

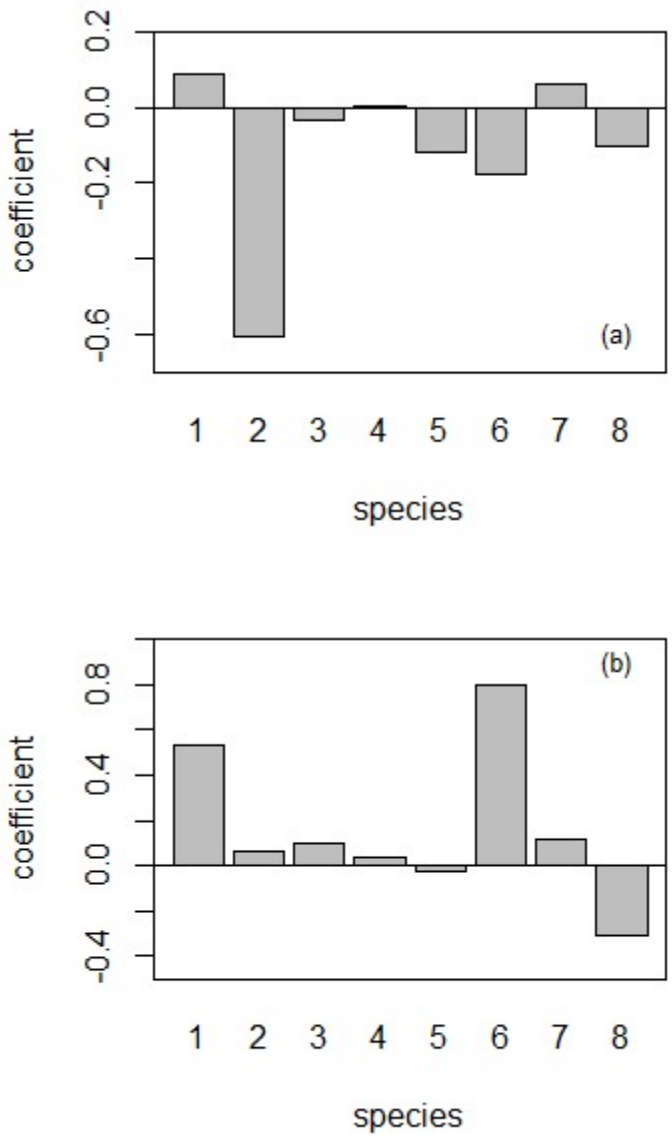

Table 4-1 Replicates of tree canopies captured by time-lapse cameras in nine sites in and around UCONN Forest.

Site name	Species and number of replicates
ASP	*Acer rubrum* (1), *Acer saccharum* (1), *Fraxinus americana* (2)
CRP	*Carya glabra* (2), *Quercus rubra* (2)
HBP	*Carya ovata* (3), *Quercus rubra* (3)
RMP	*Acer rubrum* (4), *Quercus rubra* (2)
SMP	*Acer saccharum* (4)
JohnC	*Acer rubrum* (2), *Quercus rubra* (3)
Fenton	*Betula lenta* (2), *Quercus rubra* (2)
Turf1	*Acer rubrum* (1), *Acer saccharum* (1), *Fraxinus americana* (1), *Carya glabra* (1), *Quercus alba* (1)
Turf2	*Acer saccharum* (1), *Betula lenta* (1), *Fraxinus americana* (1), *Quercus alba* (1), *Quercus rubra* (2)

Table 4-2 Mean values (and standard deviation) of SOS and EOS in Julian calendar days derived from camera images for all replicates of eight deciduous species during 2012 and 2014.

Species	SOS	EOS
Acer rubrum	123 (5.2)	285 (9.3)
Acer saccharum	123 (3.7)	282 (10.0)
Betula lenta	122 (5.2)	287 (3.0)
Carya glabra	123 (5.1)	289 (7.7)
Carya ovata	131 (3.3)	291 (4.0)
Fraxinus americana	128 (5.0)	266 (7.5)
Quercus alba	129 (4.5)	293 (7.7)
Quercus rubra	129 (3.8)	297 (9.2)

Table 4-3 Fixed variables from the best linear mixed effects models of POR and PORA. For variables names refer to Table 3-1. Subscript in each variable indicates the time period for each variable.

date	Predictor	Coefficient	SE	p-value
POR	FD_{Oct}	-0.803	0.283	0.003
	$RD_{(Sep.1- Oct.31)}$	-0.681	0.255	0.004
PORA	FD_{Oct}	-0.867	0.273	<0.001
	$RD_{(Sep.1- Oct.31)}$	-0.596	0.233	0.006

Table 4-4 Mean values and standard deviation of DOR derived from camera images for all replicates of eight deciduous species during 2012 and 2014, and the range of variation of DOR among trees in each year and among years for each tree within each species. Due to the missing data in a small sample size, there is no range value for *Betula lenta*.

Species	DOR	range of variation among trees	range of variation among years
Acer rubrum	0.131 (0.106)	0.005-0.022	0.00003-0.005
Acer saccharum	0.159 (0.097)	0.006-0.020	0.0003-0.012
Betula lenta	0.210 (0.078)	0.006	0.006
Carya glabra	0.081 (0.048)	0.002-0.007	0.00008-0.002
Carya ovata	0.116 (0.049)	0.001-0.006	0.001-0.002
Fraxinus americana	0.101 (0.065)	0.001-0.008	0.001-0.004
Quercus alba	0.155 (0.074)	0.005-0.006	0.001-0.004
Quercus rubra	0.125 (0.067)	0.003-0.006	0.00001-0.005

Appendix 4.1

Figure 4.1-1 Example of ROI selection for three different tree canopies at one site, Turf1, in 2013. Four photos showed the seasonal change of tree canopies through the growing season from spring to autumn. (a) May 10, 2013; (b) July 18. 2013; (c) October 2, 2013; (d) October 21, 2013. ROI was selected to avoid overlap of multiple tree canopies. Colors and numbers of ROI from the image indicate different tree species. 1: sugar maple, 2: white ash, 3: pignut hickory.

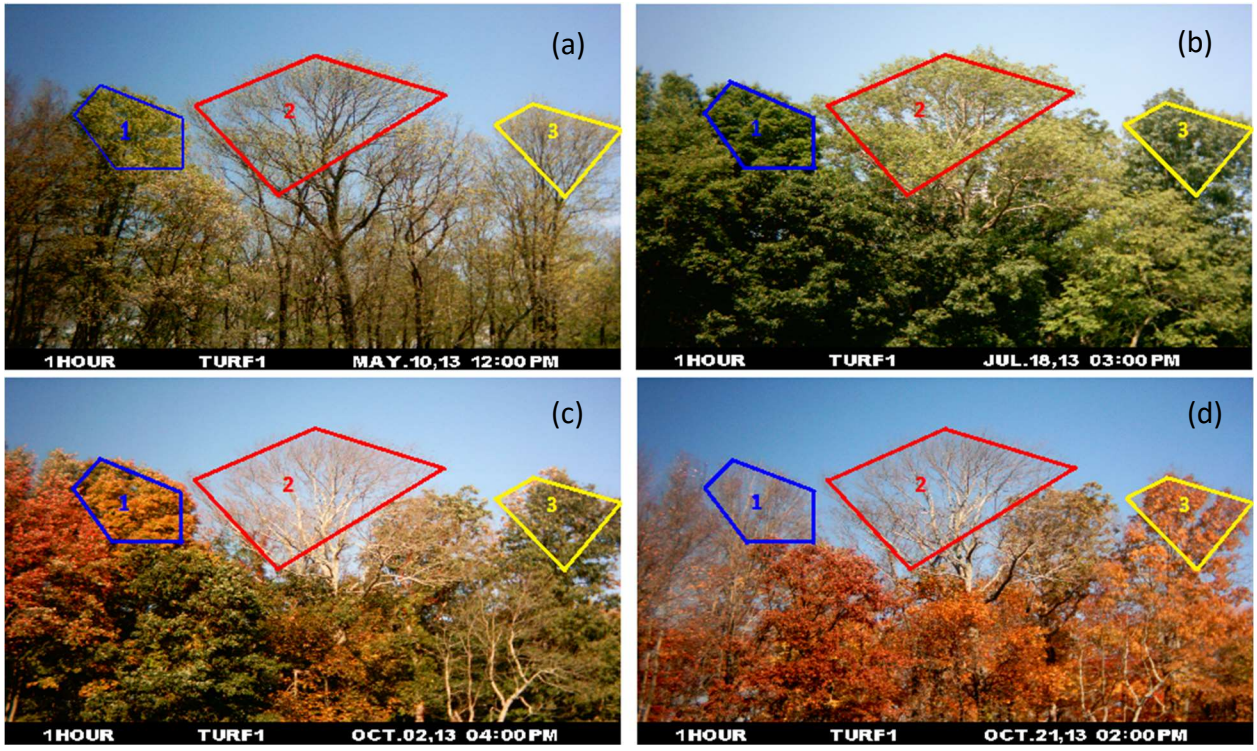

Figure 4.1-2 Time series of VARI of eight species in one growing season. a: red maple, b: sugar maple, c: white oak, d: red oak, e: pignut hickory, f: shagbark hickory, g: white ash, h: black birch. Small dots are hourly raw data, and big dots are 3-day smoothed data. Dashed lines and the numbers indicate the date of PORA.

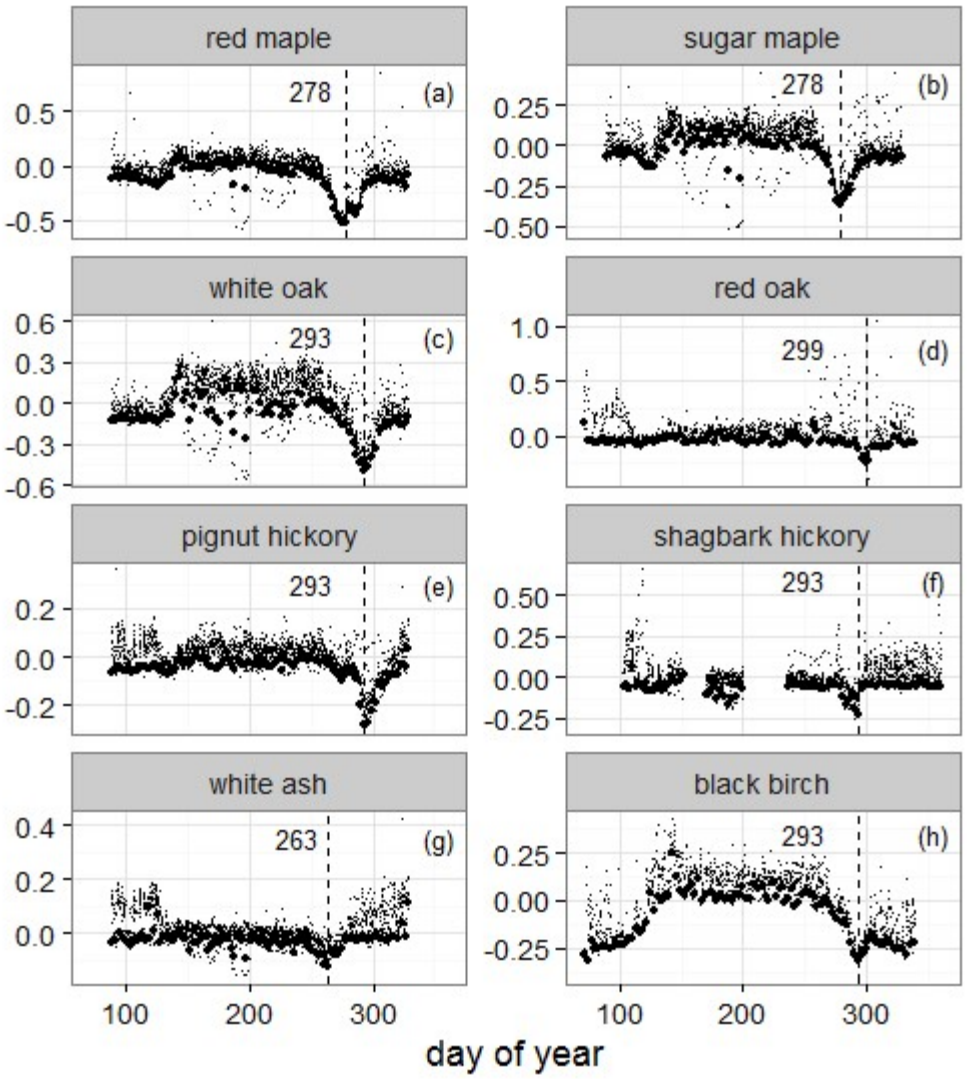

Figure 4.1-3 Comparison plots between three phenological transition dates of leaf unfolding and SOS. The solid line is 1:1 line. X axis is SOS, and y axis is observed leaf unfolding dates. a: the onset date of leaf unfolding, b: the peak date of leaf unfolding, c: the end date of leaf unfolding.

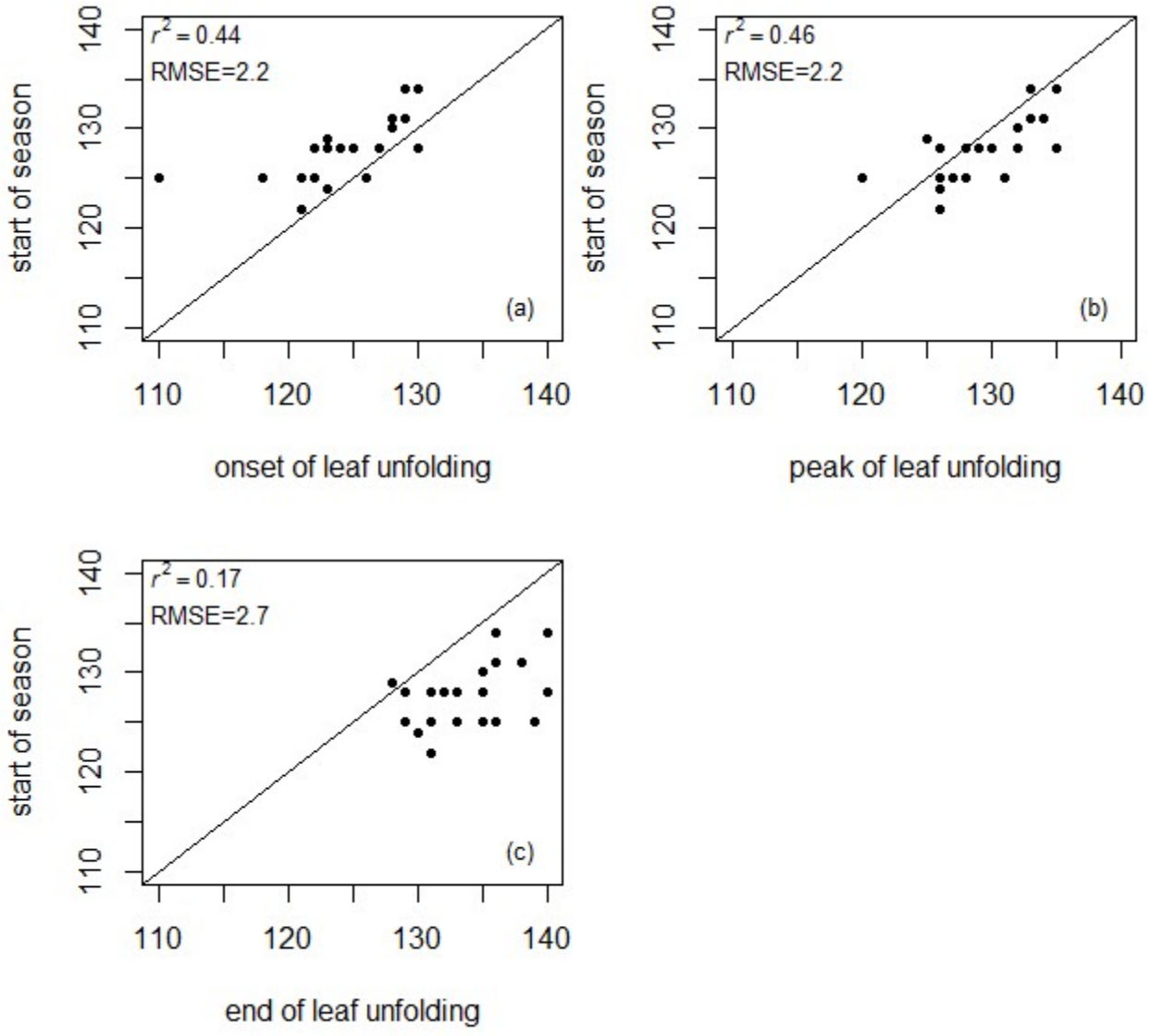

Figure 4.1-4 Spikes in time series of g_{cc} of one white ash in site Turf1 in 2013. Six spikes (pointed by arrows) were found in the time series from spring to early autumn, which were caused by dark images in cloudy and rainy days.

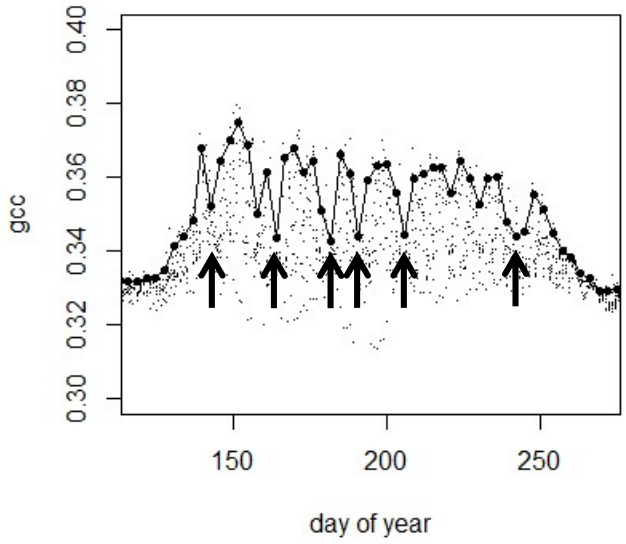

Table 4.1-1 Ground observation in four sites parallel to time-lapse camera monitoring.

Site name	Species and number of replicates
CRP	*Carya glabra* (2), *Quercus rubra* (2)
HBP	*Carya ovata* (3), *Quercus rubra* (3)
RMP	*Acer rubrum* (4), *Quercus rubra* (2)
SMP	*Acer saccharum* (3)

Table 4.1-2 Fixed variables in random intercept models for DOR of sugar maples. Random effect is intercept at individual tree level. For variables names refer to Table 3-1. Subscript in each variable indicates the time period for each variable or the base temperature in calculations.

Fixed structure of LME	Coefficient	SE	p-value
DOR ~ $T_{min\text{-}Sep}$	0.031	0.012	0.020
DOR ~ $CDDi_{Sep10}$	-0.001	0.0005	0.026
DOR ~ FD_{Oct}	-0.011	0.004	0.020

Table 4.1-3 Top four models of random intercept models of linear mixed effects models for POR and PORA. Random effects include random intercepts at species and sites levels. For variables names refer to Table 3-1. Subscript in each variable indicates the time period for each variable or the base temperature in calculations.

Fixed structure of LME	AIC	BIC
POR ~ HD_{35}	1059.47	1074.32
POR ~ $FD_{Oct} + RD_{(Sep.1\text{-}Oct.31)}$	1060.92	1078.74
POR ~ $T_{min\text{-}Sep}$	1060.69	1075.53
POR ~ $CDDi_{Sep20}$	1060.85	1075.70
PORA ~ $FD_{Oct} + RD_{(Sep.1\text{-}Oct.31)}$	1061.63	1079.45
PORA ~ HD_{35}	1062.58	1077.43
PORA ~ $T_{min\text{-}Sep}$	1063.17	1078.02
PORA ~ $CDDi_{Sep20}$	1063.38	1078.23